STUDY OF THE INTERACTIONS OF SOFTWOOD EXTRACTIVES AND MODEL COMPOUNDS WITH DIFFERENT MODEL SURFACES

Yuen Yue Tham

Bachelor of Science (Hons)

Submitted in fulfilment of the requirements for the degree of

Doctor of Philosophy

School of Physical Sciences (Chemistry)
University of Tasmania
Launceston, Tasmania
Australia

December 2015

Declaration of Originality

This thesis contains no material which has been accepted for a degree or diploma by the University or any other institution, except by way of background information and duly acknowledged in the thesis, and to the best of my knowledge and belief no material previously published or written by another person, except where due reference is made in the text of the thesis, nor does the thesis contain any material that infringes copyright.

Authority of Access

This thesis may be made available for loan and limited copying and communication in accordance with the Australian Copyright Act of 1968.

Statement regarding published work contained in thesis

The publishers of papers (comprising chapters 2 - 4) hold the copyright for that content, and access to the material should be sought from the respective journals. The remaining non-published content of the thesis may be made available for loan and copying in accordance with the above statement (Authority of access). Due to the inclusion of published material, there will be unavoidable repetition of materials in this thesis.

Sign: _____ Date: 23/12/2015

(Yuen Yue Tham)

Statement of Co-Authorship

The following people and institutions contributed to the publication of work undertaken as part of this thesis:

1. Yuen Yue Tham, School of Physical Sciences (Chem), University of Tasmania (candidate)
2. Paul J. Molino, ARC Centre of Excellence Electromaterials Science, Intelligent Polymer Research Institute, AIIM Facility, University of Wollongong
3. Michael J. Higgins, ARC Centre of Excellence Electromaterials Science, Intelligent Polymer Research Institute, AIIM Facility, University of Wollongong
4. Karen R. Stack, School of Physical Sciences (Chem), University of Tasmania
5. Desmond E. Richardson, Norske Skog Paper Mills Australia Ltd, Boyer TAS
6. Trevor W. Lewis, School of Physical Sciences (Chem), University of Tasmania

Author details and their roles:

Paper 1: Parts of results found in paper are located in chapter 2

Author 4 was the main author and presenter of the work. Candidate was a co-author that carried out parts of experimental work and results analysis. Authors 1, 4, 5 and 6 contributed to the idea, its formalisation, development and refinement of the manuscript.

Paper 2: Located in chapter 3

Candidate was the main author on this paper. Author 2 offered laboratory training and assistance. All authors contributed to the idea, formalisation and development of manuscript as well as the refinement of the manuscript.

Paper 3: Located in chapter 4

Candidate was the main author on this paper. Authors 2 and 3 offered laboratory training and assistance. All authors contributed to the idea, formalisation and development of manuscript as well as the refinement of the manuscript.

We, the undersigned agree with the above stated "proportion of work undertaken" for each of the above published peer-reviewed manuscripts contributing to this thesis:

Signed: _ _ Date: 18/7/16

Dr Trevor W. Lewis

Supervisor

School Of Physical Sciences (Chemistry)

University of Tasmania

Signed Date: 19/7/16

Prof John Dickey

Head of School

School Of Physical Sciences (Chemistry)

University of Tasmania

Abstract

Wood extractives released into the process water during the production of thermomechanical pulp from the softwood *Pinus radiata* can form colloidal dispersions that may deposit onto surfaces during paper manufacture and processing. The major components that make up wood extractives are fatty acids, resin acids, triglycerides, sterols and steryl esters. In this thesis, wood extractives were represented by three of the major components that are oleic acid (a typical fatty acid), abietic acid (a typical resin acid) and triolein (a typical triglyceride).

The major aim of this thesis is to study the interaction between wood extractives and model surfaces to give an insight into the preferential desorption of largely resin acids, in preference to fatty acids and triglycerides, from paper onto metal surfaces.

Adsorption isotherms established for interaction of wood extractives and model compounds onto pulp fibres and microcrystalline cellulose showed that multilayer adsorption would best explain the adsorption behaviour of these compounds. The effect of pH perturbations was also considered for adsorption onto pulp fibres. Multilayer adsorption behaviour was best described with the Freundlich isotherm model. The results suggest that reorganisation of the surface of wood extractive colloids most probably occurred after pH perturbations, and their behaviour was very similar to simple fatty acid colloids. This suggests the loss of abietic acid from the surface of wood extractive colloids. However, due to low solubility of abietic acid, the adsorption behaviour of abietic acid could not be determined accurately.

Additionally, interactions of wood extractives and its individual components with model surfaces (cellulose and chromium) as well as the effects of different temperatures on adsorption behaviour (25°C and 50°C) were also studied using quartz crystal microbalance with dissipation monitoring (QCM-D). Different adsorption behaviour was observed to exist between the two surfaces as a function of temperature. At the lower temperature (25°C), two phases of adsorption occurred for adsorption onto cellulose surface, whereas a single adsorption phase occurred onto a chromium surface. At elevated temperature (50°C), only a single adsorption phase occurred on both cellulose and chromium surfaces. A greater amount of abietic acid was shown to adsorb on the chromium surface than the cellulose surface. Wood extractives were shown to adsorb less onto cellulose than onto chromium, which agrees with the practical observation that a greater amount of abietic acid adsorbed onto a chromium surface than onto a cellulose surface.

A new technique of attaching soft colloids (model compounds and wood extractives colloids) onto hydrophobically functionalised tipless atomic force microscopy (AFM) cantilevers was developed to allow direct measurement of the forces of interaction between the colloid and a model surface. These measurements were carried out by atomic force microscopy (AFM). Similar to QCM-D results, it was observed that adhesion of abietic acid and wood extractives were comparable on both cellulose and chromium surfaces; whereas the adhesion of triolein and oleic acid onto a cellulose surface was much greater than onto a chromium surface. This would explain the preferential transfer of resin acids from a cellulose surface onto a chromium surface in preference to triolein or oleic acid from wood extractives. In addition to the experimental techniques, computational modelling was used to compliment the experimental data. Different levels of theories and basis sets were employed to model the interaction of the model compounds and model surfaces. However, computational modelling with *ab initio* theories was shown to be unsuitable for quantitative modelling of these interactions. Thus different modelling programs and methods may be needed to successfully model the interaction of model compounds with cellulose or chromium surfaces.

List of Publications and Conferences

Publications

1. Stack, K. R.; Tham, Y. Y.; Lewis, T. W.; Richardson, D. E. The effect of pH disturbances on the colloidal structure and fibre adsorption of *Pinus radiata* wood extractives. *Appita Journal* 2015, *68* (4), 302-321.

2. Tham, Y. Y.; Molino, P. J.; Higgins, M. J.; Stack, K. R.; Richardson, D. E.; Lewis, T. W., The study of deposition of wood extractves and model compound colloids onto chromium and cellulose surfaces using quartz crystal microbalance with dissipation (QCM-D). *Colloids and Surfaces A: Physicochemical and Engineering Aspects* 2016, *491*, 1-11.

3. Tham, Y. Y.; Stack, K. R.; Richardson, D. E.; Molino, P. J.; Higgins, M. J.; Lewis, T. W. Development of in situ soft colloidal probe atomic force microscopy for probing the adhesion between wood extractives and model surfaces. *Colloids and Surfaces A: Physicochemical and Engineering Aspects* 2016**,** *500*, 203-213.

Conference

1. Tham, Y. Y.; Stack, K. R.; Richardson, D.; Molino, P. J.; Higgins, M. J.; Lewis, T. W. In *Probing interactions between colloidal wood extractives and model surfaces with atomic force microscopy.*, The 7th Biennial Australian Colloid and Interface Symposium, Hobart, Tasmania, 1 - 5 February; 2015; Australasian Colloid and Interface Society.

Poster Presentation

1. Tham, Y. Y.; Higgins, M. J.; Molino, P. J.; Richardson, D. E.; Stack, K. R.; Lewis, T. W. In *Interaction of wood extractive soft colloids with different surfaces.*, ACES Electromaterials Symposium, AIIM Facility, Innovation Campus, North Wollongong, NSW, Australia, 13-15 February; 2013; ARC Centre of Excellence for Electromaterials Science, Intelligent Polymer Research Institute, AIIM Facility.

Acknowledgement

Firstly, I would like to acknowledge and thank my supervisors Dr Trevor Lewis, Dr Karen Stack (from University of Tasmania) and Dr Desmond Richardson (Norske Skog Paper Mills Australia Ltd), as well as Dr Paul Molino and Dr Michael Higgins (ARC Centre of Excellence Electromaterials Science, Intelligent Polymer Research Institute (IPRI), University of Wollongong) for the opportunity to work under their supervision and for their constant guidance, support and ideas, which made these past years a truly rewarding experience.

Many thanks also go to the Dr David McGuinness for allowing the use of computing time (CPU time) on the National Computational Infrastructure (NCI) for modelling calculations in this project; Dr Ruth Amos and Prof Brian Yates for guidance in carrying out the computational calculations; and Dr Nathan Kilah for sourcing crystallography structures. Thanks also to the summer research students who helped in some of the GC experiments. I would like to thank the staff within the School of Physical Sciences (Chemistry), University of Tasmania for their friendship and encouragement. I would also like to thank the other academic staff at the IPRI, University of Wollongong, for their guidance and discussion during the time I was there.

Many thanks to all the friends at the University, Mean, Melissa, Sunny, Lokman and others, who have shared all the ups and downs of going through my PhD journey and offer support and encouragements over all these years.

To my family and 'adopted' church family, I thank you all for your continual love and support, as well as keeping me sane throughout my life here in Tasmania.

Last but not least, to my husband, Jerry, I will forever be very grateful for the unwavering love, support and patience throughout these years; for putting up with me being away so much and for doing all those neglected household chores. Thank you for solving all my editing problems as well. Finally, I would like to dedicate this work, in the memory of Reuben and Amos, our darling boys who came and left this world during the course of this work. You all gave me the determination to complete this work to the best ability that I can.

Table of Contents

List of Tables

List of Figures

Glossary of Abbreviations and Nomenclature

AA	**A**bietic **a**cid
AFM	**A**tomic **f**orce **m**icroscopy
a_T	Toth isotherm constant (L/mg)
A_T	Temkin isotherm equation binding constant
b	Langmuir isotherm constant (dm^3/mg)
b_T	Temkin isotherm constant
BET	**B**runauer-**E**mmett **T**eller
C_{BET}	BET adsorption isotherm relating to the energy of surface interaction (L/mg)
C_e	Equilibrium concentration (mg/L)
CPCM	Polarizable conductor calculation model
Cr	**C**h**r**omium
C_S	Adsorbate monolayer saturation concentration (mg/L)
DFT	**D**ensity **F**unctional **T**heory
DLVO	**D**erjaguin, **L**aundau, **V**ervey and **O**verbeek (theory)
DS	**D**issolved **s**ubstances
F	Frequency
FA	**F**atty **a**cids
GC	**G**as **c**hromatography
G_{corr}	Thermal correction to Gibbs' free energy
Glc	**Gl**u**c**ose
GTO	**G**aussian **t**ype **o**rbital
H_{corr}	Thermal correction to enthalpy
HF	**H**artree-**F**ock
K_F	Freundlich isotherm constant (mg/g) $(dm^3/g)^n$ related to adsorption capacity
K^T	Toth isotherm constant (mg/g)
MD	**M**olecular **d**ynamics
MM	**M**ixed **m**odel compound
MoM	**Mo**lecular **m**echanics
n	Adsorption intensity
OA	**O**leic **a**cid
PDA	**P**hotometric **d**ispersion **a**nalyser
PEG	Methoxy**p**oly**e**thylene**g**lycol

PEI	**P**oly**e**thylene**i**mine
PEO	**P**oly**e**thylene**o**xide
PHF	**P**ost-**H**artree-**F**ock
QCM-D	**Q**uartz **c**rystal **m**icrobalance with **d**issipation
q_e	Amount of adsorbate in the adsorbent at equilibrium (mg/g)
$q_{e,\ calc}$	Amount of adsorbate in the adsorbent at equilibrium calculated from model (mg/g)
q_S	Theoretical isotherm saturation capacity (mg/g)
Q_0	Maximum monolayer coverage capacities (mg/g)
R	Universal gas constant (8.314 J/mol K)
RA	**R**esin **a**cids
SCF	**S**elf-**c**onsistent **f**ield
SE	Stabilising energy
SeE	**Se**mi-**e**mpirical methods
SPR	**S**urface **p**lasmon **r**esonance
STO	**S**later **t**ype **o**rbitals
t	Toth isotherm constant
T	**T**emperature (K or °C)
TG	**T**ri**g**lycerides
TMP	**T**hermo**m**echanical **p**ulp
TrO	**T**ri**o**lein
UAHF	**U**nited **A**tom **T**opological **M**odel
VDW	**v**an **D**er **W**aals
WE	**W**ood **e**xtractives
ΔG	Gibbs' free energy
ΔH	Enthalpy change
ΔS	Entropy change
ξ	total electronic energy values

Chapter 1 General Introduction

The Norske Skog-owned Albury and Boyer paper mills have been serving as major newsprint and related grade paper providers to the whole of Australia since 1981 and 1941, respectively.[1] However, since the start of its operation, the Albury mill has experienced fouling problems in the papermaking process. Similar problems have also been observed in the Boyer mill, though with slight differences in deposit properties due to different materials (pulps) used for papermaking.[2] Fouling is often referred to as the deposition of sticky material known as "pitch" onto paper or machine surfaces.

In recent years, both mills have made changes to their operation to conform to strict environmental guidelines and expectations such as recycling water in the plant (towards a closed-loop system) to cut down freshwater usage[3] and the use of 100 % softwood *Pinus radiata* pulp in the papermaking process (in Boyer mill only).[4, 5] These changes have caused the accumulation of wood extractives in the process water, which leads to the formation of larger agglomerates or 'pitch'. This, in turn, leads to their deposition onto surfaces of machinery that comes into contact with the process water during the paper making process.[6] A commonly used method to reduce accumulation of wood extractives has been to actively adsorb the extractives onto the paper using organic polymers or polymers mixed with minerals, without compromising paper strength.[6] However, this merely transfers the problem to the production and printing machinery contributing to desorption of extractives, consist mainly of resin acids, from the paper onto surfaces of high-pressure rollers, and even onto chromium surfaces of printing presses that are employed well-beyond the production stage (Richardson D, pers. comm.) (Figure 1).

Figure 1 Thin layer deposits (consist mainly of resin acids) found on printing rolls and paper machine surfaces, where paper comes to contact with.

Without a good understanding of how the deposit material transfers from paper surfaces onto printing machine surfaces it is difficult for the paper mill to pre-empt and minimise the occurrence of deposition problems. Hence, it is with great interest and urgency that the mechanism of deposition of pitch-related components from the paper surface onto machine surfaces is studied and understood.

Extensive studies have already been undertaken to gain a relatively good understanding of the nature and physio-chemical properties of pitch, and the development of a 'cure' for the problem.[3, 7-18] To do this, it is critical to understand the different components that contribute to the deposition problem experienced in the mill as well as in the printing press, and to incorporate the results of years of research to help solve the problem faced today.

1.1 Wood extractives

Pinus radiata thermomechanical pulp (TMP) used in the papermaking process in Australia, contains 2-4 % of wood extractives.[19] Wood extractives are lipophilic compounds – fatty acids, resin acids, triglycerides, sterols and steryl esters, which are released from the pulp material into the process water during the pulping process.[2, 13, 15, 17, 19] These compounds usually form stabilised colloidal particles in suspension, either electrostatically[14, 17] or sterically[2, 14] stabilised. Alternatively, the wood extractives can be attached to other particles, such as fines or fibres, due to their low solubility in water.[13]

Higher amounts of resin acids, located predominantly in the wood canals,[20] are found in pine wood (e.g. *Pinus radiata*) than in spruce wood[21], commonly used in northern hemisphere paper mills. This leads to the speculation that a higher resin acids concentration lead to greater pitch deposition problems.[19] Commonly found resin acids (Figure 2) are terpenoids with tricyclic carbon ring systems[20] and these can be divided into two main groups:[17, 22]

Pimarane-type – compounds have methyl and vinyl group at the C-13 position;

Abietane-type – compounds have isopropyl or isoprenyl group at the C-13 position.

Other than these common resin acids, neutral diterpenoids (and diterpenes) can also be found in minor quantities (Figure 3).

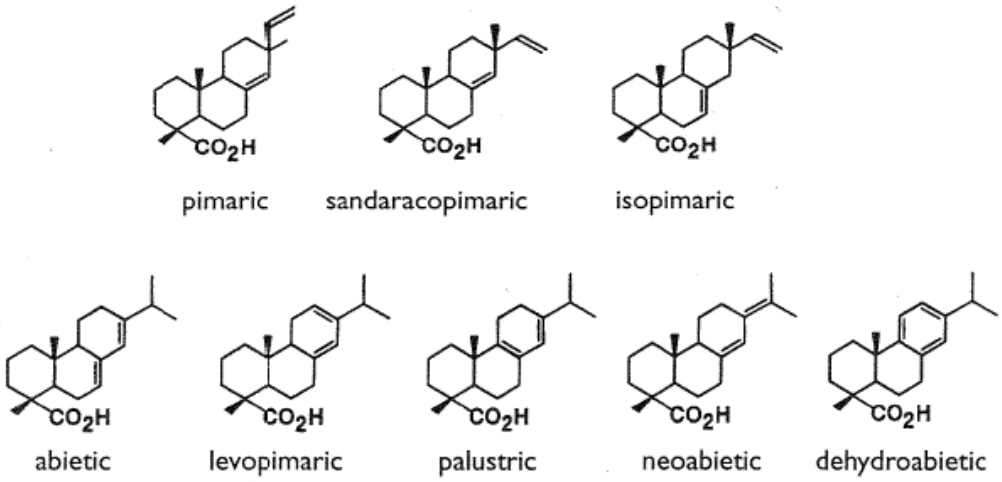

Figure 2 Structures of common resin acids.[20]

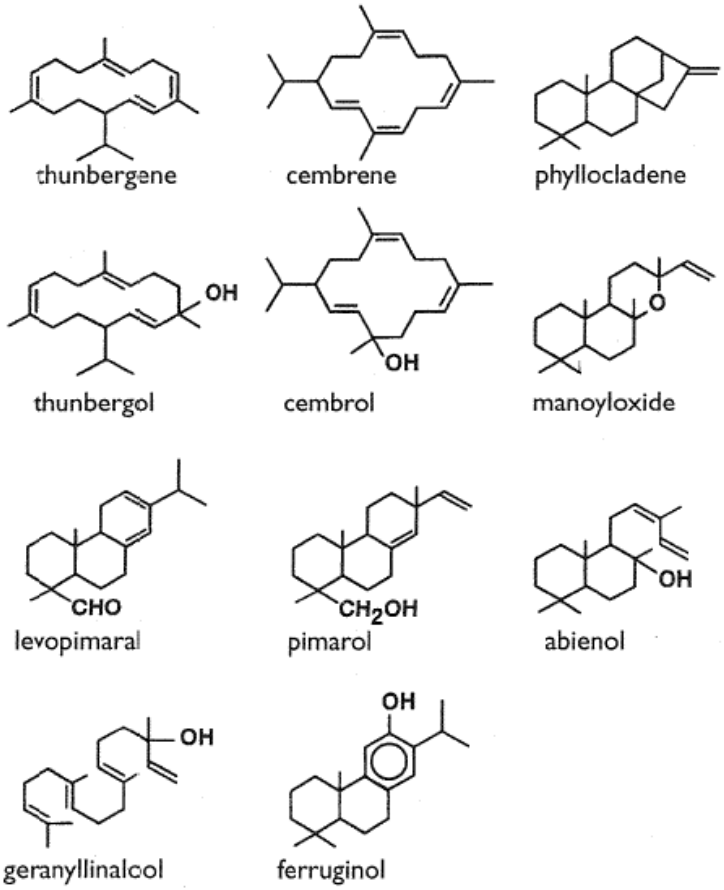

Figure 3 Examples of diterpenes and neutral diterpenoids.[20, 23]

On the other hand, extractives such as fatty acids, triglycerides and fatty acid esters (sterols) are predominantly located in parenchyma cells.[24] Saturated straight-chain and unsaturated fatty acids comprising of 16-24 carbon atoms are commonly found in plants. However, mono- (oleic), di- (linoleic), and tri-unsaturated (linolenic) fatty acids with 18-C dominate in the mixture of fatty acids in softwood species (Figure 4).[17, 22] Stereochemistry differences of unsaturated fatty acids (as compared to

saturated fatty acids) influence their physio-chemical properties such as water solubility, adhesion abilities and pK_a values.[17]

Triglycerides are hydrophobic and have low solubility in water.[17] In solution, triolein (an example of triglycerides) exists in a cyclic form, which is its lowest energy conformer (Figure 5).[25] Sterols are compounds containing tetracyclic carbon skeleton; sitosterol being the most common sterol compound (Figure 6).[22] These compounds also exist in minor amounts in wood extractives.[22]

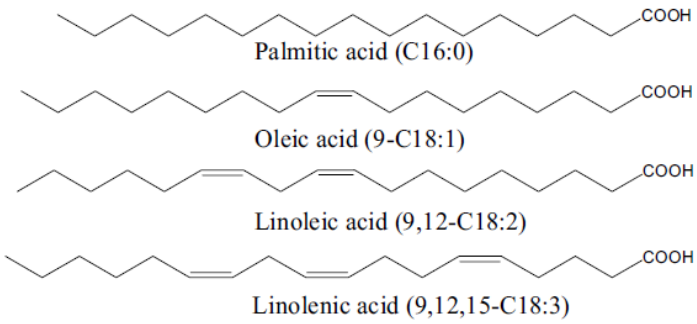

Figure 4 Structures of some common fatty acids.[26]

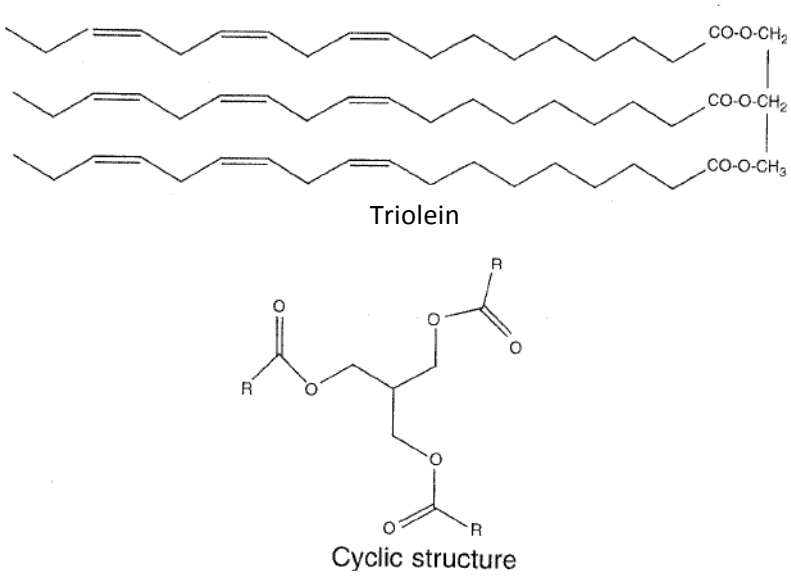

Figure 5 An example of a triglyceride (Triolein): (top) Structure commonly depicted; (bottom) structure adopting lowest energy conformation. R (in cyclic structure) represents the straight chains with straight backbone in triolein.[25]

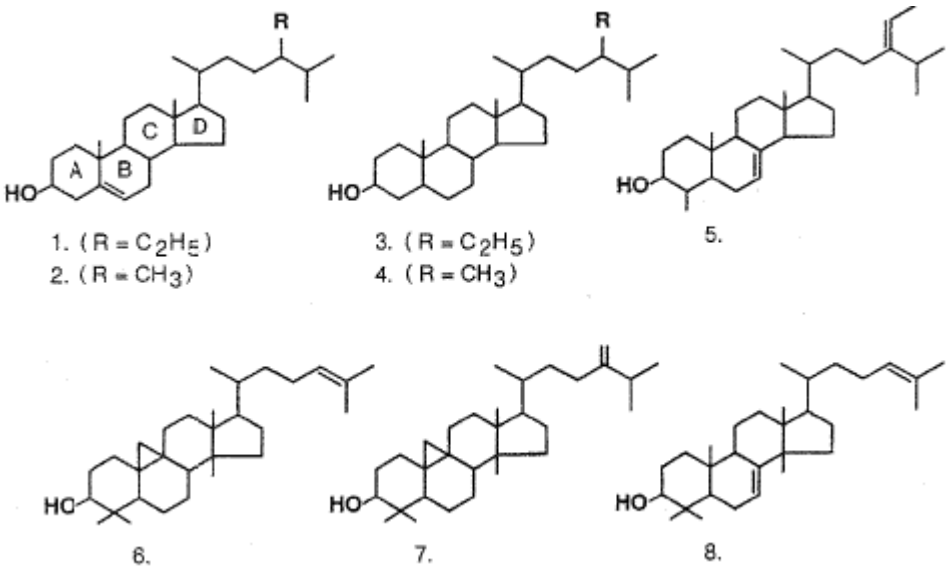

Figure 6 Structures of some common sterols: 1. Sitosterol, 2. Campesterol, 3.sitostanol, 4. Campestanol, 5. Citrostadienol, 6. Cycloartenol, 7. 2,4-methylenecycloartanol, 8. Butyrospermol.[20]

All of these groups of compounds are commonly found in paper or as deposits on machine surfaces in the paper manufacture and printing industries.[16, 26] Along with wood extractives other hydrophilic materials such as lignans, sugars and carbohydrates are also dissolved in the aqueous environment. However, these components are not found in the deposits but are factors that affect the extent of deposition.[7, 8, 16]

1.1.1 Wood pitch

Wood pitch describes wood extractives that are deposited onto surfaces such as paper or machine surfaces, commonly caused by the destabilisation of wood extractive colloids in process water. The term 'wood extractives' is quite often used interchangeably with 'wood resins', and generally has the same meaning. There are many factors that cause destabilisation of wood extractive colloids which leads to deposition problems.

Due to low solubility of wood extractive components especially at low pH, wood extractives exist as stabilised colloids in solution.[19] Wood extractive colloids were traditionally believed to adopt a two-layered droplet structure.[16] However a more recent study showed that these colloids may actually exist as a three-layered model.[27] In the two-layered model, triglycerides and steryl esters are the most hydrophobic; hence occupy the core of the two-layered structure. Resin acids and fatty acids form the outer layer with hydroxyl and carboxyl groups extending outwards into the water.[15] However, in the three-layered model, the resin acids occupy the outermost shell and the fatty acids exist as a mobile

layer between the core and the outer layer while triglycerides still occupy the core of the structure.[27] It is believed that the composition of colloidal wood extractive particles' surface plays an important role in determining wood extractive properties such as chemical reactivity, charge, colloidal stability and pitch deposition tendency.[15]

1.1.2 Factors affecting deposition of wood extractives

Extensive research carried out over the past decades, to understand the wood pitch deposition problem, has identified some factors that contributed to the deposition of wood extractives.[7-10, 12, 14-18, 22, 24, 28]

Composition of colloidal wood extractives

Resin acids are believed to be the main cause of deposition problems when using *Pinus radiata* pulp, although other components such as fatty acids and triglycerides also play important roles. Destabilisation of colloids, due to changes to solution conditions or process conditions, causes these to be deposited-onto surfaces.[19] Changes to wood extractive make-up in pulp due to seasonal or age difference of the trees will also contribute to the changes in stabilisation of colloidal wood extractives.[10] Stack and Stevens observed that composition of the wood extractive components affects the deposition tendency of the particles.[11] Correlation between resin acid levels and deposition has shown that increasing resin acid concentration will lead to increased deposition. However, complex interactions occurring between different components in the wood extractives also affects the properties of the colloidal particle, which in turn affects deposition affinity.[11]

In another study, Stack et al. showed that wood extractive components have an influence on the viscosity of the mixture, thus affecting deposition affinity. In their study, it was shown that increasing the concentration of fatty acids resulted in an increased in deposition of resin acids. This is because resin acids are highly viscous compared to fatty acids or triglycerides.[10]

In another study, Vercoe et al. hypothesised that the solubility of wood extractive components (fatty acids and resin acids) affects the deposition of pitch. Fatty acid saturation and chain length are used to explain the solubility of fatty acids, whereas the type of interactions between the resin acids was explained using deposition and molecular modelling studies.[26] In this study they not only showed that fatty acid solubility decreases with increasing chain length, they also demonstrated that less deposition occurred when fatty acids interacted with aromatic resin acids than when fatty acids interacted with non-aromatic resin acids. Most importantly they concluded that it was the interaction between the resin acids that affected the type of hydrogen bonding and stability between components in solution, affecting deposition.[26] For example, through molecular modelling studies, they showed that the aromatic resin

acids hydrogen bond to the carboxylic acid group of fatty acids through the electron rich aromatic ring of dehydroabietic acid; whereas non-aromatic resin acids form dimers with fatty acids through the hydrogen bonding of the carboxylic acid groups present in both molecules. The stabilisation energy of each complex formed was found to correlate with the likelihood of pitch deposition as increased stabilisation energy was found to correlate with increased deposition due to increased degree of unsaturation and decreased chain lengths of fatty acids.[26]

As properties such as viscosity, tackiness, wettability and surface energy differ for individual types of wood extractive components, Qin et al. attempted to identify possible relationships between wood extractive composition and deposition tendency by studying these properties of wood extractive components.[15] The authors concluded that viscosity was not only affected by wood extractives composition but also by temperature. Meanwhile, tackiness was found to be completely dependent on the wood extractive composition, where mixtures with resin acids had the greatest tackiness. From this study, the surface energy measured for resin components confirmed that colloidal resin particles form two-layered structures.[15] Similar to work done by Kallio et al.,[18] contact angle measurements were employed to understand the wettability of wood extractive components on different surfaces and their influences on pitch deposition. There, however, is no simple conclusion as to how deposition can be controlled because of vast differences in viscosity, tackiness, and wettability of different wood extractive components.[15]

Process conditions

(i) Electrolyte/salt type and concentration

Electrostatic stabilisation of colloids increases with the increasing amounts of fatty acids (or to some extent resin acids as well). This is due to the repulsive forces from increased negative surface charge of the colloids from carboxyl and hydroxyl groups on the outer layer of the colloid particle.[16] However, destabilisation of colloidal resin particles can also be easily achieved by the addition of electrolytes/salts such as Ca^{2+}.[13]

An increase in electrolyte/salt concentration will cause deposition of wood extractives to increase. This is because the added electrolytes, such as Ca^{2+} ions, will break an established stable equilibrium. Qin et al. showed about 40 % of total wood extractives deposited after the addition of 10 mmol/L $CaCl_2$; at 40 mmol/L $CaCl_2$ electrolyte concentration, almost 100 % of wood extractive colloids were deposited.[16] Richardson et al. reported an increase in deposition of wood extractives when Ca^{2+} concentration increased, which was most likely due to the formation of insoluble salts of resin acids or fatty acids.[9]

MacNeil et al. also observed that at high Ca^{2+} concentration, the solubility of resin acids and fatty acids was low.[28]

(ii) pH

In the study by MacNeil et al., at high pH (in the presence of high Ca^{2+} concentration) the solubility of resin acids was found to increase while the fatty acids remained reasonably insoluble.[28] Interestingly, results from the study also showed that not all resin acids (with the exception of dehydroabietic acid) and fatty acids reached 100 % solubility. They suggested that this might be due to changes in colloidal wood extractive composition when there was change in pH.[28] As the pH increases, the more water-soluble components in the colloidal wood extractives are drawn out by the hydroxide ions (OH^-) before the less water-soluble components. With decreased amounts of fatty and resin acids in the colloidal particles, these particles tend to agglomerate due to insufficient electrostatic stabilisation. Hence, there are less lipophilic wood extractives remaining to be released from the colloidal particles into the water phase.[28]

A similar observation was made by Richardson et al. on the change in wood extractive colloid composition when there was an increase in pH. Solubility of resin acids increased with increasing of pH. This was due to the ionisation of resin acids in the lipophilic phase that led to the formation of insoluble calcium soaps of resin acids. The resultant colloidal wood extractives become more viscous, leading to decreased flow-off rate and more deposition.[9] Likewise, Sundberg et al. also concluded that solubility of resin acids and fatty acids increase with increasing pH, even though resin acids have been shown to dissolve at a lower pH than fatty acids.[17]

Qin et al. carried out a comprehensive investigation comparing deposition tendency of different model wood extractives at pH 5 and pH 8. This investigation showed that the deposition tendency of wood extractive models with higher amounts of fatty acids and resin acids exhibited increased stability with increasing pH. Likewise, wood extractive models with more triglycerides (less fatty and resin acids) have better stability at the lower pH. The authors believed that at higher pH, the acids are dissociated and act as stabilising agents for the colloidal particles.[16]

In another deposition study at two different pHs (5.5 and 7.0), McLean et al. show that solubility and extent of dissociation of wood extractive components are both affected by pH changes. The authors also showed that a change in pH altered the interaction between wood extractive components that affect their deposition tendency. For example, at pH 5.5 (50°C), resin acids are responsible for pitch deposition; but at pH 7.0 (50°C), interactions occur, mainly between triglycerides and resin acids, that

cause deposition. The authors believed that this interaction was due to the increased ion-dipole interaction between the dissociated and un-dissociated carboxylic acid groups of the resin components.[12]

In their report to Norske-Skog Paper Mill, Stack and Stevens also studied the effects of pH on deposition of colloidal wood extractives.[11] pH is believed to affect the solubility of the colloidal wood extractives. Increased deposition has been observed from pH 4 to pH 6 with maximum deposition occurring around pH 5-6. At pHs greater than 6, deposition decreases as resin acids have increasing solubility due to dissociation of the carboxyl groups.[11]

(iii) Temperature

Stack and Stevens reported that deposition of pitch increases markedly when temperature (of process water) drops below a critical point (in laboratory experiments).[11] The study by Qin et al. noted otherwise, where they observed an increased in deposition at high temperature, which might be due to decreased viscosity that enhanced coagulation.[16]

In another study, McLean et al. showed that temperature changes the interactions between wood extractive components and thus affects deposition.[12] Interestingly, at pH 5.5 (20°C), interactions exist between resin acids and fatty acids at low triglyceride concentration, and between fatty acids and triglycerides at high triglyceride concentration, that contribute to deposition. However, at 50°C, deposition of pitch involved resin acids alone. The authors concluded that changes in temperature have a greater effect on the physical properties of wood extractive components such as viscosity, than chemical properties, such as solubility. However, it can still be used to explain the increase in solubility of wood extractive components that led to increased deposition of pitch.[12] According to Dreisbach and Michalopoulos, the temperature dependant viscosity of colloidal wood extractives will only cause deposition problems onto a surface within a narrow temperature range.[3]

(iv) Presence of fibre/fines

The study by Qin et al. also observed that reduced viscosity of resin acids in the presence of fibres boosted the deposition tendency of pitch particles.[16]

Mosbye analysed in detail the chemical composition of fines and their effect on model colloidal wood extractive adsorption and removal from solution.[13] The author also briefly summarised the factors that affect the adsorption of colloidal wood extractive onto fines, such as pH, temperature, electrolytes and dissolved substances.[13]

According to Mosbye et al., adsorption of colloidal wood extractives onto fines (for example, flake-like and fibrillar-like fines), generated during the production of mechanical pulp, can have negative effects on papers made from these pulp materials.[14, 29] In a particular study, they discovered that colloidal wood extractives adsorbed more onto flake-like fines than fibrillar-like fines.[14] They, then, went on to study the use of uncharged polyethyleneoxide (PEO) to remove these colloidal wood extractives in the presence of these fines.[29] However, they found that the efficiency of PEO to adsorb colloidal wood extractives was dependent on the presence of dissolved substances such as carbohydrates. This is because carbohydrates sterically stabilised colloidal particles through surface adsorption, preventing further surface adsorption.[14, 29]

(v) Dissolved substances (DS)

Aside from electrostatic stabilisation, colloidal wood extractives can also be sterically stabilised.[7] The amount and composition of dissolved substances will affect the behaviour of colloidal wood extractives. Sundberg noted that dissolved polysaccharides, mainly galactoglucomannans, have affinity to the surface of colloidal wood extractives thus sterically stabilising the particles, even at high electrolyte concentration.[8] On the other hand, this author also observed that dissolved pectins enhanced the aggregation of colloidal wood extractives after the pectins were precipitated with electrolytes (such as calcium ions).[8]

(vi) Others

Other than the above-mentioned changes, removal of wood extractives by adsorption has been shown to reduce the occurrence of pitch deposition. Materials such as polyethyleneoxide (PEO),[29] bentonite[19] and talc, are used to remove wood extractive components by adsorption. For example, the adsorption of wood extractives onto added bentonite was shown to decrease the deposition of pitch by decreasing the amounts of wood extractives that can be solubilised.[19]

Kallio and Kekkonen concluded that the adsorption of colloidal particles onto surfaces depends on the charge of substances in the process water as well as the absorbent surface. They suggested the use of DLVO theory to explain the adsorption of particles in moderate salt concentration. They also observed that areas with strong hydrodynamic and mechanical forces encourage adhesion of deposits onto surfaces, thus causing serious deposition problems.[30] The authors suggested changing the surface properties of the paper machines to reduce the tendency of colloidal particles to be adsorbed. For example, to take advantage of the use of hydrophilic surfaces because colloidal particles adhere poorly to hydrophilic surfaces. However, these changes are subject to its location on the paper machine and

the processes involved, so it was important to avoid unnecessary changes that might worsen the deposition problems.[30]

In another study[18], Kallio et al. studied the properties of wood extractives such as work of adhesion, contact angle, surface tension and spreading kinetics, to understand deposition/adsorption of lipophilic extractives onto surfaces. Surfaces studied include wood components, polymer used for pitch control, and paper machine surfaces. The authors concluded that wood extractive components tend to adhere to hydrophobic surfaces and/or those rich in lignin. Adhesion of wood extractives to hydrophilic surfaces such as steel, or wood components rich with cellulose and carbohydrates is low, especially under aqueous conditions. This is due to low contact angle of wood extractives with surfaces as well as weak interaction between surface and wood extractive components. The authors also noted that increase in surface roughness caused an increase in wood extractive adhesion as it impeded on water flow along the surface and allowed longer contact of wood extractive components with surfaces.[18]

A variety of techniques have been used to study the coagulation and aggregation behaviour of colloidal pitch particles in solution in order to gain understanding on how deposition of colloidal pitch particles occurs. These include photometric dispersion analyser (PDA),[31-33] impinging jet microscopy,[34, 35] surface plasmon resonance (SPR),[36] flow cytometry[37-39] and laser diffraction[37, 40].

1.2 Aim of thesis

The general aim of the thesis is to assess the interactions between wood extractives, or its components, and model surfaces that lead to segregation of wood extractive components and the transfer of these components from one surface to another. It will also investigate the physical and chemical factors that affect these interactions.

1.3 Approach of thesis

This thesis is structured as follows. This chapter – the General Introduction – gives the background to the nature of wood extractives and the chemical and physical properties that affect their behaviour.

Chapter 2 to Chapter 5 each covers the use of an experimental technique to study and understand the surface interactions of wood extractive colloids and different model surfaces. In each chapter, there will be a brief yet more specific introduction of the background to the technique used. In Chapter 2, the

deposition of wood extractives and model compounds are studied with gas chromatography (GC) and modelled with adsorption isotherms. Chapter 3 presents the use of quartz crystal microbalance with dissipation (QCM-D) to study the deposition tendency at a smaller scale than gas chromatography and without loss to surrounding surfaces that contact the colloids. Chapter 4 describes the use of atomic force microscopy (AFM) to study the interaction of colloids with model surfaces at the nano-scale level. Lastly, Chapter 5 gives details of the use of computational chemistry to model and compare the results with that of experimental chapters. The General Conclusion will combine the outcomes of each chapter of the thesis and draw any relevant conclusions.

Chapter 2 Deposition Experiments/Adsorption Isotherms

2.1 Introduction

As mentioned in the general introduction, wood extractives (WE) found in the process water during the papermaking process can deposit on paper and papermaking machine surfaces. This phenomenon, known as pitch deposition, has increasingly become a problem for the papermaking industry.

Wood extractives from *Pinus radiata* can be represented by a mix of three major components - fatty acids, resin acids and triglycerides. A model compound was chosen to represent each of these major components in the work reported in this chapter: oleic acid (OA) was chosen to represent fatty acids, abietic acid (AA) to represent resin acids and triolein (TrO) is used to represent triglycerides. OA and AA have very distinct hydrophilic and hydrophobic regions within the molecules, whereas TrO is effectively hydrophobic, with no particular polarity (Figure 7). In solution, the preferred orientation and structure of the resultant colloids at the interfaces/surfaces are determined by the nature of the interface/surface. According to Woods,[41] these model compounds either adsorb as a monolayer or hemimicelle aggregates on hydrophobic surfaces, whereas they adsorb as bilayers or admicelles on hydrophilic surfaces.[42, 43]

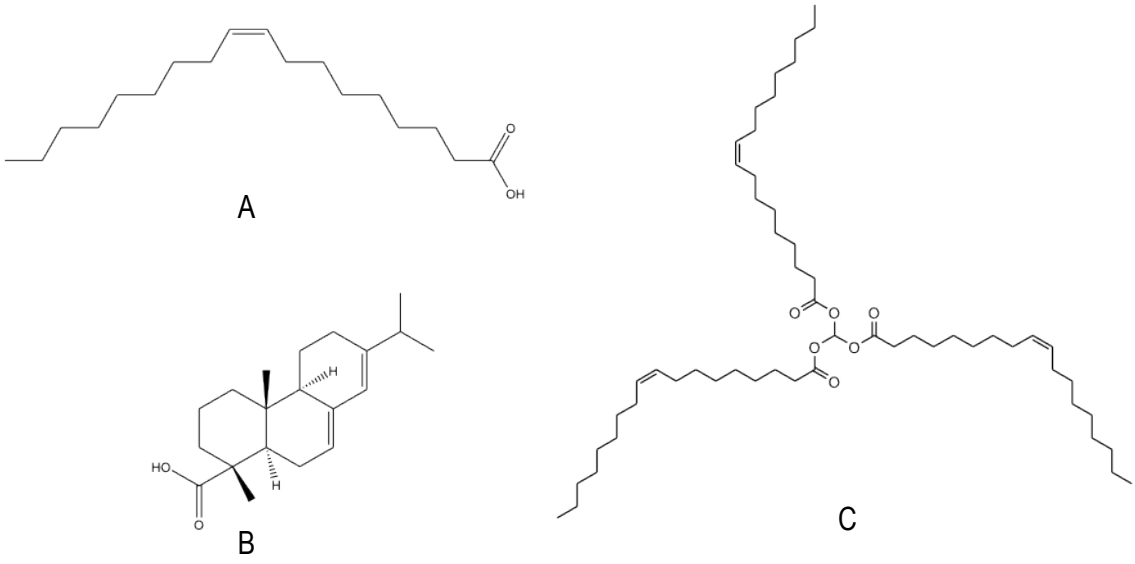

Figure 7 Chemical structures of model compounds representing each component in wood extractives. (A) Oleic acid (OA), representing fatty acids; (B) Abietic acid (AA), representing resin acids; (C) Triolein (TrO), representing triglycerides.

2.1.1 Adsorption Isotherms

"Adsorption" is the attachment of solute(s) from the bulk fluid phase onto a surface. "Adsorbate" refers to the solute participating in the adsorption process and "adsorbent" refers to the surface on which the solute attaches.[44] Adsorption isotherms describe the equilibrium of the adsorbed material at the surface (at a constant temperature);[45] they also provide information about the surface properties and affinity of the adsorbent as well as comparing the adsorptive capacities of the adsorbent.[46] Different adsorption isotherms are applied depending on whether it is monolayer or multilayer adsorption.

A wide variety of equilibrium isotherm models have been formulated over the years. A few examples of isotherm models are Langmuir, Freundlich, Temkin, Toth, and Brunauer-Emmett-Teller (BET).[47] Table 1 shows the mathematical expressions for these isotherm models.

The Langmuir adsorption describes ideal monolayer adsorption. Though it has been applied mainly to gas phase adsorption, it has also been applied in the same way to aqueous solutions.[46, 48] Graphically, the Langmuir plot reaches an equilibrium saturation point where no further adsorption takes place.

The Langmuir isotherm is derived from the assumptions that:[47]

i) the surface of the adsorbent is a two-dimensional array of energetically homogeneous sites;

ii) only monolayer coverage occurs;

iii) only one molecule (solvent or solute) is adsorbed on any one site;

iv) no interactions exist between the adsorbed molecules;

v) the bulk phase is an ideal dilute solution.

Any deviation from Langmuir adsorption is considered cooperative (multilayer) adsorption, where the adsorbed molecules have an effect on the adsorption of "new" adsorbate molecules.[44] Cooperativity is common for adsorption.

The Freundlich isotherm describes non-ideal and reversible adsorption and is not restricted to the formation of a monolayer. This isotherm does not adhere to any of the assumptions of the Langmuir isotherm, which means it can be applied to multilayer adsorption with non-uniform distribution of heat of adsorption and adsorption affinities over a heterogeneous surface. The slope of a Freundlich isotherm

mostly ranges from 0 and 1 and is a measure of adsorption intensity or surface heterogeneity.[47] The closer the value approaches zero, the more heterogeneous the surface. A value below unity implies normal adsorption (physisorption or chemisorption), where a value of $\frac{1}{n}$ above one is indicative of cooperative adsorption. A limitation of the Freundlich isotherm is that it lacks a fundamental thermodynamic basis, by not approaching Henry's Law at vanishing concentrations.[47]

The Temkin isotherm takes into account indirect adsorbate-adsorbate interactions and assumes that the heat of adsorption of all molecules decreases linearly with the increase in coverage of the adsorbent surface.[47, 49] This model is not an appropriate representation for complex liquid-phase adsorption but excellent in predicting gas phase equilibrium.[47]

The Toth isotherm was originally proposed for monolayer adsorption. It is an empirical model developed to yield an improved fit to the Langmuir isotherm and is useful in heterogeneous adsorption systems.[47, 50]

The BET isotherm is commonly used to explain physical adsorption of gas molecules on solid surfaces.[47] It is a theoretical equation and the simplest type that accounts for multilayer adsorption.[51, 52] However, it can also be used to model adsorption in aqueous settings by replacing the 'pressure' terms in the BET isotherm equation with 'concentration' terms. The BDDT (Brunauer, Deming, Denting Teller) classification describes five isotherm shapes that arise from multilayer adsorption (Figure 8).[53, 54] Type I is usually limited to adsorption of only a few molecular layers, and occurs mostly in micropores. The Type II isotherm occurs on nonporous powders; the inflection points correspond to complete coverage of the surface by the first layer, followed by multilayer adsorption of infinite layers. The Type III isotherm occurs when adsorbate-adsorbed layer interaction is greater than adsorbate-adsorbent surface interaction. Type IV and V isotherms are similar to Type II and III isotherms, except with the presence of pores with pore size ranges from 15 – 1000 Å.[54]

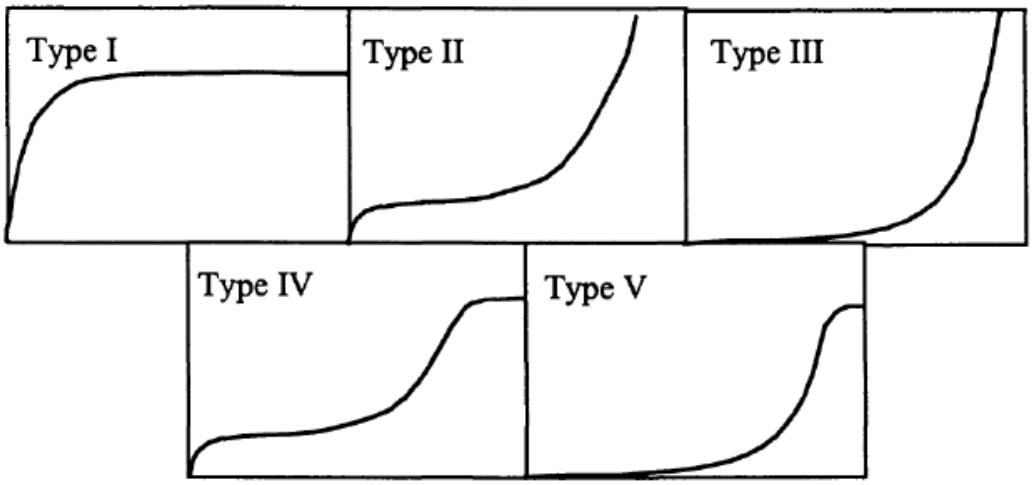

Figure 8 The BDDT classification of five isotherm shapes.[53]

There are four assumptions made by BET theory:[55, 56]

i. A single molecule can only act as a single adsorption site;

ii. Enthalpy of adsorption is the same for any layer;

iii. Energy of adsorption is the same for every layer other than the first;

iv. A new layer can start before another is finished.

Table 1 List of adsorption isotherm models.[47]

Isotherm	Non-linear form	Linear form
Langmuir	$q_e = \frac{Q_0 b C_e}{1 + bC_e}$	$\frac{C_e}{q_e} = \frac{1}{bQ_0} + \frac{C_e}{Q_0}$
Freundlich	$q_e = K_F C_e^{\frac{1}{n}}$	$logq_e = logK_F + \frac{1}{n} logC_e$
Temkin	$q_e = \frac{RT}{b_T} lnA_T C_e$	$q_e = \frac{RT}{b_T} \ln A_T + \left(\frac{RT}{b_T}\right) lnC_e$
Toth	$q_e = \frac{K_T C_e}{(a + C)^{\frac{1}{t}}}$	$\ln\left(\frac{q_e}{K_T}\right) = lnC_e - \frac{1}{t}\ln\left(a_T + C_e\right)$
BET	$q_e = \frac{q_s C_{BET} C_e}{(C_s - C_e)\left[1 + (C_{BET} - 1)(\frac{C_e}{C_s})\right]}$	$\frac{C_e}{q_e(C_s - C_e)} = \frac{1}{q_e C_{BET}} + \frac{(C_{BET} - 1)}{q_e C_{BET}} \frac{C_e}{C_s}$

2.1.2 Aim(s)

This chapter compares the deposition affinity of wood extractives and the major classes of compounds within the wood extractives onto pulp fibres (PF) and microcrystalline cellulose (MCC).

The aims of the study reported in this chapter were:

1. To establish adsorption isotherms for each model compound colloidal system and the wood extractive colloidal system onto pulp fibres and microcrystalline cellulose.
2. To investigate the effect of pH perturbation (increasing and decreasing the pH) on the deposition behaviour of the colloids onto pulp fibres.

2.2 Method and Materials

2.2.1 Preparation of model compound colloidal suspension

The model compounds used to represent individual components found in wood extractive are oleic acid (fatty acid, 90 % Aldrich), abietic acid (resin acid, 75 % Fluka Analytical), and triolein (triglyceride, 65 % Sigma). A range of concentrations of the individual colloidal suspensions (50 mg L^{-1} to 700 mg L^{-1}) were prepared *in situ*. A fixed mass of each compound was weighed out (to give the required concentration) and dissolved in 3.50 mL of acetone (AR grade, Chem-supply). For experiments with pulp fibre slurry, 54.0 mL of 1 mM KNO_3 (aq) was added to a flask and stirred at 400 rpm, before 1.00 mL of model compounds in acetone was added, with force, using an autopipette. For experiments with microcrystalline cellulose slurry, 94.0 mL of 1 mM KNO_3 (aq) was added to a flask and stirred at 400 rpm, before 1.00 mL of model compounds in acetone was added, with force, using an autopipette. In both cases, the colloidal suspensions were stirred for 15 min to allow for stabilisation before pulp fibre slurry or microcrystalline cellulose mixture was added to the flasks.

2.2.2 Preparation of wood extractive colloidal suspension

Thermomechanical pulp (TMP) from the Norske-Skog Boyer mill was freeze-dried then soxhlet extracted for 8 h with hexane. The hexane was removed by rotary evaporation and the resulting wood extractive product was stored at < 10°C until required. Wood extractive colloidal suspensions of a range of concentrations (50 mg L^{-1} to 400 mg L^{-1}) were used in deposition experiments. As stated under 2.2.1, a fixed mass of extracted wood extractives was weighed (to give the required concentration) and

dissolved in 3.00 mL of acetone (AR grade, Chem-supply). For experiments with pulp fibre slurry, 54.0 mL of 1 mM KNO_3 (aq) was added into each flask and stirred at 400 rpm, before 1.00 mL of wood extractives in acetone was added, with force, using an autopipette. For experiments with microcrystalline cellulose mixture, 94.0 mL of 1 mM KNO_3 (aq) was added into each flask and stirred at 400 rpm, before 1.00 mL of wood extractives in acetone was added, with force, using an autopipette. In both cases, the colloidal suspensions were stirred for 15 min to allow for stabilisation before the pulp fibre slurry or microcrystalline cellulose mixture was added to the flasks.

2.2.3 Preparation of TMP pulp fibre slurry

The TMP pulp, from which the wood extractives had been extracted, was used as an adsorbent representing a cellulose surface and simulating the adsorption occurring in the papermaking process. A pulp slurry of 2.0 % consistency was made by stirring 4.0 g TMP pulp in 196 mL of 1 mM KNO_3 (aq), overnight. This was diluted to a final concentration of 0.5 % pulp consistency by mixing 25.0 g of prepared pulp slurry, 20.0 mL of 1mM KNO_3 (aq) and 55.0 mL of the colloidal suspension before the start of each experiment.

2.2.4 Preparation of microcrystalline cellulose mixture

Microcrystalline cellulose mixture was employed as a further representation of the cellulose surface. In the current chapter this was in the form of an aqueous suspension while in the QCM experiments (Chapter 3) it was in the form of a solid coating. The aqueous suspension was made by mixing 3.5 g microcrystalline cellulose (Serva-Avicel PH 105, ca. 0.019 mm) with 35.0 mL of 1 mM KNO_3 (aq) and stirred overnight. 5.0 mL of microcrystalline cellulose slurry was then added to 95.0 mL colloidal suspension before the start of the experiment to ensure 0.5 % microcrystalline cellulose consistency in each flask.

2.2.5 Adsorption experiment methods

A Radleys parallel 6-carousel reactor fitted with 250 mL wide neck round bottom flasks and 25 mm rare earth elliptical Teflon stirring bars, was used to prepare colloidal suspensions *in situ* and carry out adsorption studies in triplicate. Experiments were conducted at a temperature of 50°C and pH of 5 - 5.5.

For experiments with the pulp slurry and microcrystalline cellulose mixture, colloidal suspensions were prepared as described in 2.2.1 (for model compound suspensions) and 2.2.2 (for wood extractives suspensions). The suspensions were stirred for 15 min to allow for stabilisation before the pulp slurry or microcrystalline cellulose suspension was added to the flask.

For experiments with pH perturbations, after the addition of the pulp slurry or microcrystalline cellulose mixture, the suspension was stirred for about 5 - 10 min before pH perturbations were applied. The pH of the suspension was initially increased to 7 - 8 with KOH (aq). After stirring for about 5 min the pH was returned to 5 with HNO_3 (aq) before the process of deposition commenced.

Sample 'A' was taken before the commencement of the 2 h deposition period at 50°C. Sample 'B' was taken straight from the reaction flask at the end of the 2 h deposition period. At the same time, a larger sample was transferred to a glass centrifuge tube. This sample was centrifuged at 1800 rpm for 10 min to sediment the pulp fibres/microcrystalline cellulose particles. Sample 'C' was then taken from the supernatant of the centrifuged sample. All sample volumes were measured using an auto-pipette and known to at least 3 significant figures.

2.2.6 Extraction method

Samples 'A', 'B' and 'C' were extracted with tertiary-butyl methyl ether (t-BME, HPLC grade, Scharlau) by the following method. An internal standard solution containing heptadecanoic acid (C17, >98 %, Sigma), pentadecanoic acid (C15, 99+ % Aldrich), cholesteryl stearate (CS, 99% Sigma) and glyceryl triheptadecanoate (GTH, ≥99 % Sigma) was prepared in toluene (99.9 % purity, Sigma-Aldrich), at concentrations of approximately 50 µg/ 100 µL each, known accurately. After adjustment of the sample pH with nitric acid to pH <4,100 µL of the internal standard solution was added to each sample, followed by 2 mL of t-BME. The samples were shaken vigorously for 30 sec before being centrifuged at 1800 rpm for 10 min. After centrifugation, the t-BME layer of each sample was transferred, using Pasteur pipettes, into clearly labelled GC vials. The solvent in each GC vial was evaporated to dryness before 1.00 mL of toluene was added.

2.2.7 Analysis by gas chromatography

Each sample was analysed using a Varian CP-3380 gas chromatograph, fitted with a Varian 8100 auto-sampler and flame ionisation detector (FID). A 15 m Zebron capillary GC column, with internal diameter and film thickness of 0.53 mm and 0.15 µm, respectively, was used. An on-column method was employed, at a set pressure flow of 4 psi of a mixture of helium gas (carrier gas) and nitrogen gas (make-up gas) over a period of 50 min using a temperature ramping programme. The injector was set at 100°C for 1.5 min, ramped at 180°C/min to 325°C then held for 11 min. The column oven was set at 100°C for 2 min then ramped at 15°C/min to 320°C and held until the end of the run. The FID was set at 350°C for the entire run.

A spike solution, containing the internal standard solution along with oleic acid (GC standard, Fluka), dehydroabietic acid (99+ %, Helix Biotech) and triolein (65 %, Sigma) in toluene, at concentrations approximately 50 µg/100 µL each, known accurately, was used to determine the response factors for each set of results. All response factors were based on the C17 standard. The internal standards CS and GTH were used to correct the concentrations of fatty acids and triglycerides, and resin acids, respectively. Results were analysed using Varian Star version 6.20 software.

2.3 Results and discussion

2.3.1 Composition of wood extractives

The relative percentage of each class of compounds in the wood extractives was determined by analysing the wood extractive sample using gas chromatography. Table 2 shows the average percentage of each class of compounds in the wood extractive samples obtained at the start of the adsorption experiments. The results show that the ratio of fatty acids to resin acids to triglycerides (FA:RA:TG) is about the same for the wood extractive sample used in adsorption experiments involving pH perturbations as well as those with no pH perturbation, i.e. FA:RA:TG = 1:5:4. This shows that the samples are consistent throughout the experiments thus eliminating this variable from these adsorption results.

Table 2 Relative average composition of fatty acids, resin acids and triglycerides in wood extractive samples.

	With pH perturbations	With no pH perturbation
Fatty acids (FA)	7 %	6 %
Resin acids (RA)	54 %	58 %
Triglycerides (TG)	39 %	35 %

2.3.2 Adsorption experiments

2.3.2.1 Adsorption isotherms

Adsorption isotherms were obtained by plotting equilibrium concentration, C_e (i.e. concentration of the un-adsorbed component that remained in suspension) against the concentration of material adsorbed onto the fibres called the loading concentration, (B-C). Equilibrium concentration, C_e was obtained directly from results of sample 'C' mentioned under 2.2.5; loading concentration, (B-C), was obtained as the difference between the concentrations of samples 'B' and 'C'.

The adsorption experiments carried out on pulp fibres and microcrystalline cellulose yielded a number of representative isotherm profiles. Figure 9 shows a typical isotherm profile, referred to as "T1", which was obtained from the adsorption of wood extractive colloids onto pulp fibres with or without pH perturbations. This isotherm profile is most prevalent and appeared for adsorption of OA and AA onto pulp fibres without pH perturbation and OA and TrO adsorption onto microcrystalline cellulose without pH perturbation. The isotherm profile for the adsorption of AA onto pulp fibres without pH perturbation and WE onto microcrystalline cellulose showed a resemblance to that of Figure 9 however without an inflexion point. Two regions were identified on this isotherm profile and labelled as "ideal" and "non-ideal", as indicated in Figure 9. The "non-ideal" region refers to the region after the point of inflexion on the isotherm profile and occurs when the concentration of wood extractives in solution becomes sufficiently high to saturate the solution. Data points before the point of inflexion on the isotherm profile fall within the "ideal" region. Heier has previously observed this type of isotherm profile in her adsorption experiments onto bentonite and explained that the occurrence of the "non-ideal" region may be due to the formation of larger agglomerates, after the saturation point of the colloidal dispersion, which may have been lost during centrifugation, which may indicate that it is an artefact of the experiment.[57]

Another possible isotherm profile, referred to as "T2", shown in Figure 10, was observed for adsorption of OA and AA onto pulp fibres with pH perturbations as well as AA onto microcrystalline cellulose particles. This profile resembled that of Figure 9, where the point of inflexion turns downwards instead of upwards. The third profile observed (T3) is that of TrO adsorption onto pulp fibres without pH perturbations, where the saturation point was not achieved (Figure 12).

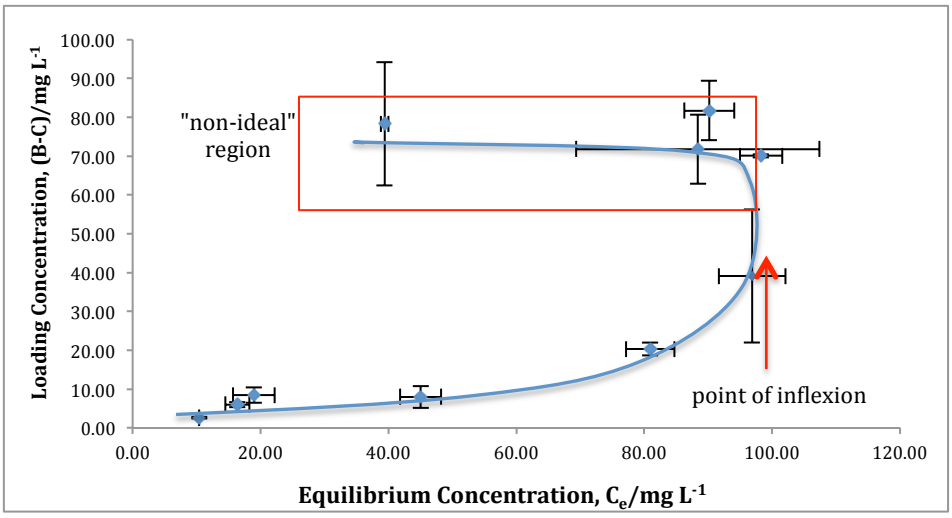

Figure 9 Type 1 (T1) isotherm profile of loading concentration vs equilibrium concentration, C_e of adsorption of wood extractive colloids onto pulp fibre (without pH perturbation). The "non-ideal" concentration region is denoted by the box in the graph, an arrow points to the 'point of inflexion' where any result points prior to this point belongs in the "ideal" region.

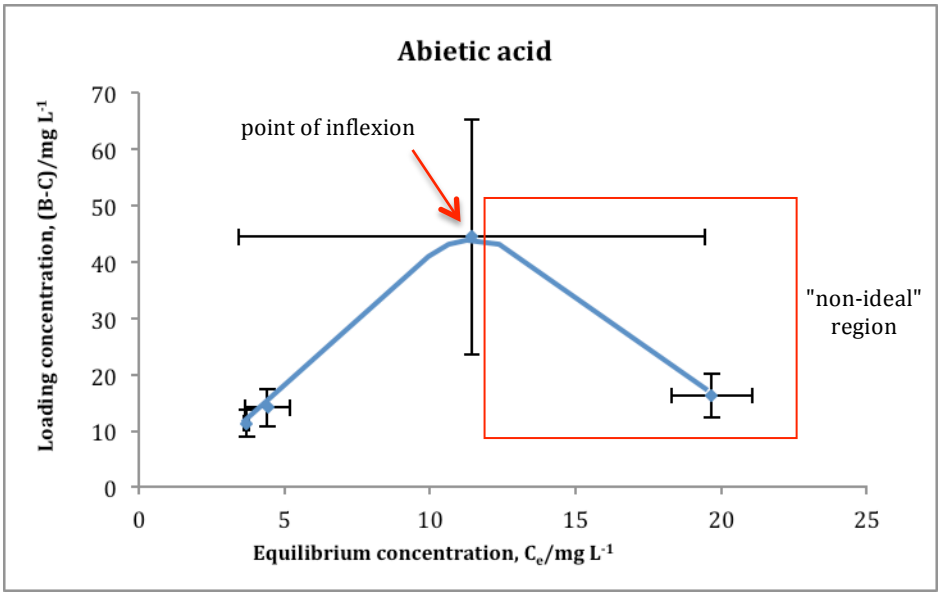

Figure 10 Type 2 (T2) isotherm profile of loading concentration vs equilibrium concentration, C_e of adsorption of abietic acid colloids onto pulp fibres (with pH perturbations). The "non-ideal" concentration region is denoted by the box in the graph, an arrow points to the 'point of inflexion' where any result points prior to this point belongs in the "ideal" region.

2.3.2.2 Modelling of the adsorption isotherms

Three adsorption isotherm models, Langmuir, Freundlich and BET isotherms, were considered to determine which adsorption model was the best fit for the experimental results. The Langmuir adsorption isotherm was still considered even though a cursory glance at the plotted data showed that adsorption did not cease at monolayer coverage. For each colloidal type, a broad range of concentrations was studied for the adsorption isotherms, ensuring that saturation of the solution was

achieved. The modelling constants of adsorption of each colloidal type to pulp fibres or microcrystalline cellulose particles were determined from the linear form equations of the three isotherms and are compared in the following sections.

For modelling the Langmuir isotherm, the linear (isotherm) equation (Equation 1) was used and the Q_0 and *b* (Langmuir isotherm constant) were determined. For the Freundlich isotherm, the linear equation (Equation 2) was used and the $\frac{1}{n}$ and K_F were determined and for BET isotherm calculations the linear isotherm equation (Equation 3) was used. Only the points before the inflexion point (C_s) were used to plot the Langmuir, Freundlich and BET isotherms. R^2 values for each graph were included in the tables to indicate the fit to the curves.

For the Freundlich isotherm, $\frac{1}{n}$ values indicate whether normal adsorption (between the adsorbate and adsorbent which may be either via chemisorption or physisorption) or cooperative adsorption is occurring, as mentioned in the introduction. When $n > 1$, the adsorption process is favourable over the entire range of concentration.[58] In this case, the graph would be approaching a more Langmuir-shaped curve and so at lower concentrations there is a favourable interaction with the surface. However, as the surface sites become filled the amount adsorbed decreases until no further adsorption can occur, effectively as the surface sites are saturated (monolayer adsorption). However, when $n < 1$, the adsorption process is more favourable at high concentration than at lower concentration.[58] In this case there is a lower affinity with the surface and a greater interaction between the adsorbates adsorbed onto the surface than with the surface itself. This indicates greater cooperativity between adsorbates, which leads to multilayer adsorption.[59]

Langmuir	$\frac{1}{q_e} = \frac{1}{bQ_0}\frac{1}{C_e} + \frac{1}{Q_0}$	(Equation 1)
Freundlich	$logq_e = logK_F + \frac{1}{n}logC_e$	(Equation 2)
BET	$\frac{C_e}{q_e(C_s - C_e)} = \frac{1}{q_s C_{BET}} + \frac{(C_{BET}-1)}{q_s C_{BET}}\frac{C_e}{C_s}$	(Equation 3)

The best fit among the isotherm models was assessed by the coefficient of determination (R^2) value and the non-linear Chi-square (χ^2) values.[60] The mathematical equation for calculating the χ^2 values is

$$\chi^2 = \sum \frac{(q_{e,calc} - q_e)^2}{q_{e,calc}} \qquad \text{(Equation 4)}$$

The smaller the total $\Sigma\chi^2$ values, the more accurate the model. By comparing the values in Table 3, the χ^2 varies in the following order BET < Langmuir < Freundlich, with some exceptions. Based on the χ^2 values this indicates that the BET isotherm modelling may be the most accurate model for studying adsorption of these colloid types onto pulp fibres or microcrystalline cellulose particles with some exceptions in cases when BET isotherm could not be fitted.

Table 3 Total chi square (χ^2) calculated for each colloid type from each different adsorption isotherm model, under the different experimental conditions.

Treatment	Colloid type	Total chi square ($\Sigma\chi^2$) calculated for different adsorption isotherm model		
		Langmuir	Freundlich	BET
(A) Pulp without pH perturbation	WE	3.23	28.5	0.63
	OA	-984	2.32×10^6	13.2
	AA	0.82	2.60	0.52
	TrO	2.67	1.61	-
(B) Pulp with pH perturbations	WE	4.29	236	0.02
	OA	5.63	1220	2.33
	AA	5.71	10.2	-
	TrO	27.4	-	-7.40
(C) Microcrystalline cellulose without pH perturbation	WE	18.6	137	1.33×10^{-4}
	OA	4.75	98.3	0.26
	AA	0.21	10.3	-
	TrO	75.8	-	-4.82

2.3.2.3 Adsorption of wood extractives and model compounds onto pulp fibres without pH perturbation

In the case of adsorption of wood extractive (WE) colloids and model compound colloids (OA, AA and TrO) onto pulp fibre, only TrO did not seem to reach any saturation of the colloidal concentration ("non-ideal" region) as shown in Figure 11 and Figure 12. Figure 13 is a representative graph of Freundlich isotherm fit using the "ideal" region of the adsorption results.

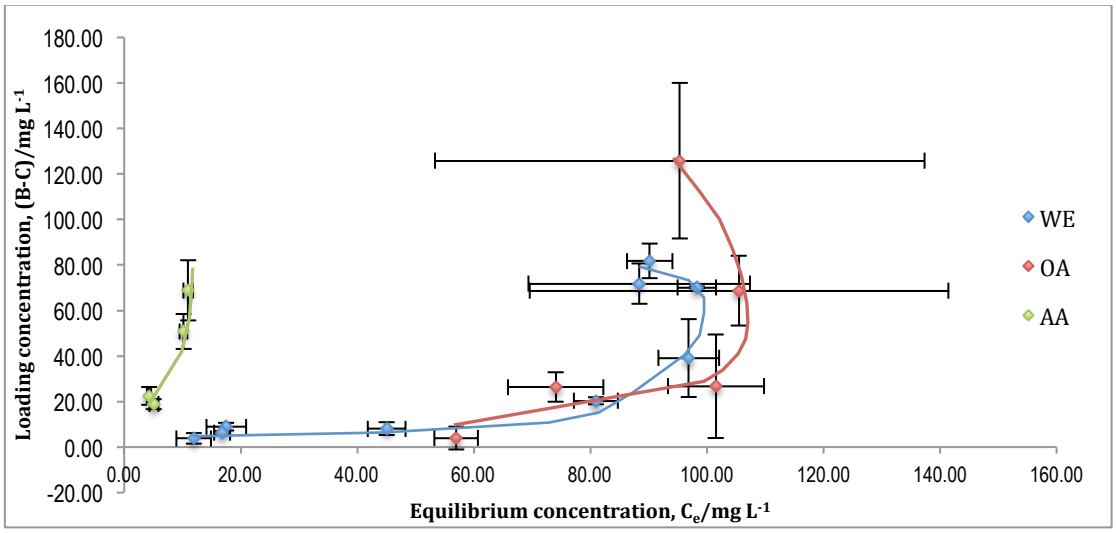

Figure 11 Adsorption curves of wood extractives (WE), oleic acid (OA) and abietic acid (AA) onto pulp fibres without pH perturbation that have "T1" isotherm profiles.

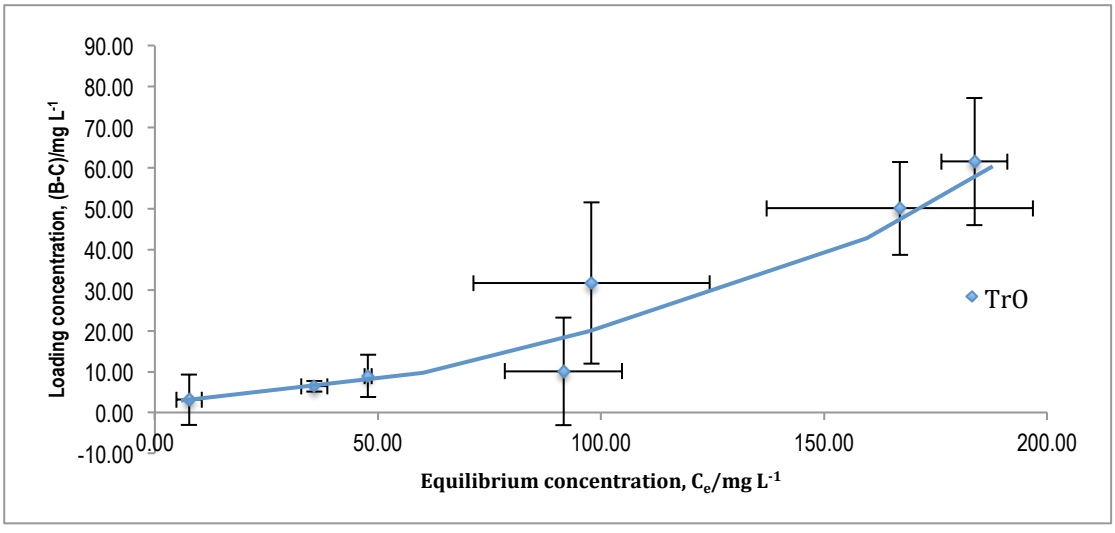

Figure 12 Adsorption isotherm of adsorption of triolein (TrO) onto pulp fibres without pH perturbation that did not show saturation of colloidal suspension (no "non-ideal" region). This isotherm profile is also labelled as Type 3 (T3).

The following Table 4 - Table 6 show the results from modelling these results with Langmuir, Freundlich and BET equations.

Table 4 Langmuir isotherm modelling results - *b*, Q_o, and R^2 values for adsorption of each colloidal type on pulp fibres without pH perturbation.

	Q_0, max. monolayer coverage capacities(mg/g)	*b,* Langmuir isotherm constant	R^2 for Langmuir
WE	10.7	7.39×10^{-3}	0.81
OA	-0.79	-9.49×10^{-3}	0.83
AA	-49.3	-17.0×10^{-3}	0.84
TrO	7.49	1.56×10^{-2}	0.58

Table 5 Freundlich isotherm modelling results - $\frac{1}{n}$, K_F and R^2 values for adsorption of each colloidal type on pulp fibres without pH perturbation.

	Slope of graph, $\frac{1}{n}$	Adsorption intensity, n	K_F, Freundlich isotherm constant (mg/g)	R^2 for Freundlich
WE	0.86	1.16	0.38	0.82
OA	4.58	0.22	3.29×10^{-4}	0.75
AA	1.24	0.81	0.81	0.91
TrO	0.94	1.07	6.33×10^{-2}	0.84

Table 6 BET isotherm modelling results - q_s, C_{BET}, and R^2 values for adsorption of each colloidal type on pulp fibres without pH perturbation.

	q_s , theoretical isotherm saturation capacity (mg/g)	C_s, adsorbate monolayer saturation concentration (mg/L)	C_{BET}, BET adsorption isotherm relating to energy of surface interaction (L/mg)	R^2 for BET
WE	0.72	97.8	-16.4	0.98
OA	0.25	106	-1.20	0.63
AA	0.71	11.0	-1.98	0.99
TrO	-	-	-	-

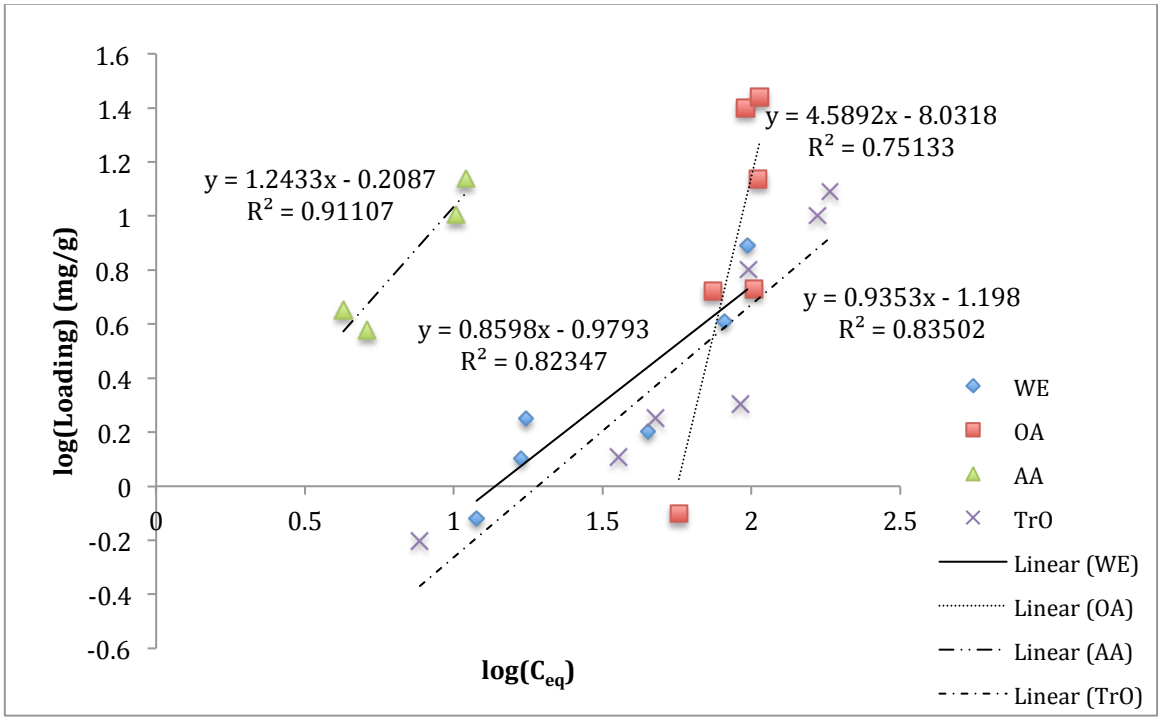

Figure 13 Freundlich isotherm fit for adsorption of wood extractives, oleic acid, abietic acid and triolein onto pulp fibres without pH perturbation.

Table 4 shows that the Langmuir model cannot be used to explain adsorption of all colloidal types. Negative Q_0 values for model compounds are unrealistic, whereas for WE the adsorption plot does not portray a Langmuir-shaped curve. The results in Table 5 and Table 6 show a better fit of the experimental data to the Freundlich and BET models than to the Langmuir model due to the larger R^2 results. For modelling with BET model, the results in (Table 6) showed better fit of the experimental data

for WE and AA (R^2 > 0.98) than for the Freundlich model, however the negative C_{BET} values indicate that the BET model is not suitable over the experimental concentration ranges used to fit the linearized BET model.

From the adsorption curves (Figure 11 and Figure 12), multilayer adsorption is suggested for all the colloidal types (WE, OA, AA and TrO). Using the Freundlich model, the $\frac{1}{n}$ values (Table 5) may suggest that OA and AA colloids underwent cooperative adsorption and had a weaker affinity for the pulp fibres, compared to WE and TrO. K_F values of WE and AA are at least a magnitude or more greater than that of OA and TrO, indicating that WE and AA have greater adsorption capacity onto pulp fibres than OA and TrO colloids.

2.3.2.4 Adsorption of wood extractives and model compounds onto pulp fibres with pH perturbations

The effect of pH perturbations on the adsorption of wood extractives and model compounds was investigated and model fitting of the data was undertaken in the same way as described in 2.3.2.2. As mentioned in the "Methods and Materials" section, the pH of the suspension was increased (to about 7 - 8) before returning it to the starting pH of about 5 at the start of the deposition experiment. Adsorption of WE onto pulp fibres subjected to pH perturbations resulted in isotherm profile "T1"; whereas the adsorption of OA and AA resulted in isotherm profile of "T2" (Figure 14). Negative adsorption of TrO, shown in Figure 15, can be read as no adsorption due to the size of the error bars. Therefore the TrO results cannot be used conclusively for any modelling calculations.

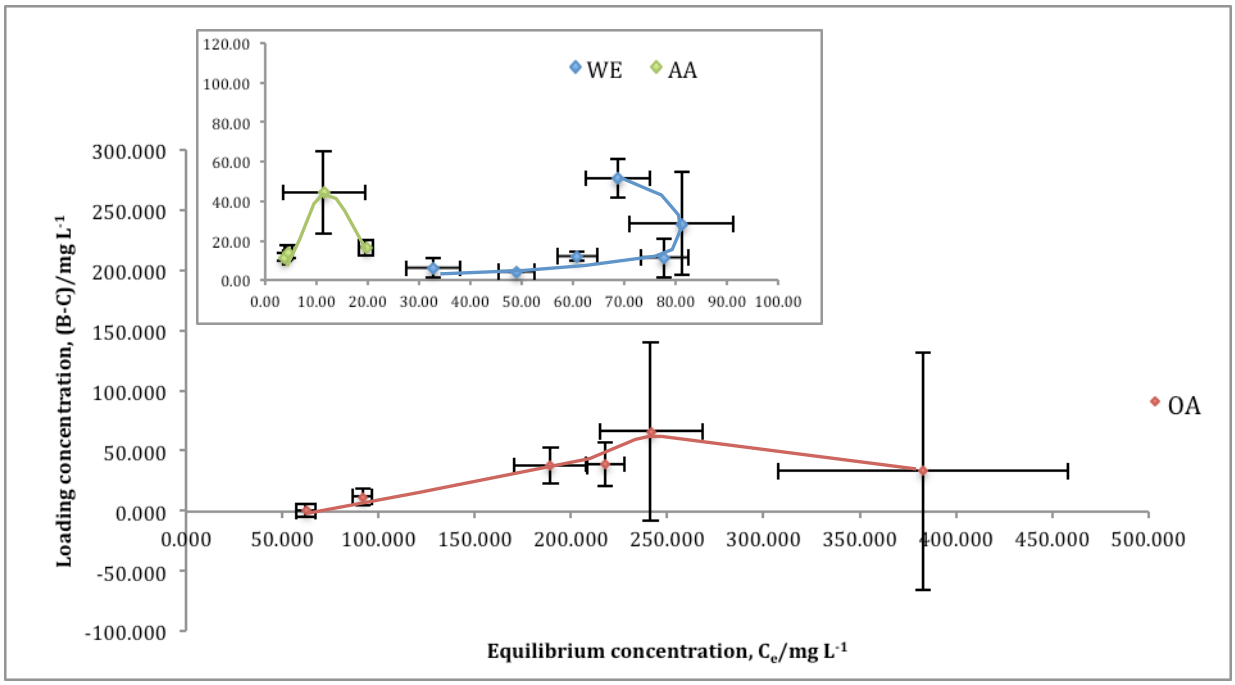

Figure 14 Adsorption of wood extractives (WE), oleic acid (OA) and abietic acid (AA) onto pulp fibres with pH perturbation.

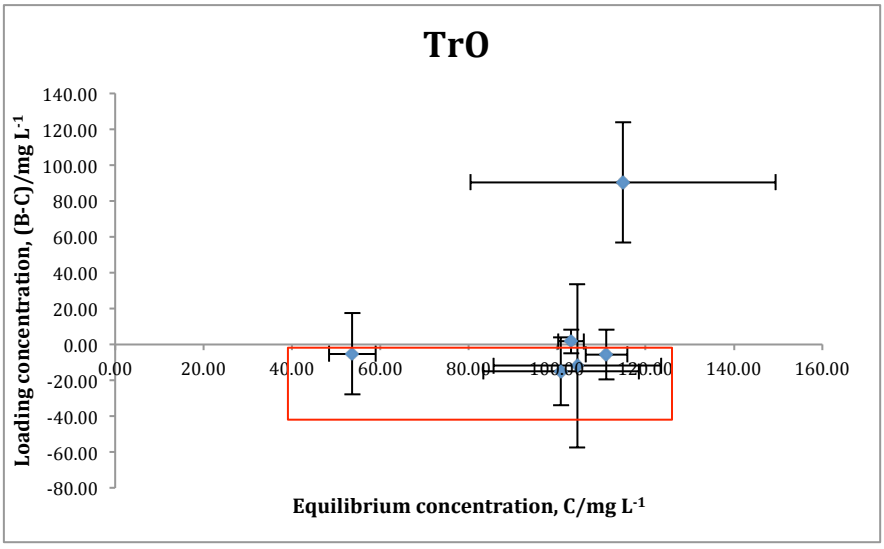

Figure 15 Plot of adsorption of triolein (TrO) onto pulp fibres with colloidal suspension subjected to pH perturbations. Points in boxed region show no or negative adsorption, which will be read as no adsorption.

The results of the Langmuir, Freundlich and BET model fitting are shown in Table 7 - Table 9 respectively. With the exception of OA, the model fitting after pH perturbations is not as good as that obtained for the experiments in which the pH was not changed. This is shown by the lower R^2 values for all tests except OA in Table 7 – Table 9 compared to Table 4 – Table 6. Table 7 shows that the Langmuir model is a poor fit for experimental data for the adsorption experiments for all the colloidal types except OA. Even though the R^2 value for OA (Langmuir) was very high (R^2 = 0.96), the negative constant values (Q_0 and *b*) are unrealistic. Therefore, the Langmuir model is also unsuitable for adsorption of OA. Similarly, with negative C_{BET} values, the BET model is unsuitable for modelling adsorption of OA and WE (Table 9). Insufficient points for AA also result in unsuccessful modelling with the BET isotherm.

Table 7 Langmuir isotherm modelling results - *b*, Q_o, and R^2 values for adsorption of each colloidal type on pulp fibres with pH perturbations.

	Q_0 max. monolayer coverage capacities (mg/g)	*b,* Langmuir isotherm constant	R^2 for Langmuir
WE	-14.7	1.82×10^{-3}	0.46
OA	-10.1	-1.83×10^{-3}	0.96
AA	6.52	0.16	0.52
TrO	-	-	-

Table 8 Freundlich isotherm modelling results - $\frac{1}{n}$, K_F and R^2 values for adsorption of each colloidal type on pulp fibres with pH perturbations.

	Slope of graph, $\frac{1}{n}$	Adsorption intensity, *n*	K_F, Freundlich isotherm constant (mg/g)	R^2 for Freundlich
WE	1.55	0.65	8.86×10^{-2}	0.60
OA	1.63	0.61	5.80×10^{-2}	0.96
AA	0.39	2.56	1.24	0.26
TrO	-	-	-	-

Differences in the modelling constants were observed for experiments with pH perturbations of the suspension (treatment (B)) compared to the experiments with no pH perturbation (treatment (A)), where adsorption intensity values, *n* provide information on how favourable the adsorption is. The modelling results indicate that, with the exception of TrO, the adsorption process for all the colloidal types subjected to pH perturbation is best described as multilayer adsorption (Table 8).

Table 9 BET isotherm modelling results - q_s, C_{BET}, and R^2 values for adsorption of each colloidal type on pulp fibres with pH perturbations.

	q_s, theoretical isotherm saturation capacity (mg/g)	C_s, adsorbate monolayer saturation concentration (mg/L)	C_{BET}, BET adsorption isotherm relating to energy of surface interaction (L/mg)	R^2 for BET
WE	0.12	81.2	-1.17	0.69
OA	0.91	241	-3.05	0.68
AA	-	-	-	-
TrO	-	-	-	-

Based on modelling with the Freundlich isotherm equation, WE showed stronger adsorption intensity to pulp fibres when there is no pH perturbation compared to when pH was perturbed, whereas WE reached lower saturation concentration after pH perturbation (81.2 mg L^{-1}) than with no pH adjustment (98.0 mg L^{-1}). These observations would explain why WE adsorption to pulp fibres increases when there has been a pH perturbation to the colloidal suspension, where the colloidal stability of WE in suspension is reduced. The colloidal instability of WE subjected to increased pH can be explained by the observation by Richardson et al.[9], Sundberg et al.[17] and Palme.[61] Both studies by Richardson et al. and Sundberg et al. observed that ionisation and solubilisation of fatty and resin acids increased with increasing pH.[9, 17] Similarly, Palme observed that when wood extractive (WE) colloids are subjected to pH perturbations, different components are solubilised as pH is increased. When WE colloids re-formed after the pH was returned to pH 5, the amount of resin acids (RA) within the re-formed WE decreased. The author proposed that resin acids might form smaller aggregates of pure colloids than reforming into droplets with the fatty acids and triglycerides. This would lead to decreased resin acids in WE colloid droplets, causing instability in the colloids.[61] As pH of these experiments (of this chapter) was increased to about 7, it can be rationalised that more resin acids would be solubilised before fatty acids from WE

colloid as most resin acids have lower pK_a values than that of fatty acids.[62] Therefore, when results in Table 8 show that AA have higher *n* and K_F values, whereas WE and OA have similar *n* and K_F values after pH perturbation may suggest that the surface properties of WE (when re-formed as pH was returned to 5) resemble that of OA rather than AA. This would agree with the observation of Palme, where fatty acids remained in the WE colloids even after pH perturbation. Additionally, it would also support the notion that AA would form smaller aggregates of pure colloids rather than return into the WE colloids with the fatty acids and triglycerides, thus causing a change to the surface properties of the WE colloids. The K_F value of AA, being much greater than that of OA and WE, may also be an indication of colloidal instability, thus greater deposition capacity onto adsorbent than remain suspended in solution.

Conversely, OA had a lower saturation concentration without pH adjustment (105.5 mg L^{-1}) than with pH adjustments (241.0 mg L^{-1}). When pH increased to about 7, some ionisation of OA occurred but would be very minimal as pK_a of OA is 8.29[62], which may contribute to the colloidal stability of OA colloid when pH perturbations occurred. As AA adsorption, the saturation concentrations were similar with or without pH perturbation but very low compared with that of the other colloidal types, being 11.4 mg L^{-1} and 11.0 mg L^{-1}, respectively. This may be due to AA colloids being very unstable and the difficulty in incorporating AA into solution, regardless of whether it was subjected to any pH perturbation.

2.3.2.5 Adsorption of wood extractives and model compounds onto microcrystalline cellulose (MCC) particles without pH perturbation

Table 10 – Table 12 show the results from Langmuir, Freundlich and BET model fitting of adsorption onto microcrystalline cellulose (MCC) particles with no pH perturbation (referred to as treatment (C)). The pH of the colloidal suspensions were not subjected to any changes and measured to be around pH 5 throughout the experiments.

All colloidal types showed a point of inflexion marking the start of the “non-ideal” concentration region. Only results before the “non-ideal” region were considered in the modelling calculations.

Table 10 Langmuir isotherm modelling results - *b*, Q_o, and R^2 values for adsorption of each colloidal type on microcrystalline cellulose particles without pH perturbation.

	Q_0 max. monolayer coverage capacities (mg/g)	*b,* Langmuir isotherm constant	R^2 for Langmuir
WE	10.4	4.90×10^{-3}	0.79
OA	47.4	5.10×10^{-4}	0.94
AA	5.66	0.70	0.69
TrO	1.09	-8.46×10^{-3}	0.96

Table 11 Freundlich isotherm modelling results - $\frac{1}{n}$, K_F and R^2 values for adsorption of each colloidal type on microcrystalline cellulose particles without pH perturbation.

	Slope of graph, $\frac{1}{n}$	Adsorption intensity, n	K_F, Freundlich isotherm constant (mg/g)	R^2 for Freundlich
WE	1.13	0.89	0.20	0.81
OA	1.02	0.98	0.21	0.87
AA	0.15	6.58	1.69	0.59
TrO	-	-	-	-

As there are no negative values for Q_0 the results in Table 10 show that the Langmuir model can be applied to all the colloidal types. However, this might not be correct, as the adsorption of colloidal materials failed to reach a limiting concentration due to saturation of the adsorption sites.

Table 12 BET isotherm modelling results - q_s, C_{BET}, and R^2 values for adsorption of each colloidal type on microcrystalline cellulose particles without pH perturbation.

	q_s, theoretical isotherm saturation capacity (mg/g)	C_s, adsorbate monolayer saturation concentration (mg/L)	C_{BET}, BET adsorption isotherm relating to energy of surface interaction (L/mg)	R^2 for BET
WE	1.11	198	1280	1.00
OA	1.39	233	179	0.96
AA	2.66	28.5	-85.4	0.99
TrO	0.73	248	-2.02	0.94

R^2 values for the BET modelling all show very good fit to the experimental results (Table 12). However, negative C_{BET} values for AA and TrO are unrealistic, hence the BET model is not suitable for modelling AA and TrO undergoing treatment (C). On the other hand, the BET model was found to be appropriate for the adsorption of WE and OA effectively under the experimental concentrations, both having positive C_{BET} values.

Freundlich modelling (Table 11) shows that multilayer adsorption occurs for all but TrO colloids. The results of TrO adsorption cannot be used conclusively for any Freundlich modelling calculations as there was very little or no adsorption. AA colloids once again have a higher adsorption intensity than WE and OA, evident with its higher *n* values. AA also has the highest K_F values, followed by WE and OA (with comparable K_F values). As previously mentioned in 2.3.2.4, higher *n* and K_F values for AA and comparable *n* and K_F values for OA and WE, may indicate that the WE surface properties are similar to that of OA, or other fatty acids, due to AA leaving the WE colloid when the pH is perturbed. This may also suggest that MCC had a much higher adsorption capacity for AA compared to WE and OA. As previously proposed, colloidal stability as well as the insolubility of AA may contribute to greater deposition onto MCC. The Freundlich constant values of treatments (A) and (C), showed that OA has a stronger adsorption intensity and capacity on MCC than onto pulp fibres, while the adsorption intensity and capacity of WE on MCC and pulp fibres are the same order of magnitude. Unlike the adsorption of AA onto pulp fibres (treatment (A)), the deposition curve of AA onto MCC approached a more Langmuir-shaped curve, which is supported by values of *n* being greater than 1. As for WE and OA, where $0 < n$

< 1, cooperative adsorption is favoured. Some form of cooperative adsorption between solute molecules may still occur for AA in addition to interaction between solute molecules and the surface.

As for the adsorption of AA, Asselman et al.[63] determined that adsorption of AA colloids occurs between a molecular and a colloidal monolayer. The results here show that AA colloids do not follow a monolayer adsorption pattern for treatment (A), though full surface coverage may not be achieved at the concentrations used, C_e. However, for treatments (B) and (C), results may point towards AA colloids having a Langmuir type adsorption, where normal adsorption occurred. This may be due to difficulty in obtaining a good concentration range of AA in suspension (in these adsorption experiments), as AA colloids are very unstable and are not easily incorporated into a stable dispersion as shown by previous work by Heier.[57]

2.4 Conclusion

Adsorption isotherms of wood extractives and model compounds onto pulp fibres (with and without pH perturbation of the colloidal suspensions) and microcrystalline cellulose were modelled and results compared. The Langmuir model was found to be unsuitable for modelling the adsorption of these compounds, since the adsorption is believed to be more than monolayer coverage while the negative constant (*b*) values determined are unrealistic. For multilayer adsorption of wood extractives and model compounds the BET adsorption model or the Freundlich model can be used to model the adsorption process. However, negative constant (C_{BET}) values as a result of the BET modelling also showed that this model is not suitable for modelling except for adsorption of WE and OA onto microcrystalline cellulose. Therefore the Freundlich model is the appropriate model for most of the adsorption experiments, even though the total chi-square test ($\Sigma\chi^2$) showed that the BET and the Langmuir models had better fits. In general, all colloidal types are believed to exceed monolayer coverage during the adsorption process and multilayer (cooperative) adsorption is shown to occur for all colloidal types.

The results show that OA and AA have the greatest adsorption intensity (*n*) to microcrystalline cellulose than to pulp fibres, whereas WE have greater adsorption intensity to pulp fibres than to microcrystalline cellulose. Similarly, OA and AA also have greatest adsorption capacity (K_F) onto microcrystalline cellulose than to pulp fibres and WE showed greatest adsorption capacity onto pulp fibres than onto microcrystalline cellulose. In addition, the surface properties of WE colloids have shown to be modified to become more fatty-acid-like when subjected to pH perturbations. This is because the Freundlich adsorption isotherm constants for WE become more similar to that of OA as compared to the Freundlich

adsorption isotherm constants for WE being similar to that of AA when not subjected to pH perturbations. This may be explained by the ability of abietic acids in the WE colloids to ionise and solubilise when pH was increased from 5 to 7, but when pH was returned to 5 the solubilised AA component did not return to the WE colloid.

Studies of adsorption of AA for all three treatments (A-C) were found to be problematic as the solubility of abietic acid was quite low. This may contribute to inaccuracy of isotherm modelling and thus may affect the conclusion of the AA adsorption. Similarly for TrO during treatments (B) and (C), no isotherm models could be fitted due to negative loading experimental values.

Chapter 3 Adsorption with Quartz Crystal Microbalance with Dissipation (QCM-D)

3.1 Introduction

Quartz crystal microbalance with dissipation (QCM-D) is a technique that measures the mass and viscoelastic properties of molecular layers as they build up on a crystal surface. The technique enables precise, time resolved measurements of the frequency shift (Δf) with an energy dissipation factor (ΔD).[64] Originally, QCM was developed solely for use as a highly sensitive mass detector for use in vacuum environments.[65, 66] Technological advances in resonator electronics have since seen QCM-D widely used to measure minute mass changes occurring on a crystal surface in vacuum, gas or liquid phase. Capturing of both the frequency and dissipation data on modern QCM instruments provides an opportunity to obtain information other than simply the mass and thickness of the adsorbed layer, but also layer viscoelastic properties, such as shear modulus and viscosity.[67]

QCM-D consists of a thin quartz disk with electrodes plated on either face (Figure 16).[65, 68] The piezoelectric quartz disc is made from a precisely cut section of a natural or synthetic crystal of quartz.[68] The thin quartz crystal disk is cut to a specific orientation with respect to the crystal axes - either AT-cut or BT-cut. BT-cut crystal is cut at an angle approximately opposite that of the AT-cut. Both types have the same vibration mode but the BT-cut is slightly thicker than the AT-cut.[69] However the AT-cut crystals are widely used due to its excellent temperature and frequency characteristics, providing close to zero values for both the temperature coefficient and resonance frequency drift (induced by alternating electric field) within the range 0 – 50°C.[65, 68, 70] The QCM is fundamentally driven by the piezoelectric effect in quartz crystals, where an electrical field applied between the two electrodes plated on each side of the crystal generate an internal mechanical stress in the crystal, producing an oscillation frequency typically in the MHz range.[68] The crystal oscillation is parallel to the surface of the sensor, with height changes at the sensor surface estimated at 1-2 nm.

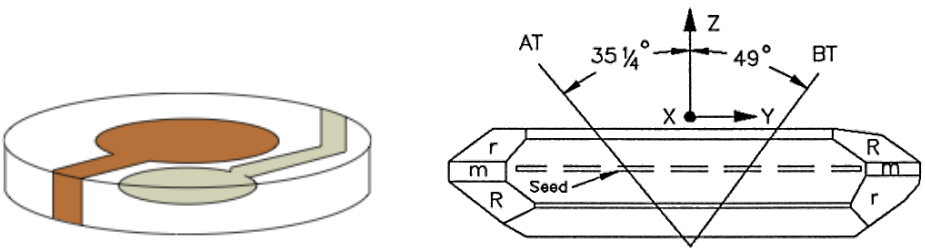

Figure 16 A piezoelectric disc forming the resonant transducer for QCM-D.

The theoretical foundation for the use of piezoelectricity was first explored by Raleigh and thoroughly investigated by Jacques and Pierre Curie in the 1880s.[68] The decrease in resonance frequency of the quartz crystal is proportional to the mass deposited on the surface. Sauerbrey was the first to develop the relationship (given by Equation 5) that quantifies and correlates a change in frequency with the change in mass.[71]

$$\Delta f = -\frac{\Delta m}{nC} \qquad \text{(Equation 5)}$$

where *C* is the mass sensitivity constant and *n* is the overtone number.

Equation 5 will only hold if the adsorbed layer is rigid and/or thin and the mass is small as compared to the mass of the crystal. The physical properties of the material deposited (such as mechanical stress and damping) should not affect the material constants of the quartz.[72] When the coverage exceeds a value of approximately 0.5 % with respect to the weight of the bare quartz resonator, the relationship between Δf and Δm is no longer linear.[71]

The sensitivity of the mass determination is restricted by the interval during which the resonance frequency is subject to stochastic fluctuation (random fluctuation). Mechanical oscillators react sensitively to ambient factors such as temperature, pressure, humidity and interfering fields. These (systematic) deviations can be corrected or compensated. Ageing can also be a source of error.[72]

The second measurement parameter, the dissipation factor (*D*) provides information on the mechanical or viscoelastic properties of the adsorbed layer on the QCM electrode sensor surface.[73-75] The dissipation changes are measured when the driving voltage to the crystal is shut off and the energy from the oscillating crystal dissipates from the system. As the quartz crystal oscillates, an acoustic wave propagates perpendicular to the crystal surface, estimated to be ~250 nm in deionised (DI) water at room temperature and 5 MHz.[67]

A range of factors affect the frequency changes in QCM-D. The fundamental frequency depends on the quartz disc, its chemical structure, its shape and mass. Other factors that affect the oscillating frequency include the thickness, the density, and the shear modulus of the quartz.[68] According to a review by Handley, the environment at the crystal's surface, the mass and characteristics of the coating, and the properties of the solution near the electrode surface affect the resonant frequency change experienced by the oscillating crystal.[76] Other factors such as viscosity and density of the interacting fluid, as well as concentration and charge density can impact frequency changes.[76]

The choice of quartz crystal is important especially when used in a solid/liquid environment, as resonant frequency will be affected by surface roughness.[65, 71] Other than crystal surface roughness, the thickness of the crystal will also influence its sensitivity and resonance frequency. Thinner devices are more sensitive as they resonate at higher frequencies but are also harder to handle due to their fragility.[65] The frequency of the acoustic wave depends on the mass of the entire piezoelectric disc. Therefore, the mass of deposited film on the surface of the disk can be calculated from the measured change of the resonant frequency of the device.[65] Coupling mass change and resonance frequency enables mass determination to be registered quickly and with high precision.[68, 72]

The temperature of the crystal affects the stability of the frequency (*f*) of the oscillator strongly. The angle of cut of the crystal plates determines the "turning points" (zero-temperature coefficient), which is the static frequency-temperature (*f-T*) characteristics of the quartz crystals.[77] For example, a turning point for an AT-cut crystal is 26-80°C. A study by Bouzidi et al. summarized and listed the other temperature-dependent factors that affect the *f-T* characteristics of the oscillator crystal – frequency jumps, activity dips, thermal gradients, thermal history and thermal hysteresis. Some cause temporary changes while others cause permanent frequency shifts.[77]

Quartz crystal microbalance with dissipation (QCM-D) is a relatively new instrumental technique used in the area of colloidal chemistry. It has gained popularity in interfacial phenomena studies such as mechanism and kinetics studies of gas adsorption,[78] adsorption/desorption in liquids,[71, 79] and wetting velocities of surfactants.[80, 81] It is also used to investigate the mechanical properties of film coatings[82, 83] as biosensors, as well as for monitoring fluids and deposition at high temperatures. Other than that, it has been used extensively in biological research such as immunology and cell biology to investigate issues such as cell and protein adhesion kinetics. [84-86]

Bouzidi et al. improved on the fundamental principles of QCM and developed a high stability QCM-D to study quantitatively the chemisorption of gases on metal surfaces.[77] Dultsev et al. have applied QCM-D to measure the onset of bond rupture by increasing the amplitude of the acoustic wave applied on the instrument. They were able to measure molecular interactions from relatively weak interactions such as hydrogen bonding to full covalent bonds.[87] Pham et al. used QCM-D to study the interfacial phenomena occurring between solid/liquid environments.[88] They utilised QCM-D to monitor the different modes of colloidal droplets during evaporation and analysed sessile droplet evaporation. The changes of crystal oscillating frequency and damping are observed and linked to the different stages of the evaporation process.[88] They achieved understanding by comparing QCM-D measurements of colloidal droplets drying to that of a model system, which included a range of particle sizes (1.9 to 10 μm) of

monodispersed spherical latex particle droplets, as well as with the behaviour of evaporation of suspensions known from optical observations.[88]

The use of QCM-D, to understand the properties and behaviour of wood extractives when in contact with different surfaces, is a relatively new application of the technique to wood chemistry. Johnsen et al.[89] have used the QCM technique to study the adsorption of wood extractive colloids and dissolved hemicelluloses onto cellulose, which had been deposited onto polystyrene coated QCM quartz crystal. They concluded that dissolved hemicellulose sterically stabilise the colloids and promote adsorption onto flake-like fines instead of fibrillar fines. Similarly, Tammelin et al. also studied the adsorption of wood extractive colloids and dissolved hemicelluloses onto fibre surface components such as lignin and extractives other than cellulose.[90] They have concluded that the adsorption onto cellulose was the greatest for electrostatically stabilised extractive colloids. Whereas, dissolved hemicelluloses sterically stabilise wood extractives and prevent adsorption of extractives to itself.[90] QCM-D was also used to study the adsorption mechanism of fatty acids[91] as well as sodium oleate adsorption to a hydroxyapatite surface.[92]

There have been several different methods used by other researchers to functionalise the crystal surface for a particular application. In this project, where interactions with cellulose are fundamental, it is necessary to modify a crystal surface to represent cellulose. Many methods of developing and modifying a surface with cellulose can be found in the literature. These include the Langmuir-Schaefer (LS) method with trimethylsilyl cellulose (TMSC),[93] layer-by-layer (LbL) technique with cellulose nanocrystals (CNC), or cellulose nanofibrils (CNF) in combination with cationic polyelectrolytes,[94] spin-coating regenerated cellulose (RC), CNC and TMSC onto substrate[95-97] and others.[98] These methods require sophisticated instrumentation setup, expensive materials and are usually time-consuming.

3.1.1 Aim

The aim of this research is to use QCM-D to study the interaction between wood extractive colloids, in the water phase, and the different surfaces these colloids come in contact with during papermaking and printing. This is achieved by tracking the mass changes on a crystal surface. Model compounds that represent the major components in the wood extractive colloids were also used to study the interaction with the different surfaces. They were then compared to that of wood extractive colloids in order to provide some insight into what constitutes the surface chemistry or the make-up of the colloids of wood extractives. In this research, we have developed a new method for coating a surface with relatively inexpensive microcrystalline cellulose particles to represent a cellulose surface.

3.2 Method and Materials

The quartz crystal microbalance with dissipation (QCM-D) instrument used was a Q-sense E4 (Q-sense AB, Västra Frölunda, Sweden). The instrument was set up to measure changes to mass and viscoelastic properties of molecular layers as changes occur on the sensor surface. The 6 mM NaCl (aq) (Univar, AR grade) solution was used as the aqueous background electrolyte in all suspension preparation as well as in each rinsing process for QCM-D adsorption experiments.

3.2.1 QCM-D crystal sensors and preparation

The QCM-D crystals were A-T cut crystals with a 10 mm diameter gold (QSX301) or 15 mm diameter chromium (QSX315) (Cr) electrode surface with a fundamental resonance frequency of 5 MHz (Q-Sense AB). Prior to each experiment, the quartz crystals' surface was cleaned with Piranha solution (70 % sulphuric acid and 30 % hydrogen peroxide) for 3 min, rinsed with MilliQ water (18 MΩ) and dried under a gentle stream of nitrogen gas. The crystals were then UV-cleaned for 10 min in a Bioforce Nanosciences UV/Ozone Procleaner™, rinsed with 70 % ethanol and dried under a stream of nitrogen gas. Chromium-coated QCM-D crystal sensors were then directly used in adsorption experiments, while gold-coated sensors were subsequently modified with microcrystalline cellulose (MCC) prior to the measurement of colloidal adsorption to the sensor surface.

3.2.1.1 Preparation of cellulose surface

Microcrystalline cellulose-coated (MCC) quartz crystals were prepared *in situ* in the QCM-D flow cells using the gold-coated quartz crystals. Crystal sensor surface was first modified with polyethyleneimine (PEI*) in situ* in the QCM-D flow cells by passing a 5 mg mL^{-1} PEI (25000 MW, Aldrich) solution through the cells for 15 min at 40 μL min^{-1}. After rinsing with MilliQ water (18 MΩ) for 40 min at 40 μL min^{-1}, a MCC suspension was introduced into the cells for 2 h at 40 μL min^{-1}. The microcrystalline cellulose (Serva-Avicel PH 105, ca. 0.019 mm) suspension was prepared by sonicating a 5 % w/v MCC suspension (in MilliQ water, 18MΩ) for 12 min. The MCC suspension was then filtered through a 0.22 μm filter to ensure a uniform dispersion of MCC particles to the flow cells. This MCC suspension was introduced into the flow cells after the PEI modification of QCM-D crystals. After 2 h of incubation in the MCC suspension, the QCM-D flow cells were rinsed with 6 mM NaCl (aq) until the QCM-D parameters were stabilized, at which time the modified sensors were ready to be used for adsorption experiments.

3.2.2 Preparation of colloidal suspension

3.2.2.1 Model compound colloidal suspension

Model compounds used to represent individual components found in wood extractives are oleic acid (OA, model for fatty acids, Aldrich, 90 %), abietic acid (AA, model for resin acids, Fluka Analytical, 75 %), and triolein (TrO, model for triglyceride, Sigma, 65 %). Colloidal suspensions of approximately 600 mg L^{-1} were prepared by weighing about 0.012 g of each compound and dissolving in acetone (<1 mL) (AR grade, Chem-supply). The acetone-model compound mixture was then added to 20 mL of 6 mM NaCl (aq) and stirred for 15 min before use. An additional colloidal suspension of a mixture of all three model compounds (MM) was also prepared following the above method by measuring out equal amounts of oleic acid (OA), abietic acid (AA) and triolein (TrO) into 20 mL of 6 mM NaCl (aq).

3.2.2.2 Wood extractives colloidal suspension

Wood extractives (WE) were extracted from *P. radiata* thermomechanical pulp (TMP) according to the method described by Stack et al.[99] Aqueous dispersions of wood extractives were prepared by dissolving about 0.0200 g of extracted wood extractives in <1 mL of acetone, followed by dispersion of acetone-extractive mixture into a stirred 20 mL aqueous 6 mM NaCl (aq) to give a stable colloidal dispersion of the wood extractives.

3.2.3 Characterisation of model surfaces

3.2.3.1 Scanning Electron Microscopy (SEM)

Microcrystalline cellulose modified and gold-coated glass cover slips were sputter coated with a thin layer (~2 nm) of platinum and glued in place on the scanning electron microscopy (SEM) stub with silver paint. SEM images of the sample surface were obtained using a field emission SEM (JOEL JSM-7500FA).

3.2.3.2 Atomic Force Microscopy (AFM)

AFM images were obtained in tapping mode under ambient condition with a μMash NSCI5 cantilever (spring constant 40 N/m) fitted to a MFP-3D atomic force microscope (Asylum Research). Three AFM images (at 1 μm x 1 μm resolution) were taken per sample for each model surface and the mean surface roughness measurement (R_{RMS} roughness) obtained.

3.2.3.3 Contact Angle Measurement

A Dataphysics Contact Angle System in conjunction with SCA20 software was used to calculate the contact angle of a 1 µL sessile drop (MilliQ water, 18 MΩ) on the film surfaces. Contact angle measurements were run in triplicate for three samples of each surface.

3.2.4 QCM-D adsorption experiments and analysis

Prior to each experiment, the quartz sensor surface was cleaned with Piranha solution for 3 min. After the cleaning step, the sensors were rinsed twice with MilliQ water (18 MΩ) and dried with nitrogen gas. Baseline was achieved by allowing the frequency and dissipation measurement parameters of the QCM-D sensors to stabilize in a 6 mM NaCl (aq) at the relevant temperature prior to the adsorption experiments. For experiments at elevated temperature, the modification (if any) of the quartz sensor surface was carried out at 25°C and the temperature of the system was increased to 50°C only after the surface modification was completed and before the colloidal suspension was passed through the cells.

In this study, the adsorption experiments of colloidal model compounds and wood extractives onto MCC-modified and chromium surfaces were carried out at 25°C and 50°C. Colloidal materials were introduced into the flow chamber at 20 µL min^{-1} for 2 h before rinsing with 6 mM NaCl (aq) for at least 4 h. QCM-D measurement parameters were recorded during rinsing in order to quantify the desorption of the adsorbed colloidal material during this time. All QCM-D experiments were run in triplicate to check repeatability of adsorption measurements.

Thirteen different frequency overtones and dissipation energies were recorded on the QSoft software. Qualitative comparison can be achieved by comparing frequency-dissipation (*f/D*) plots. Frequency and dissipation measurements from the 5^{th}, 7^{th} and 9^{th} overtones were used for viscoelastic modelling (using the QTools analysis program) in order to estimate the adsorbed mass to the sensor surface. The Voigt model has previously been used to characterise the adsorption of fatty acids, including oleic acid[91, 92] using QCM-D and therefore the Voigt representation has been employed here using the following modelling parameters (fluid density and viscosity of 1000 kg m^{-3} and 0.001 kg m^{-1} s^{-1}, respectively, layer density of 1150 kg^{-1} m^{-3}, layer viscosity of $1^{-6} \leq 1^{-2}$ kg kg^{-1} ms^{-1}, shear modulus of $1^{4} \leq 1^{8}$ Pa and mass of $115 \leq 1.15^{5}$ ng^{-1} cm^{-2}).

3.3 Results

3.3.1 Colloidal suspensions

The concentrations of the colloidal suspensions were chosen to ensure there was an excess of colloidal material always passing through the QCM-D flow cells, in order to minimise the loss of material to other surfaces before the sensor surface.

3.3.1.1 Wood extractives colloidal suspension

The concentrations of each major component in the wood extractives (WE) mixture are listed in Table 13. There are two different wood extractive samples used for these experiments and Table 13 shows that there is a slight difference in the resin acids-to-triglyceride ratio between the two samples. Sample #1 has a resin acids-to-triglyceride ratio of 1:2, while sample #2 has a ratio of about 1:1.

The effect on deposition due to the difference in the resin acids-to-triglycerides (RA:TG) ratio is shown in Figure 17 in terms of the frequency changes on the sensor. At the lower temperature (25°C), the deposition onto both cellulose and chromium was not significantly different for both samples #1 and #2. However, at 50°C, there is a higher deposition onto both surface types when the RA:TG is similar (#2). The difference in ratio is most likely due to sample #1 being stored for some time before use and so the resin acids are likely to have undergone oxidation thus resulting in a lower concentration of resin acids in the sample. The ratio of RA:TG is believed to be important in determining the stability of the colloid and the distribution of the thickness of each layer in the colloid structure. Sample #2 has been used in further experiments as the RA:TG composition is closer to sample ratios present in the papermaking process.[9]

Table 13 Mean concentration and standard deviation (mg L^{-1}) of each component of wood extractives at the commencement of the experiment.

Colloid	Concentration (mg L^{-1})	
	#1 (old)	#2 (new)
Wood extractives (WE)		
Fatty Acids	7.8 ± 1.1	11.5 ± 1.1
Resin Acids	112.1 ± 15.3	190.0 ± 6.0
Triglycerides	206.8 ± 29.7	245.1 ± 8.9
Total	326.7	446.6

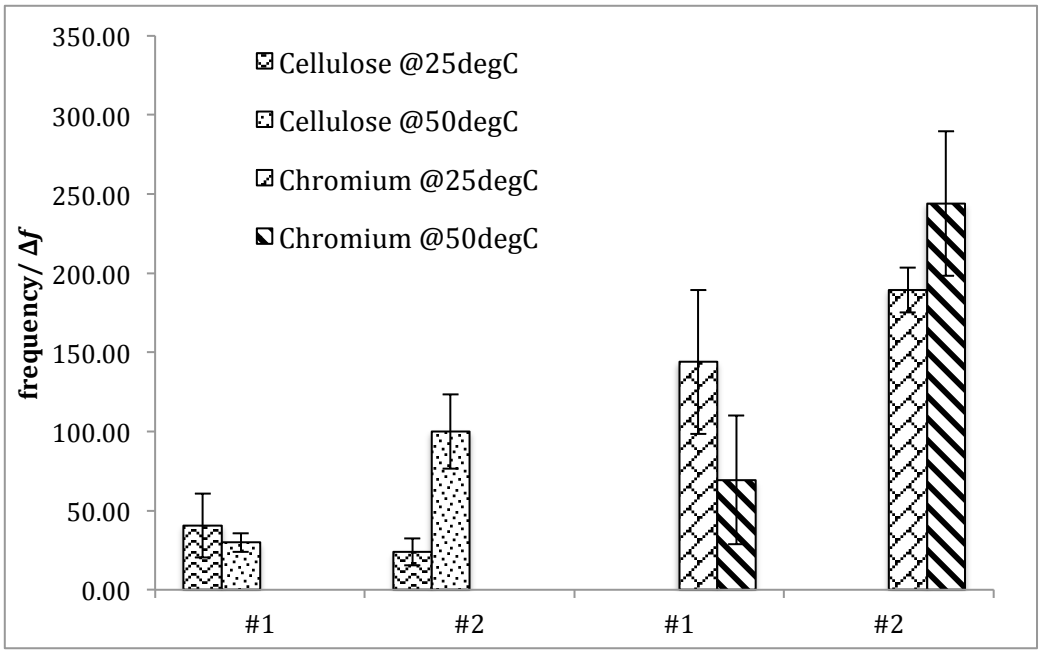

Figure 17 Frequency change (Δf) at point of maximum amount deposited comparing between the two different wood extractives (WE) samples on both cellulose and chromium surfaces.

3.3.1.1 Model compounds colloidal suspension

The concentrations of oleic acid (OA), abietic acid (AA), triolein (TrO) and mixed model (MM) colloidal suspensions used in the experiment are listed in Table 14. The mixed model (MM) colloidal suspension is a suspension mixture of OA, AA and TrO.

Table 14 Mean concentration and standard deviation (mg L^{-1}) of colloidal material at the commencement of the experiment. The concentration of each individual component is listed for mixed model colloidal material.

Colloid	Concentration (mg L^{-1})
Mixed Model (MM)	
Oleic Acid	195.9 ± 75.2
Abietic Acid	33.9 ± 12.0
Triolein	221.4 ± 94.8
Total	451.2
Oleic Acid (OA)	216.7 ± 18.3
Abietic Acid (AA)	86.0 ± 66.2
Triolein (TrO)	407.0 ± 68.7

3.3.2 Characterisation of surfaces

3.3.2.1 Scanning Electron Microscopy (SEM)

SEM images (Figure 18) show that the MCC-modified surface was homogenous and smooth and had a similar surface appearance to a gold-coated glass cover slip in terms of smoothness and homogeneity.

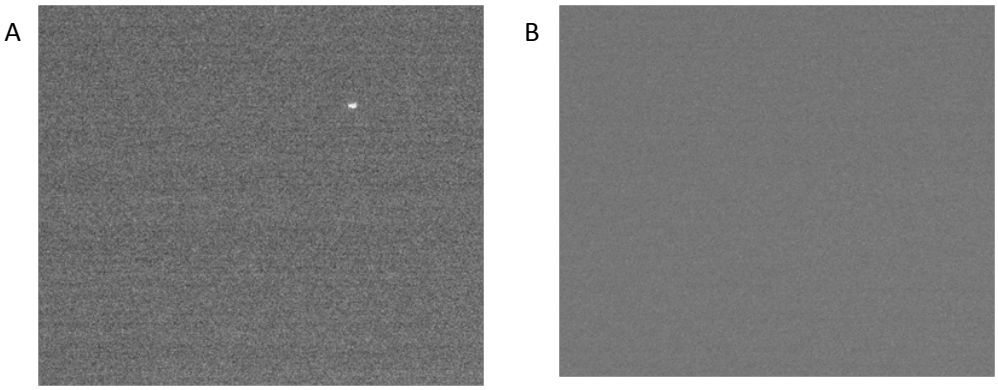

Figure 18 SEM images of microcrystalline cellulose (MCC) surface (A), which represents cellulose surface and gold-coated glass cover slip (B), which is the control surface.

3.3.2.2 Atomic Force Microscopy (AFM)

AFM images of the three prepared surfaces (gold QCM sensor surface, MCC-modified sensor surface, and chromium QCM sensor surface) are shown in Figure 19. The MCC-modified surface showed nodule-like structures[100] (R_{RMS} roughness = 0.80 ± 0.10 nm), whereas the chromium-coated sensors appeared more homogenous with no features greater than 5 nm in height (R_{RMS} roughness = 0.92 ± 0.08 nm). The R_{RMS} roughness of gold QCM-D sensor is 3.44 ± 0.10 nm.

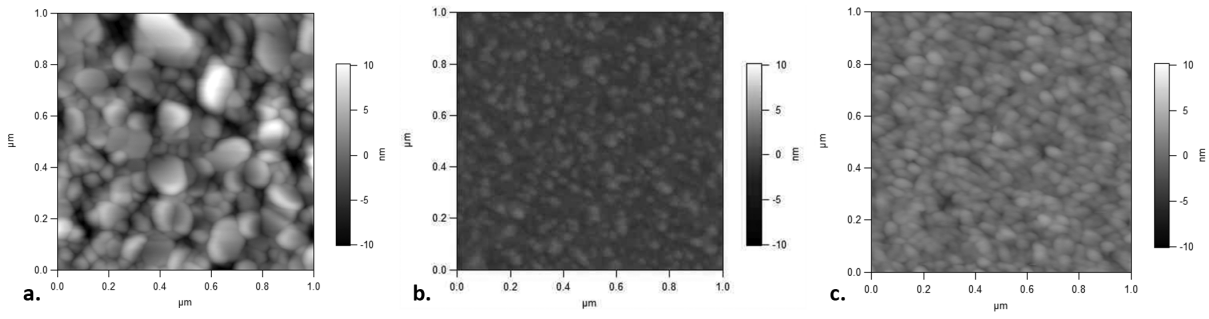

Figure 19 AFM images of gold QCM crystal surface (a), a microcrystalline cellulose-modified gold QCM crystal (b) and a chromium QCM crystal (c). All images obtained in AC mode. Dimensions 1.0 µm x 1.0 µm.

3.3.2.3 Contact angle measurements (Goniometry)

Figure 20 compares the contact angle measurements of the three different model surfaces – gold-coated, MCC-modified and chromium-coated surfaces. The mean experimental contact angle values of these model surfaces are compared with literature values in Table 15. Variability in contact angle measurements between experimental and literature values may be due to droplets on the surface not fully reaching their equilibrium shape. The gold and polyethyleneimine (PEI) surfaces were included for comparison purposes. Modification of the QCM sensor surface with MCC led to an increase in surface hydrophilicity. The chromium surface is shown to be the most hydrophilic among the three different surfaces.

Table 15 Experimental contact angle mean values of each model surface compared with literature contact angle values.

Model Surfaces	Experimental Contact Angle (°)		Literature Contact Angle (°)	
	Angle	SD	Angle	SD
Gold	96	2	70[101]	-
Microcrystalline Cellulose (MCC)	62	9	64.3[102]	1.1
Chromium	49	3	20-60[103], 70[104]	-
Polyethyleneimine (PEI)	74	9	-	-

Contact angle measurements were also obtained for each stage during the method development of the microcrystalline cellulose coated surface and shown in Figure 21, where different periods of incubation of the glass cover slip with MCC suspension were trialled (1 h, 2 h and 4 h). Finally, an incubation time of 2 h was used in adsorption experiments to ensure full coverage of the surface in a reasonable timeframe. Even though experimentally the incubation period of 1 h and 2 h fall within the error, the latter was chosen to ensure that sensor was definitely covered.

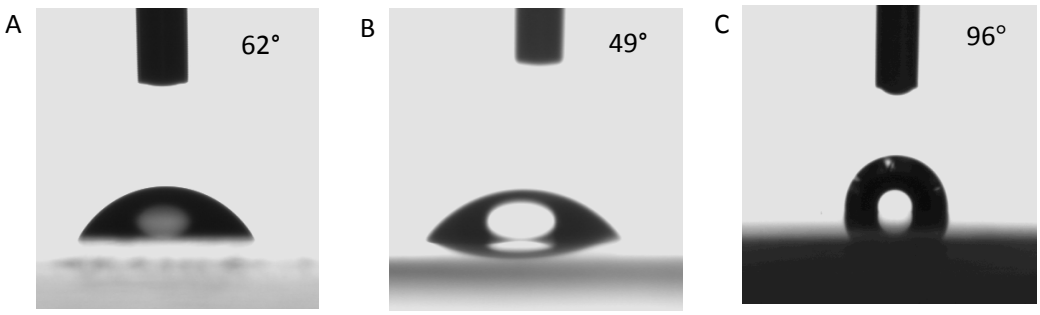

Figure 20 Contact angle measurements of surfaces – (A) cellulose (62° ± 9°), (B) chromium (49° ± 3°) and (C) gold (96° ± 2°).

3.3.3 QCM-D adsorption experiments

Adsorption and desorption experiments were carried out on cellulose and chromium surfaces. The colloidal suspensions used were OA, AA, TrO, MM, and WE colloidal suspensions. A qualitative comparison can be achieved by comparing plots of frequency, *f* and dissipation, *D*. Figure 23 and Figure 22 present annotated plots of *f* and *D* for the *in situ* functionalization of the QCM sensor with MCC, followed by the adsorption and desorption of wood extractives on the cellulose at 25°C and 50°C, respectively. In Figure 23, the background solution was passed through the flow cell until a constant baseline was achieved. Then, as mentioned under section 3.2.1.1, the PEI solution was passed through the flow cells for about 20 – 25 min, where the saturation of PEI on sensor surface was achieved quickly (I). The rinsing process with background electrolyte solution was carried out until a constant baseline was achieved (II). This was to ensure that any excess PEI solution was removed from the system. Filtered MCC suspension was introduced into the flow cells for 2 h (III). Before the introduction of WE colloidal suspension (V), the flow cells were rinsed to remove excess MCC suspension until a constant baseline was achieved (IV). At the end of adsorption process, rinsing with the background solution was carried out (for about 4 h) (VI). In Figure 22, the temperature of the flow cells was increased (Figure 22V) after rinsing the flow cells post-MCC deposition, and before the introduction of colloidal suspension (Figure 22VI). The rest of the process was similar to that described for Figure 23. Figure 24 and Figure 25 show plots of *f* and *D* for adsorption and desorption of wood extractives on chromium surface at 25°C and 50°C, respectively. Figure 24 shows that the colloidal suspension was introduced into the flow cells once a constant baseline was achieved (I). Rinsing of the flow cells commenced after 2 h of the adsorption process (II). For adsorption onto chromium at the higher temperature of 50°C, the temperature of the flow cells was increased (prior to I) before the introduction of the colloidal suspension (Figure 25(III)). These example plots of *f* and *D* shifts are typical of what was observed for other colloidal suspensions, with the only difference being the magnitude of the shifts for each colloidal system.

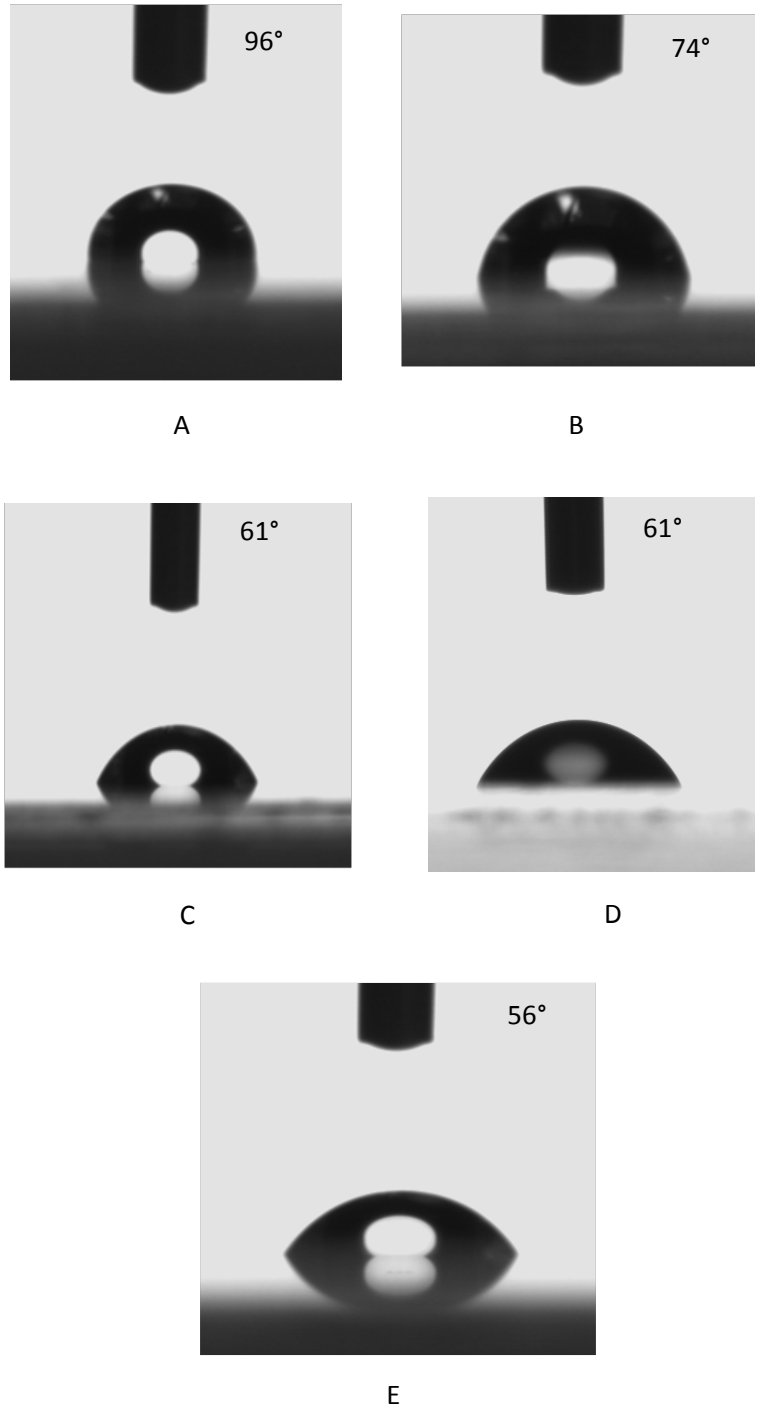

Figure 21 Contact angle measurements of surfaces – (A) Gold-coated surface (96° ± 2°), (B) Polyethyleneimine (PEI) coated (74° ± 9°), (C) – (E) are PEI-coated surfaces that are incubated in microcrystalline cellulose mixture for various period of time: (C) 1 h (61° ± 3°), (D) 2 h (61° ± 9°) and (E) 4 h (56° ± 7°).

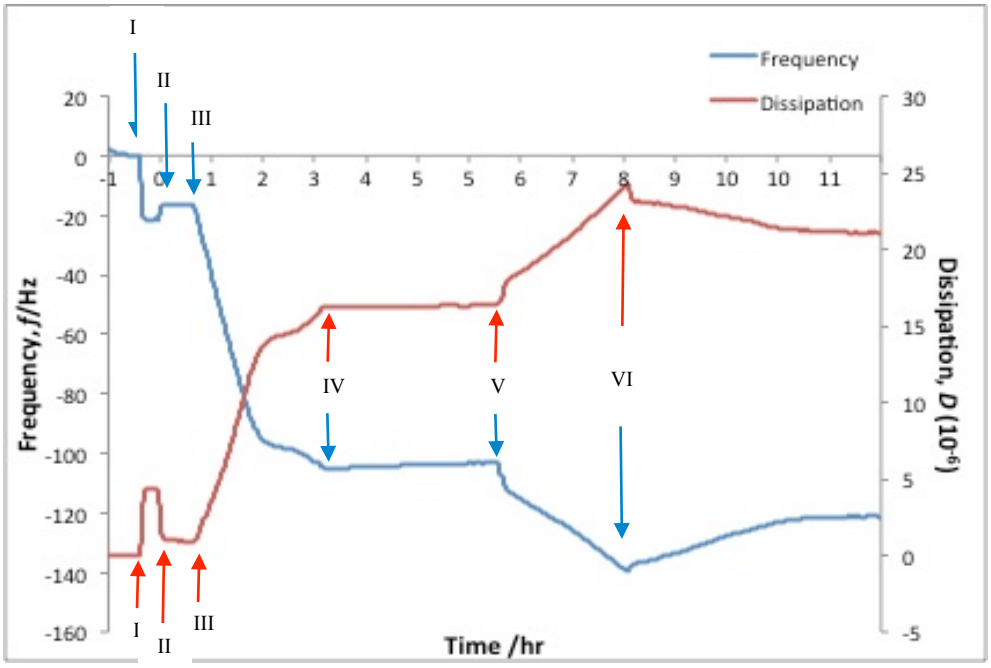

Figure 23 An example of the changes in frequency and dissipation (of the 5th overtone) for wood extractives adsorption onto microcrystalline cellulose (MCC) surface at 25°C, as different modification and solutions are introduced into the QCM-D sensor chambers.

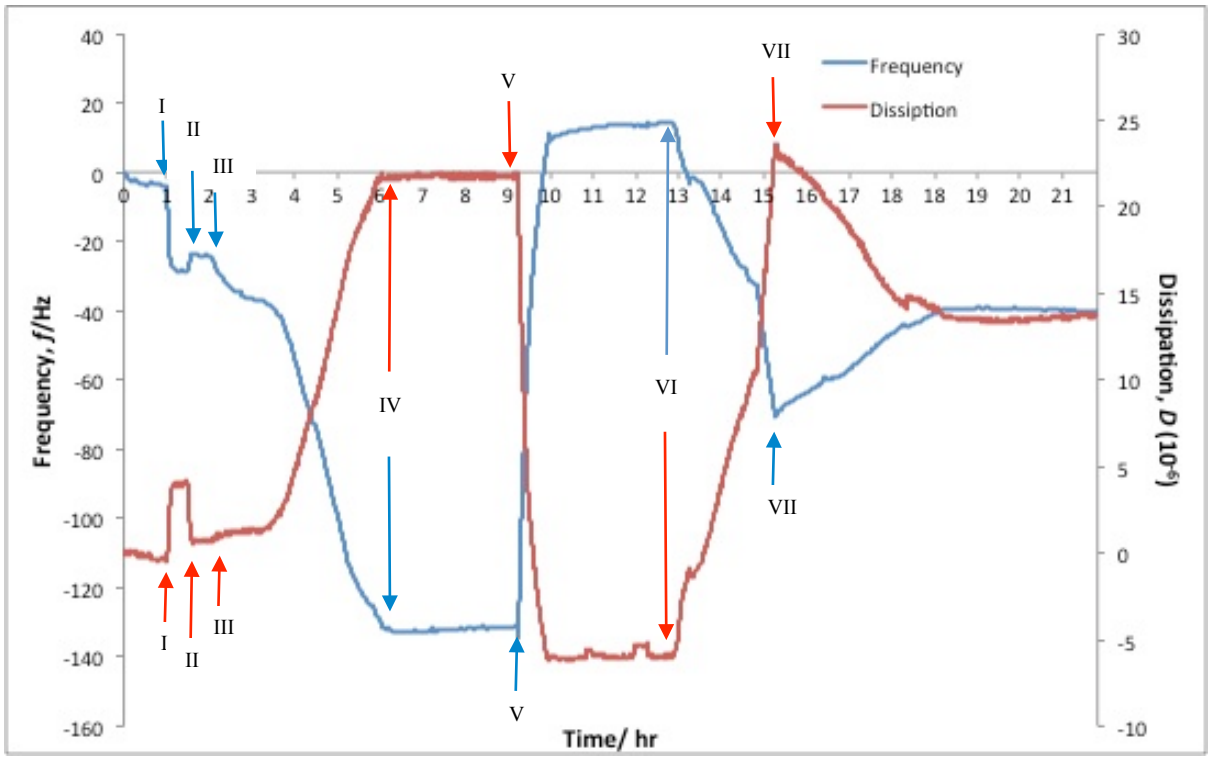

Figure 22 An example of the changes in frequency and dissipation (of the 5th overtone) for wood extractives adsorption onto microcrystalline cellulose (MCC) surface at 50°C, as different modification and solutions are introduced into the QCM-D sensor chambers. Steps (I) – (IV) were carried out at 25°C and similar to that in Figure 22. Steps (V) – (VII) were carried out at 50°C.

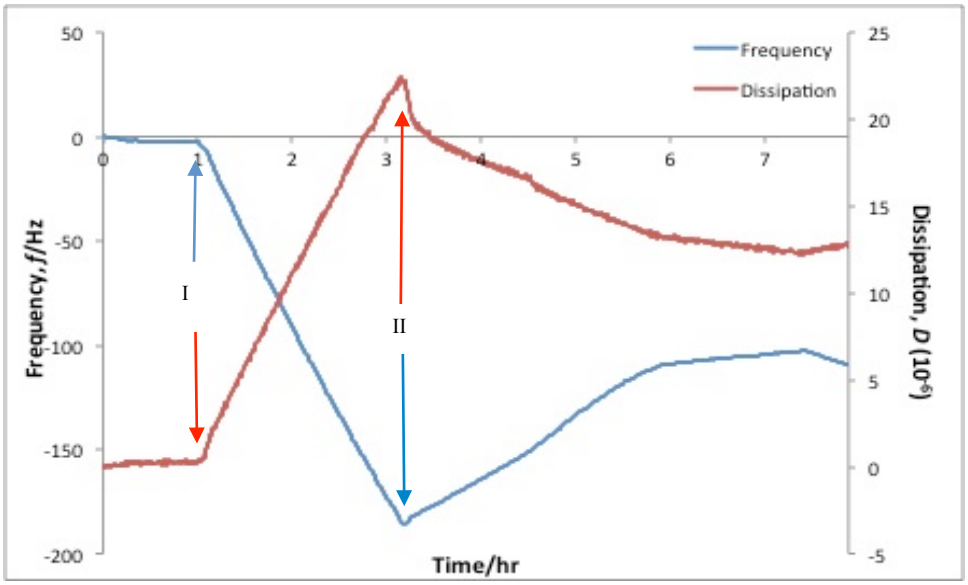

Figure 24 An example of the changes in frequency and dissipation (of the 5th overtone) for wood extractives adsorption onto chromium surface at 25°C as solutions were introduced into the QCM-D chambers. (I) WE colloidal suspension was introduced into the chambers for 2 h once a constant baseline was achieved. (II) Rinsing commenced with background solution for 4 h.

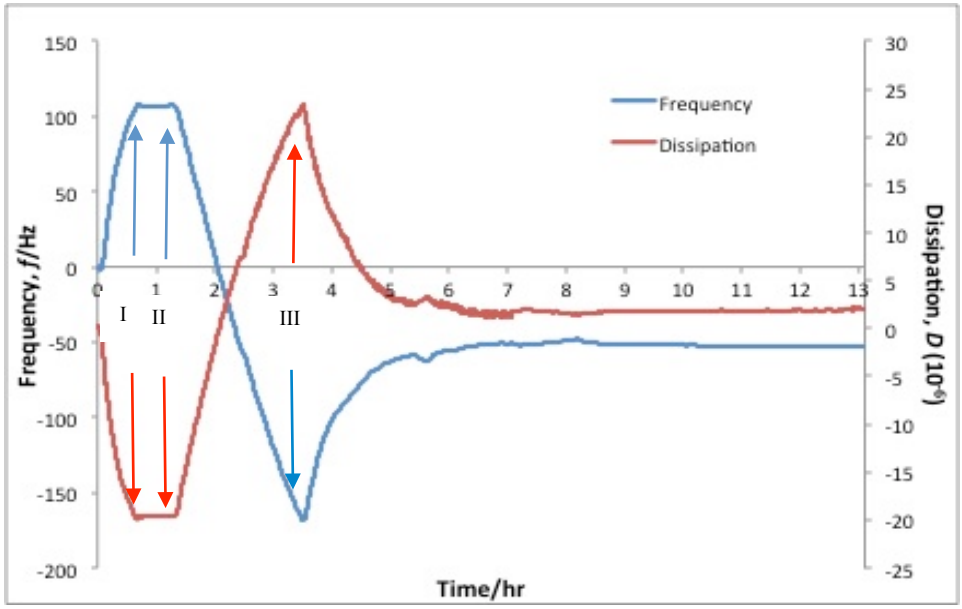

Figure 25 An example of the changes in frequency and dissipation (of the 5th overtone) for wood extractives adsorption onto chromium surface at 50°C, as solutions were introduced into the QCM-D chambers. (I) Temperature of the chambers was increased from room temperature to 50°C. (II) WE colloidal suspension was introduced into the chambers for 2 h once a constant baseline was achieved. (III) Rinsing commenced with background solution for 4 h.

From the *f* and *D* results, the frequency-vs-dissipation (*f/D*) results (value of *f* divided with *D* value) were calculated at the maximum mass adsorption relative to the baseline. Figure 26 compared the *f/D* of the adsorption experiments for all colloidal materials on the cellulose and chromium surfaces at both 25°C and 50°C. Increasing the temperature from 25°C to 50°C for adsorption onto the cellulose surface showed a decrease in *f/D* values for OA and MM colloids, whereas it increased for AA colloids and remained the same for TrO and WE colloids. With chromium, the *f/D* values were very similar for all the colloidal materials studied as the temperature increased from 25°C to 50°C.

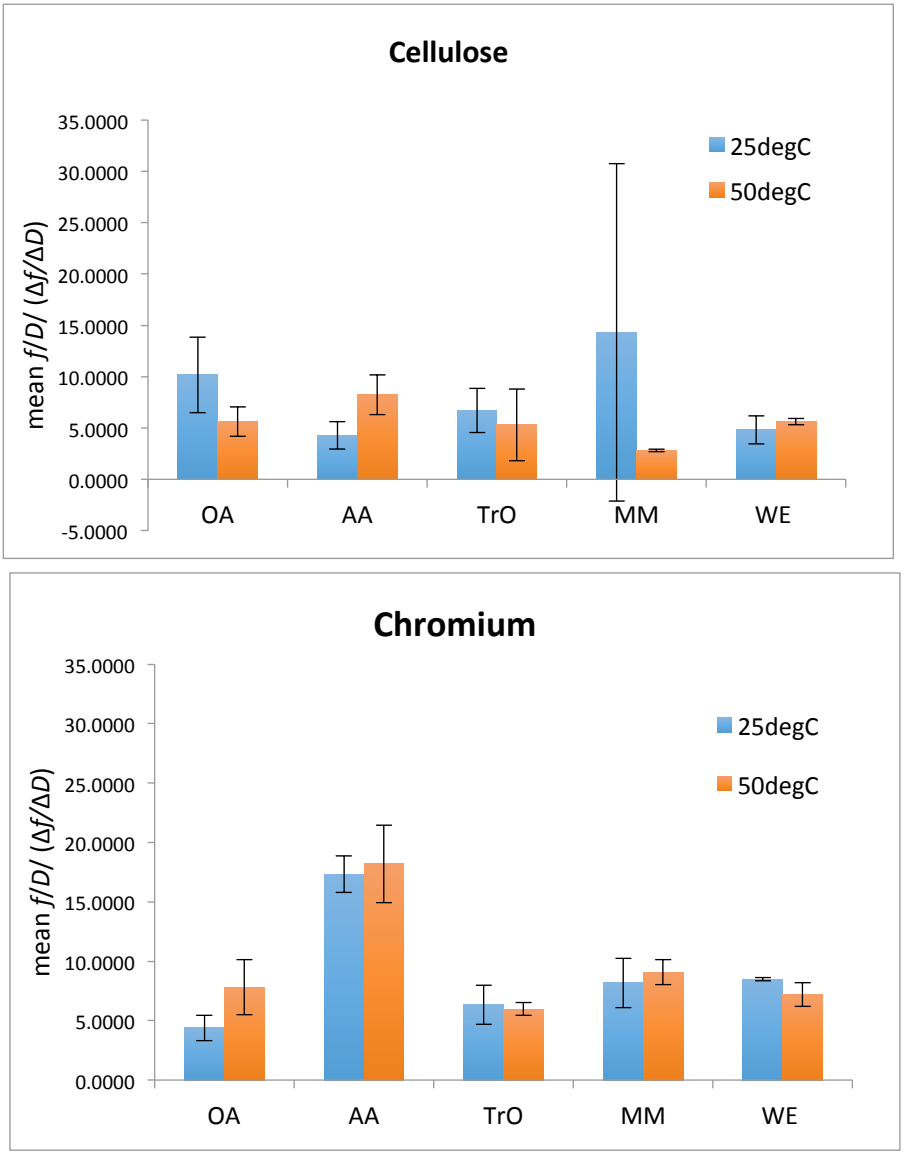

Figure 26 Mean *f/D* values (with 95 % confidence interval) of all colloidal materials at point of maximum adsorption on both cellulose (MCC) and chromium surfaces at both 25°C (25degC) and 50°C (50degC).

Figure 27 and Figure 28 show representative plots of the calculated mass deposited onto the cellulose and chromium surfaces at 25°C and 50°C as a function of time. The adsorption of all colloidal types, except OA, at 25°C onto a cellulose surface showed a two phase adsorption – a rapid adsorption phase at the start (denoted by 'fast' in Figure 29), followed by a slower adsorption phase (denoted by 'slow' in Figure 29) that continued until the rinsing of the flow cell commenced at about 2 hr. At 50°C the adsorption onto the cellulose surface exhibited only a single phase adsorption for all colloidal materials, except for the MM colloidal material.

There was only a single adsorption phase for all colloidal materials at both 25°C and 50°C for adsorption onto the chromium surface. In some cases for AA (at 25°C) and TrO (at 25°C and 50°C), the adsorption onto the chromium surface reached a plateau before rinsing was commenced, whereas for the other colloidal types the adsorption continued until the rinsing was commenced.

The rates of adsorption of the different colloidal types onto the cellulose and chromium surfaces at 25°C and 50°C, estimated from the slopes of the quasi-linear region(s) in Figure 27 and Figure 28, were compared in Figure 29. Where there were two apparent linear regions, the different rates were estimated by considering each quasi-linear region up to the point of inflexion. In general, the rates of adsorption of AA and TrO colloidal materials onto a cellulose surface were much greater than that of MM and WE colloids, while the rate of adsorption of OA was the lowest. On the chromium surface, AA colloids showed the greatest adsorption rate followed by TrO and MM colloids. OA and WE colloids exhibited the lowest rate of adsorption on the chromium surface.

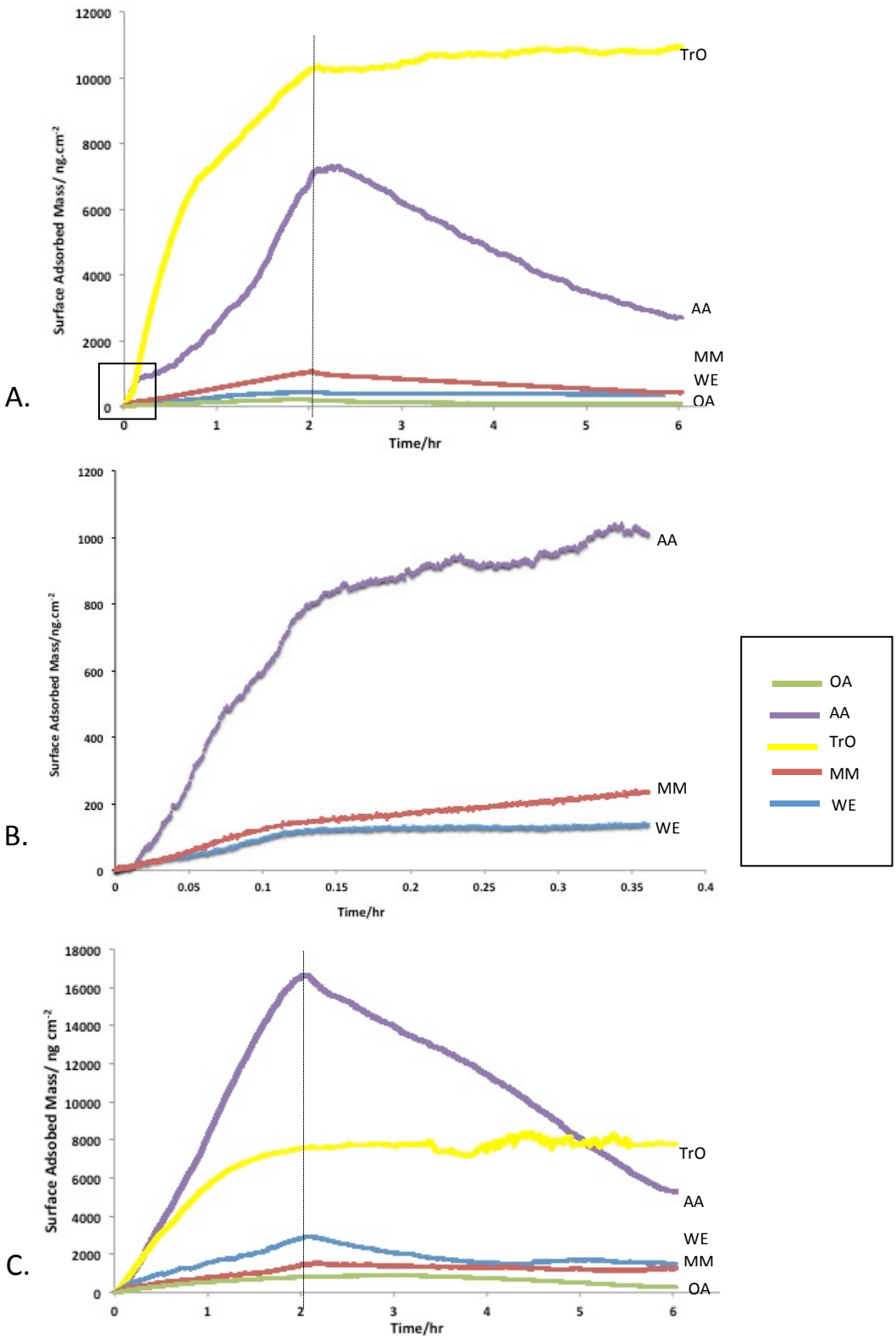

Figure 27 Representative plot of the time dependent adsorption of different colloidal materials on cellulose at 25°C (A) and 50°C (C). Graph (B) is a high-resolution plot of initial adsorption region of abietic acid (AA), wood extractives (WE) and mixed model (MM) on cellulose at 25°C (delineated by boxed area in (A)).

a.

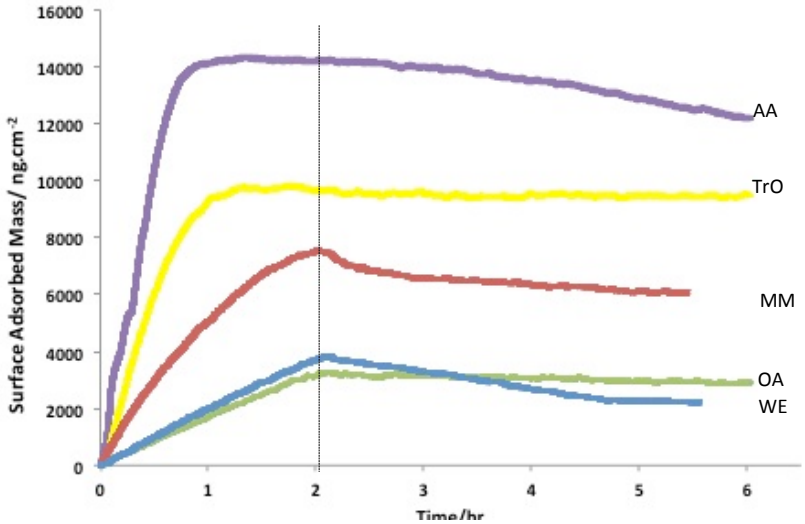

b.

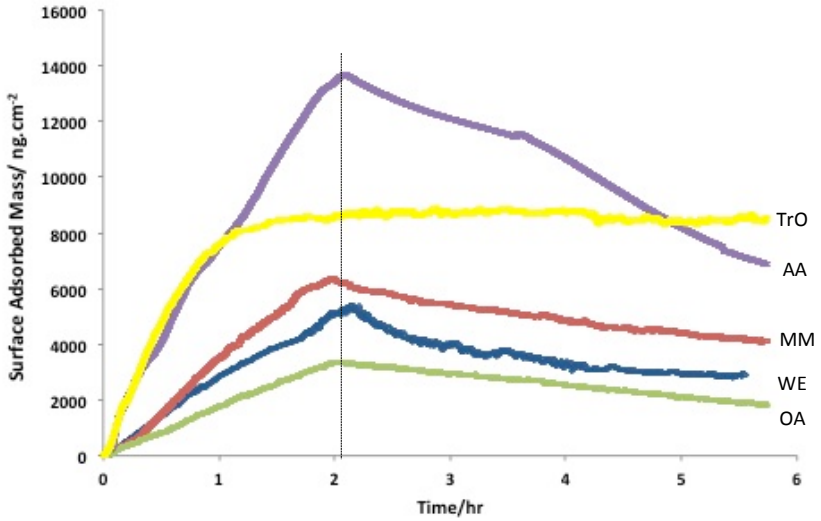

Figure 28 Representative plot of 'mass deposited per unit area against time' of different colloidal materials on chromium surface at 25°C (a) and at 50°C (b).

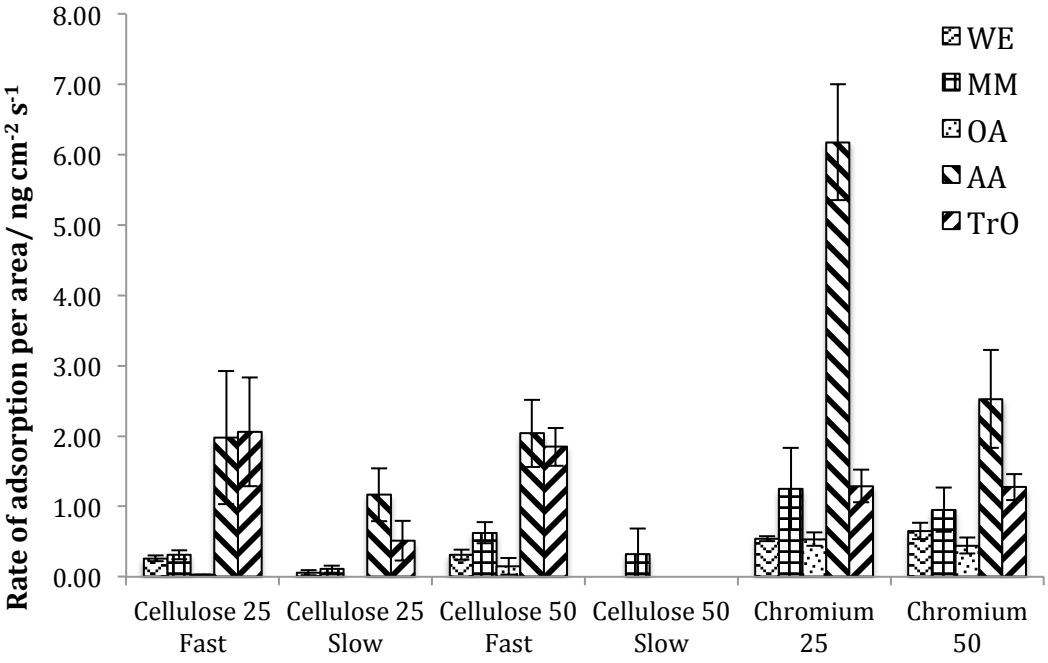

Figure 29 Rate of adsorption (ng cm^{-2} s^{-1}) of different colloid types on cellulose and chromium surfaces at both 25°C and 50°C. ('Fast' and 'Slow' denotes the different regions of rate on the adsorption process.)

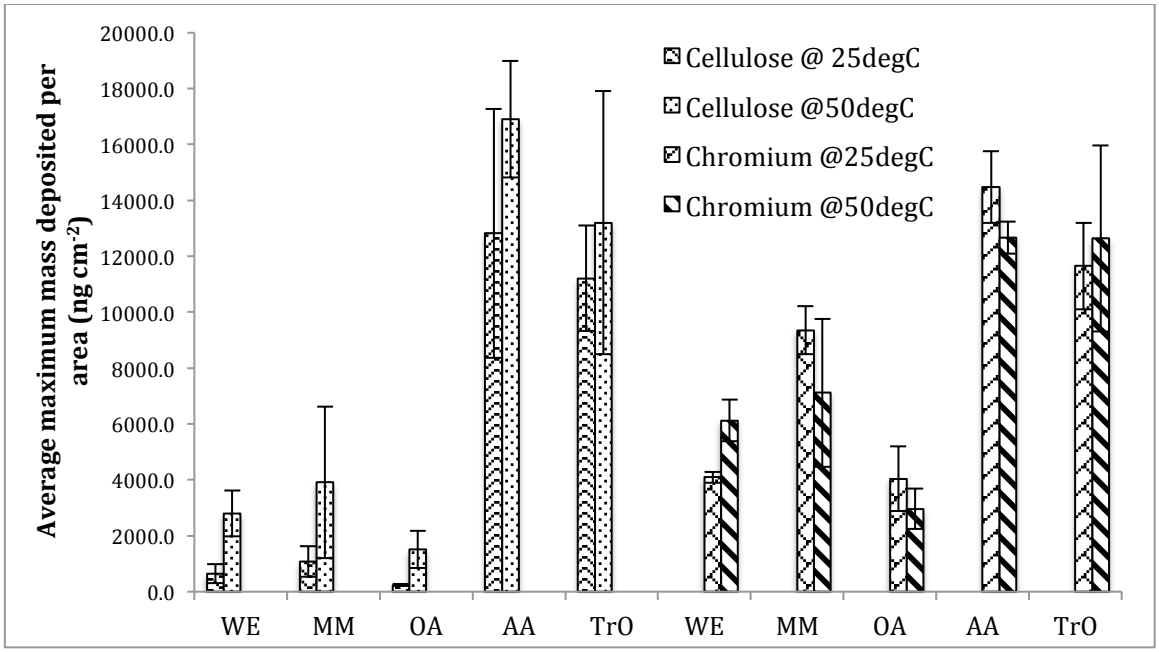

Figure 30 Average maximum mass deposited per unit area (ng cm^{-2}) for different colloidal materials comparing two different temperatures (25°C and 50°C) on two types of surfaces: cellulose and chromium surfaces.

Figure 31 compares the average maximum mass of each colloidal material deposited at 25°C and 50°C onto the cellulose and chromium surfaces. Several key observations can be made from Figure 31 with regards to the effect of temperature, model surface type and colloidal material being deposited. In the case of cellulose surface, more material was deposited at 50°C than at 25°C for all colloidal material. For the chromium surface, the average mass of colloidal material adsorbed was less at 50°C than at 25°C, with the exception of wood extractives and triolein colloidal types, though the difference was not statistically significant. Generally, the mass of colloidal material adsorbed on chromium at 25°C was higher than on cellulose at this temperature for all colloids tested. Abietic acid and triolein were found to adsorb onto cellulose by as much as a factor of ten compared to other colloidal material onto cellulose at both temperatures. A significantly greater mass of wood extractives, mixed model and oleic acid were adsorbed onto the chromium than on the cellulose surface at 50°C. Overall, the total mass of colloidal materials adsorbed on the cellulose and chromium surface followed a similar trend, with abietic acid and triolein clearly demonstrating the greatest mass adsorbed on both surfaces. The average mass adsorbed was slightly higher for the mixed model compounds, followed by wood extractives. Oleic acids have the lowest average mass adsorbed on the cellulose and chromium surfaces. This is especially significant when the relatively low concentration of abietic acid in solution is considered. From an 86 mg L^{-1} suspension of abietic acid, 12800 ng cm^{-2} was deposited on cellulose at 25°C. In comparison, only 240 ng cm^{-2} of oleic acid was deposited from an initial concentration of 217 mg L^{-1} and 11200 ng cm^{-2} of triolein was deposited from an initial concentration of 407 mg L^{-1} under the same conditions.

Figure 31 shows the final percentage of material desorbed from each surface when rinsed with 6 mM NaCl (aq) for a 4 h period. Triolein was found to adsorb very strongly to both the cellulose and chromium surfaces, as it did not desorb during the rinsing process. Oleic acid, abietic acid and mixed model colloids desorbed more readily from the cellulose surface than from the chromium surface at 25°C. At 50°C, there is no significant different in the amount of colloidal material desorbed from both surfaces for any of the colloidal material except wood extractive colloidal material. On the cellulose surface, almost double the amount of WE colloidal material was lost at the higher temperature (50°C), whereas a comparable amount of WE colloidal material desorbed from the chromium surface at both 25°C and 50°C. However, unlike the adsorption process, the desorption process was found to be very variable.

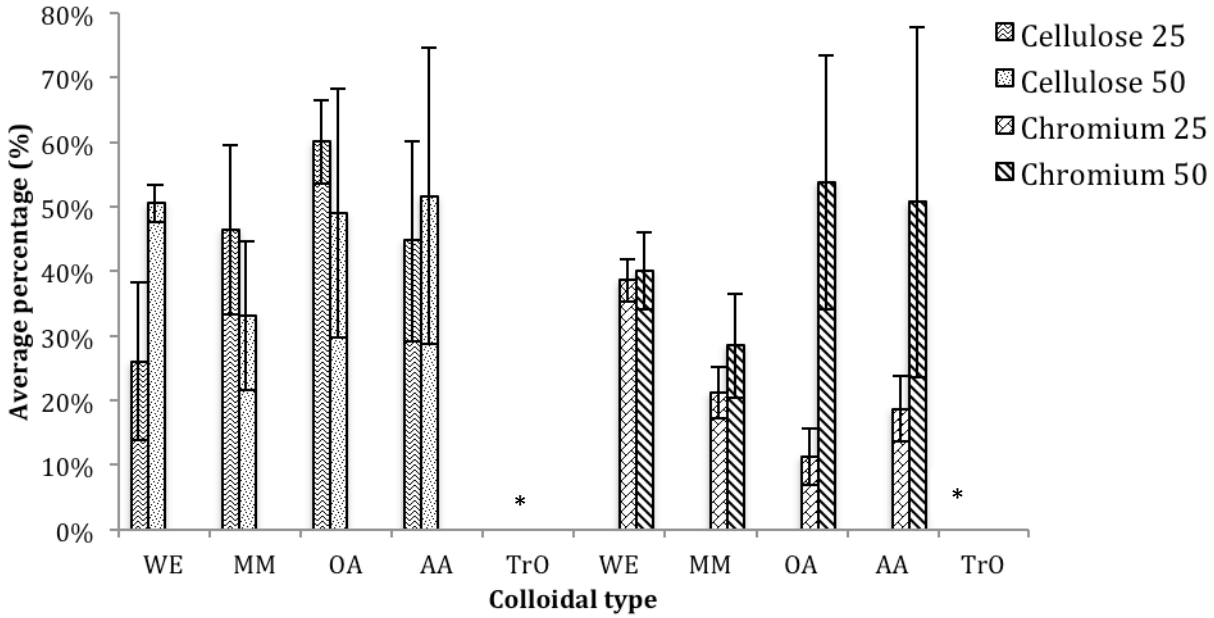

Figure 31 Average percentage of colloidal materials desorbed from cellulose and chromium surfaces at 25°C and 50°C. Asterisks marked no desorption of triolein (TrO).

3.4 Discussion

Surface chemistry of the materials plays an important part in determining the type of interaction occurring between the surface and the colloids. Microcrystalline cellulose surface is believed to be rich in hydroxyl (-OH) groups while a chromium surface in ambient conditions will form, at least in part, an oxide layer. In aqueous environment, both of these surfaces are assumed to be weakly anionic in nature, as well as hydrophilic as shown by contact angle measurements (Table 15).[90] The adsorption of oleic acid and abietic acid onto these weakly anionic surfaces is likely due to hydrogen bonding between the carboxyl groups on the fatty acid and resin acid and the oxygen groups on the surface. The pK_a value of oleic acid is reported to be 8.22 at 25°C and 8.29 at 50°C,[62] while the pK_a value of abietic acid is 7.26 at 25°C and 6.18 at 50°C.[62] As the experiments were conducted at pH 4 – 5, the carboxyl groups on the fatty acid and resin acid colloids are predominately protonated, which will support the postulation of hydrogen bonding between the functional groups on the colloids and the model surfaces.

Frequency-vs-dissipation (*f/D*) values give an insight to how 'soft' or 'hard', or 'viscoelastic' or 'elastic', the adsorbed layer is. The higher the *f/D* value, the 'stiffer' the adsorbed material, and vice versa. The difference observed in *f/D* values (Figure 26) may be caused by the variation in colloidal size when adsorption occurs on the QCM sensors. It may also be caused by the different mode of adsorption of

colloids during the adsorption process. The use of *f/D* values allows the consistency of deposited colloidal materials to be checked. Results showed that AA colloidal material forms the most rigid layer on the surface, whereas deposited OA, TrO and WE colloidal materials are relatively soft. This is consistent with the observation made during the attachment of colloids onto an AFM cantilever tip, where AA colloids maintained a spherical shape but OA, TrO and WE colloids spread during the attachment process (chapter 4).

In general, adsorption onto surfaces occurs when molecules achieve greater stability by precipitating or adsorbing onto these surfaces than when they are in solution. Adsorption of a solute from suspension also involves competition between the solute and solvent for the adsorption sites.[42] The adsorption process can result in either monolayer coverage or multilayer coverage of materials on the surface. Figure 32a shows a simple monolayer coverage that could occur with no particular orientation of the molecule on the surface. Figure 32b represents multilayer adsorption that could precede monolayer adsorption or remain as a partial multilayer coverage, while Figure 32c shows multilayer adsorption after complete monolayer coverage. For molecules with charged or polar groups such as fatty acids and resin acids, Figure 32d shows a monolayer of molecules that can either interact with the surface via a head to surface interaction or tail to surface interaction. The orientation of the molecules on the surface is governed by the relationship between the surface and the adsorbate properties such as hydrophobicity and the presence of active sites that could lead to specific adsorption. For an aqueous suspension with fatty acids and resin acids adsorbing onto a hydrophilic surface (such as cellulose and chromium surfaces), the carboxylic head groups are more likely to interact with the active sites on the surface and the hydrophobic tails would protrude into the aqueous solution. This particular single layer adsorption is not stable in aqueous solution as the hydrophobic tails are exposed to the aqueous environment. Thus a second layer of molecules would interact with the exposed hydrophobic tail to form a bilayer, where the polar head groups interact favourably with the aqueous environment as shown in Figure 32e.

Differences in the shape of the adsorption curves and also the mass of the adsorbates onto the two different surfaces provide information about the dynamic adsorption process. The adsorption of the colloids onto the cellulose and chromium surfaces indicates continual multilayer adsorption, evident through the measured mass being far beyond that expected for a monolayer adsorption with the maximum amount adsorbed not reached prior to the rinsing process (with the exception for adsorption of abietic acid and triolein onto the chromium surface at 25°C where saturation of surface occurred as indicated by the plateau region achieved in Figure 28a). The single adsorption rate onto chromium may

indicate non-specific interactions occurring between the surface and the colloidal molecules as shown in Figure 32b and Figure 32c.

The two different adsorption rates observed with the abietic acid, triolein, mixed model compounds and the wood extractive colloids onto cellulose may be explained by a two-step adsorption in which a monolayer is formed on the surface followed by multilayer adsorption. The point of inflexion at which the rate changes should correspond to the point where monolayer coverage occurred. The theoretical mass adsorbed at monolayer coverage (M_a) for each compound (assuming full surface coverage) can be determined by Equation 6.

$$M_a = \frac{Mw}{(S_a \text{ x } N)} \qquad \text{(Equation 6)}$$

where S_a is the molecular area of the molecule adsorbed onto the surface, Mw is the molecular weight of the molecule and N is Avogadro's number.

For abietic acid molecule, with Mw of 302 g mol^{-1} and cross section area of 1.4 nm^2 (obtained from molecular modelling using Gaussview), the estimated mass of a molecular monolayer is 35 ng cm^{-2}, or 70 ng cm^{-2} if a bilayer occurs. This is significantly less than the 800 ng cm^{-2} observed at 25°C in Figure 27 (at the point where the second adsorption phase commenced). The concentration of abietic acid in solution is well above the critical micelle concentration (CMC), determined previously as 3 mg L^{-1}.[105] This indicates that abietic acid is not adsorbing as individual molecules but as colloids or agglomerates. Likewise with the adsorption of triolein onto cellulose at 25°C, (Mw = 885 g mol^{-1} and cross sectional area of 1.26 nm^2), the 7000 ng cm^{-2} adsorbed at the point of inflexion is significantly higher than the estimated mass adsorbed at molecular monolayer coverage (approximately 116 ng cm^{-2}) again indicating that adsorption is not of individual molecules on the surface but as agglomerates. As for oleic acid, the molecules can either adsorb in a flat configuration on the surface or a close-packed configuration with the hydrocarbon chain orientated perpendicular to the surface or something between the two. Applying the same calculations as before, the theoretical mass of an adsorbed monolayer of oleic acid would be 42 ng cm^{-2} adopting a flat orientation (assuming cross sectional surface of 1.14 nm^2 [106]) and 234 ng cm^{-2} for a perpendicular orientation (assuming a surface area of 0.2 nm^2). The estimated maximum mass of oleic acid adsorbed is about 230 ng cm^{-2} at 25°C and about 1500 ng cm^{-2} at 50°C (Figure 27). Therefore, at 25°C, adsorption of oleic acid seems to reach monolayer coverage if the molecules are adsorbed perpendicularly, however this orientation would be unfavourable as it leaves the hydrophobic tail of the oleic acid exposed to the aqueous environment. The concentration of oleic acid is also much greater than the CMC value of 4.5 mg L^{-1}. Therefore, oleic acid is more likely

also adsorb as colloids or admicelles[43] onto the cellulose surface. The agglomerates or admicelles of these adsorbed colloidal materials may spread to form a thin film when in contact with the surface.[34]

The adsorption of colloids onto the chromium surface can be explained by multilayer adsorption where molecules randomly adhere to the surface and interact with each other non-specifically, resulting in non-specific adsorption (Figure 32f). As the interactions between the surface and the colloids are non-specific, the adsorption mechanism would be controlled by solubility limitations. The molecules adsorbed onto the surface may be stabilised by a cooperative interaction with other solute colloids already on the surface. This means that multilayers may begin to form before monolayer surface coverage is achieved. Based on the mass adsorbed and the calculated theoretical masses at monolayer coverage, the adsorption of abietic acid and triolein onto the chromium surface (at 25°C) is not of molecular monolayer coverage. The observed plateau in the adsorption (example in Figure 28) may be due to either equal rates of adsorption and desorption of colloids or saturation of the adsorption surface, which prevents further interaction between surface colloids and other molecules or colloids in suspension.

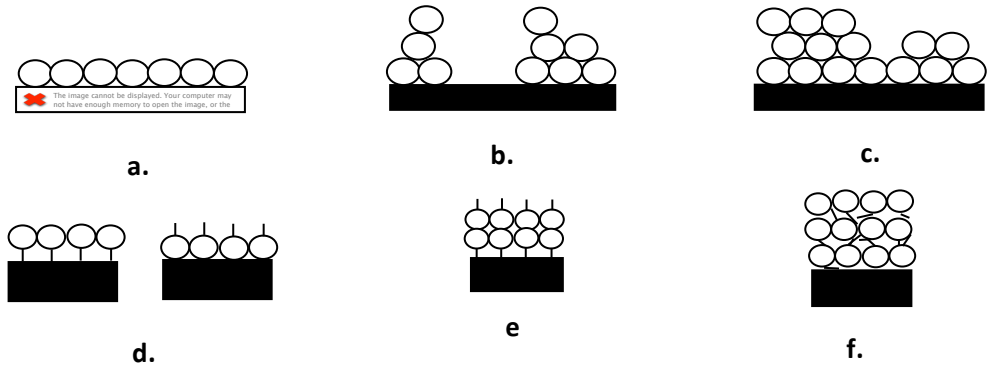

Figure 32 Possible adsorption process of material onto test surfaces: (a) Monolayer coverage; (b) Multilayer adsorption without full monolayer coverage achieved; (c) Multilayer adsorption after full monolayer coverage achieved; (d) tail-to-surface interaction or head-to-surface interaction of monolayer adsorption; (e) head-to-head and tail-to-tail multilayer adsorption; (f) non-specific multilayer adsorption. For (d) – (f), the sphere represents oxygen-containing groups, sticks represent hydrophobic portion.

Based on Figure 29 and Figure 30, abietic acid adsorbed more rapidly and to a greater extent than oleic acid. This suggests that abietic acid has a stronger interaction with both surfaces compared to oleic acid. Maher et al. has shown that, as a single component, abietic acid has a stronger tendency to deposit onto fibre or non-fibre surfaces than oleic acid or triolein.[107] However, the observation of triolein remaining in the dissolved colloidal phase in the study by Maher et al. contradicts the observation made in this study where triolein deposits onto surfaces as quickly as deposition of abietic acid. The

difference in behaviour could be explained by the presence of stabilising carbohydrate materials in the extracted pulp fibres used by Maher. These carbohydrate materials help to stabilise the colloidal material (namely triolein) in solution.[107]

During the desorption process twice the amount of abietic acid desorbed from the cellulose surface than from the chromium surface (Figure 31). This indicates that the abietic acid was adsorbed more strongly and with a more stable arrangement on the chromium surface, an observation in line with the previously mentioned phenomena where abietic acid preferentially deposits on chromium surfaces in the papermaking and printing processes. Even though both cellulose and chromium surfaces can be considered “hydrophilic”, contact angle measurements of these two surfaces showed that the chromium surface is more hydrophilic than the cellulose surface. This may explain the stronger interaction of polar aggregates such as abietic acid with chromium than with a cellulose surface.

The adsorption of triolein (TrO), representative of triglycerides, is very different to the adsorption of oleic acid or abietic acid. The lowest energy molecule conformation of a triolein molecule is where all the hydrophobic tails are directed into the surrounding aqueous solution.[25] Dispersion forces can be assumed to be very strong between triolein molecules as compared to oleic acid and abietic acid molecules because triolein has a greater surface area of interaction. More importantly, the interaction between triolein molecules and a hydrophobic surface is stronger than its interaction with water. This can be extended to strong interactions between triolein molecules due to poor solute-solvent interaction, leading to negligible or no desorption of triolein over the 4 h of rinsing after deposition (Figure 31).

Temperature has been shown to effect the properties of wood extractives, including viscosity[15] and phase distribution or solubility of wood extractive components.[17, 108, 109] Solubility of colloids are shown to increase with increasing temperature[17, 108, 109], while the viscosity of these suspensions decreases at higher temperature.[15] This may infer that the colloidal suspension becomes more fluid-like, increasing the probability of both the attraction of the molecule to the surface and the attraction between molecules. As the papermaking process generally operates at around 60°C, it is necessary to consider how higher temperature would affect the deposition process of these materials onto these surfaces. Increasing temperature from 25°C to 50°C was found to have greater effect on adsorption onto cellulose surface than onto chromium surface. As well as decreasing the viscosity of the colloids, increasing the temperature may also expose more active sites on the cellulose surface.[110] With these contributing factors, the deposition of colloids onto the cellulose surface would be expected to be greater at a higher temperature, as is shown to occur in Figure 30. Though much the same logic should apply on the chromium surface, the deposition of all colloidal material remained reasonably constant at

higher temperature. This may indicate that the increased deposition onto cellulose at higher temperatures may be largely due to the increase in the active sites exposed on the cellulose surface caused by swelling of the structure allowing increased exposure of the cellulose chains. These active sites may have been previously tightly bound when at a lower temperature.[110]

A three-layered model for wood extractive colloid structure was proposed by Lee et al[27], where the triolein occupies the hydrophobic core, resin acids on the outermost shell and the fatty acid layer exists as a mobile layer between the outer layer and inner core. Interactions between different components in mixed model and wood extractive colloids have been found to stabilise the colloids to a greater extent than colloids composed of the single components.[111, 112] In addition to these interactions between the primary components of the colloid itself, it is known that there may exist components in wood extractives such as wood carbohydrates and lignin components that will help stabilise the colloids in solution.

Our results for both the mixed-model and wood extractive colloidal materials demonstrate significantly lower adsorption to both chromium and cellulose substrates at 25°C and 50°C, compared to single component abietic acid and triolein colloids (Figure 30). Additionally, the rates of adsorption of mixed model and wood extractives were less than for triolein and abietic acid on cellulose at both 25°C and 50°C (except for the second adsorption phase at 50°C where a two phase adsorption was only demonstrated for the mixed model colloid). On the other hand the rate of adsorption of abietic acid on chromium was significantly greater than both the mixed model and wood extractives colloids, while the rate for triolein adsorption on this surface was significantly greater than wood extractives, but comparable to the mixed model colloid. The oleic acid colloid exhibited generally comparable or smaller values than both the mixed component colloids (Figure 29 and Figure 30).

There is clearly an indication of stabilisation effects in the mixture of oleic acid, abietic acid and triolein - mixed model compound colloids, even though the effects are not as significant as with wood extractives due to the lack of other components that may exist in the wood extractive sample. However despite having different ratios of oleic acid and abietic acid within mixed model compound colloids and wood extractives, the amount adsorbed and desorbed onto microcrystalline cellulose and chromium surfaces were quite similar (Figure 30 and Figure 31).

3.5 Conclusion

QCM-D was shown to be a useful technique for studying the adsorption of different colloidal materials onto both cellulose and chromium surfaces. On both the model surfaces, the greatest adsorption occurred for abietic acid and triolein, pointing to these compounds being the least stable in solution and having greatest interaction with the surfaces. Triolein, in particular, was found to adsorb strongly to the surface as no desorption occurred during the rinsing process. Comparatively, OA, MM and WE colloidal materials exhibited lower adsorption, showing that these colloids may be more stable in solution and have less interaction with the cellulose and chromium surfaces.

Adsorptions of these colloidal materials are believed to follow multilayer adsorption pattern, which was also observed in chapter 2. Differences in the adsorption curves between the two different surfaces were observed. Adsorption onto cellulose appeared to be two-phase process in which it is proposed that complete or nearly complete surface coverage occurs prior to further multilayer deposition of colloids interacting with each other. The layers of colloid aggregates on the surface readily desorb with rinsing of the surfaces. On the chromium surface, it is proposed that multilayer adsorption occurs slightly differently with colloids interacting with each other and cooperatively stabilising the interaction with the surface thus building up layers prior to achieving full surface coverage. Less of the materials are removed in the rinsing stage compared with the cellulose surface indicating that the aggregate interactions are slightly stronger when formed in this way on the chromium surface.

From the experimental results, increasing temperature had a greater effect on the deposition of all colloidal types onto cellulose surface than onto chromium surface. Deposition was greater on the chromium surface at both temperature tested (25°C and 50°C). As for deposition onto cellulose surface, more AA was deposited at 50°C. TrO deposition were quite similar onto both surfaces at 50°C. This indicates that increasing the temperature changes the surface properties of colloidal materials as well as the cellulose surface, which leads to greater deposition on the cellulose surface. However, as the surface properties for a chromium surface do not change significantly with increased temperature, the changes to deposition can only be attributed to changes in properties of the colloidal materials.

When compared with results from adsorption isotherm modelling for deposition of colloidal material onto microcrystalline cellulose at 50°C (chapter 2), both experiment methods yield similar trend of adsorption, where deposition of AA was the greatest over the other colloidal types.

Chapter 4 Atomic Force Microscopy (AFM) – Force Measurements

4.1 Introduction

Atomic force microscopy (AFM) was developed as an extension to scanning tunnelling microscopy (STM) to allow topographic imaging of both conductive and insulating surfaces down to atomic resolution. It also allows measurement of interaction forces of colloid(s) that are influenced by microscopic effects such as fluctuations in thermal energy, osmotic stress, specific ion effects, hydrophobic interactions and so on.[113, 114] The ability to measure the microscopic effects enables the imaging of surfaces,[113] while force measurement (of interaction forces) allows the study and understanding of the properties between tip, surface and any medium between them.[114]

For the imaging function, the AFM consists of a cantilever with a sharp tip at its end that is used to scan the specimen surface. When the tip is brought into proximity of a sample surface, the forces between the tip and sample lead to a deflection of the cantilever according to Hooke's Law, F = kd, where k is the spring constant of the cantilever and d is the cantilever deflection.[113] The deflection is measured using a laser spot reflected from the tip surface of the cantilever into an array of photodiodes. Adjustment of the z-piezo coupled with feedback mechanism of the instrument is usually employed to adjust the tip-to-sample distance to maintain a constant force between the tip and the sample, to avoid causing surface damage. The topographical image of the sample will be generated by plotting the height position of the cantilever deflection against its position on the sample.[113, 114]

Force measurement is a widely used application of AFM, where the AFM probe is moved to approach the surface and makes contact. The deflection is recorded as the cantilever continues to push into the surface when the tip is lowered by the z-piezo and any deflection will be converted to distance and force values (Figure 33).[115] The change in distance recorded reflects the physical separation between the probe and the surface. When the probe and surface have no contact, the cantilever is not deflected. However, when there is interaction between the probe and surface, deflection of the cantilever will be a combination of static deflection and the piezo displacement. If the interaction is strongly attractive, the gradient of the force exceeds the spring constant, spring instability occurs and the tip "snaps" into the surface. When the probe and surface make 'contact' on an infinitely hard surface, the deflection of the cantilever (in volts) is equivalent to the distance moved by the z-piezo (referred to as constant compliance). The inverse of the slope of the deflection (volts) versus distance in the contact region give the optical lever sensitivity of the cantilever (nm/V), which can be used to convert the cantilever

deflection in volts to a distance, typically in nanometers. By knowing the cantilever deflection the interaction force can be determined using Hookes Law.[113]

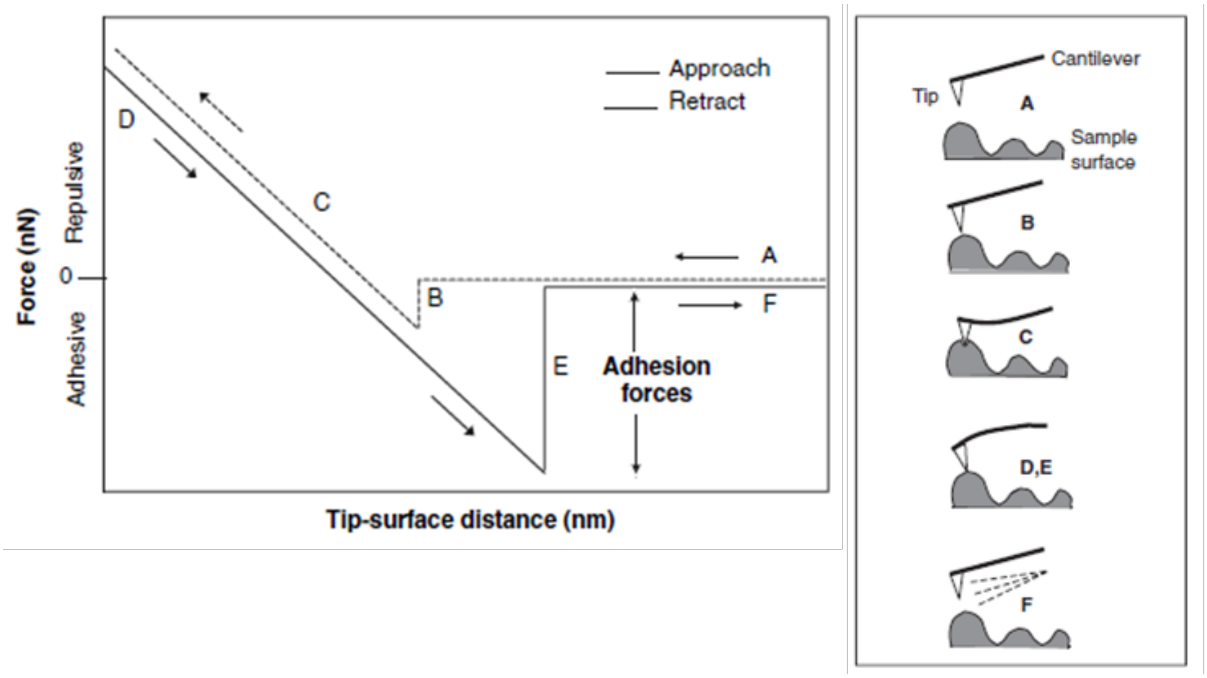

Figure 33 Idealised force-distance curve describing a single approach-retract cycle of the AFM tip during surface scanning. (A) The AFM tip is approaching the sample surface. (B) The initial contact between the tip and the surface is mediated by the attractive van der Waals forces that lead to an attraction of the tip toward the surface. (C) A contact and default force applied on the tip upon the surface leads to sample indentation and cantilever deflection. (D) The tip undergoes retraction and break loose from the surface. (E) The adhesive force that hampers the tip from breaking loose from the surface measured. (F) The tip withdraws and loses contact with the surface after overcoming the adhesion forces.

AFM is capable of measuring forces of interaction between colloids or between a colloid and a surface using the colloidal probe technique of attaching a colloid to the end of an AFM tip using glue and a micromanipulator. Smooth, spherical hard particles with a defined radius were used when the technique was first introduced. Hard microspheres commonly and traditionally used are silica, zirconia, alumina and polymeric microspheres. By attaching a particle with a defined geometry and contact radius to a cantilever surface, the force can be quantitatively analysed with greater sensitivity, as the total force is higher. It is also easier to manipulate the chemical composition of the surface of the particle and substrate making possible a variety of interaction and hydrodynamic force measurements.[114] Different types of colloids can also be attached to mimic and study the colloidal system of interest. The forces experienced between the tip and substrate can be measured and quantified,[113, 114] then represented as force-versus-distance curves. These force curves may be used to provide information such as the

Hamaker constant, surface charge densities, elasticity, and adhesion. Colloidal force measurements are carried out:

1) to understand surface forces in the stabilisation of dispersions;
2) to gain better understanding of adhesion;
3) to study nanomechanical properties of materials; and
4) to study properties of single molecules (such as rupturing force or stretching of polymer chains).[116]

AFM force measurements can be carried out in both air and aqueous environment which overcomes the limitation of other similar instrumentation such as scanning tunnelling microscopy (STM) or scanning near-field optical microscopy (SNOM).[114] Factors that will affect force measurements are surface roughness, the spring constant and resonance frequency of cantilever, and the design, type and shape of the cantilever.[114]

Research with soft particles is a fairly new area as most force measurement studies have been carried out with hard particles as mentioned above.[114] In the last decade, there have been a limited number of studies carried out using AFM with soft particles such as bubbles and oil droplets.[117-120] The purpose of these investigations is to model and understand specific interactions between soft particles. Dagastine et al. studied the attractive interaction between a rigid silica microsphere with a polar organic liquid droplet in a series of inorganic electrolyte aqueous environments.[117] The outcome of the experiment showed that whether the force-separation behaviour is due to DLVO or non-DLVO behaviour depends on the type of electrolyte present. In their research, the attractive force is consistent with DLVO prediction when sodium nitrate or similar systems are used. However, systems in sodium perchlorate and calcium nitrate do not display the typical DLVO interaction behaviour.[117] Manor et al. developed a theoretical model for dynamic forces of a bubble with smooth mica plate, then with varying boundary conditions and electrical double layer thickness.[118] In another study, Dagastine et al. developed a methodology to analyse dynamic interactions between two deformable oil droplets.[119] Lockie et al., by studying interactions between two organic droplets[120], were able to propose understanding to aqueous film drainage and ion-specificity for deformable colloidal interactions using colloidal probe AFM.

A study by Wallqvist et al. is highly relevant to this thesis as their research involved model compounds or wood extractives. They studied forces acting between abietic acid/pitch colloid (as a colloidal probe) and talc (a common pitch control additive) with the aim of investigating the forces of interaction and

mechanism between these materials. In their study, they developed a number of methods of making colloidal probes for force measurements. The first method involved coating a silica sphere with extracted wood extractive, then gluing the coated sphere onto the cantilever. The second method, known as the precipitation method, attached dried colloids with glue in air directly onto the cantilever. The final method, known as the melt method, heated a piece of material on the cantilever that formed a hemisphere, attached by molecular forces only. The force measurements collected were carried out with the colloidal probes and results (of approach force curves) were compared with theoretically calculated forces. The study concluded that forces were repulsive initially then became attractive due to bridging of submicroscopic bubbles existing on the hydrophobic surfaces on the talc and colloids. The surface nature of the colloid was found to influence the nature of the interaction between the colloid and talc.[2]

In this chapter, a new and novel technique to attach soft colloids to a tipless cantilever to measure the adhesion force between a colloid and a surface has been developed. To our knowledge, the research carried out in this project is the first to use soft wood colloid directly in force measurement experiments.

4.1.1 Aim(s)

The main aim is to measure the surface forces for the interaction between soft wood extractive colloids and model compound colloids (used to represent individual components of wood extractive) with three different model surfaces – glass, cellulose and chromium. This should provide an insight into why there is a greater tendency of resin acids to desorb from paper surfaces rather than fatty acids and triglycerides and resin acids' propensity for binding onto metal (especially chromium) surfaces.

The first part of this chapter describes the development of a new method of *in situ* attachment of the colloid to the tip from the colloidal suspension without modification to the colloid itself. This is advantageous in this research as it maintains the native structure of the colloids for adhesion experiments. The second part presents the adhesion force measurements between different colloidal probes consisting of softwood extractive colloids and model compound colloids of the different components in the wood extractives (oleic acid, abietic acid and triolein) and different model surfaces (glass, microcrystalline-cellulose and chromium surfaces). The interaction between wood extractives and model compounds with microcrystalline cellulose is used to model the interaction of wood extractives with pulp; while the interaction of wood extractives and the model compounds between chromium surfaces models the wood extractive interaction with rollers and printing press chromium-coated surface.

4.2 Method and Materials

4.2.1 Preparation of model compound colloidal suspension

The model compounds used to represent individual components found in wood extractives are oleic acid (OA, model for of fatty acids, Aldrich), abietic acid (AA, model for resin acids, Fluka), and triolein (TrO, model for triglycerides, Sigma). To make individual colloidal suspensions of approximately 600 mg L^{-1}, about 0.012 g of each compound was weighed and dissolved in acetone (<1 mL). The acetone-model compound mixture was then added to 20 mL of 6 mM NaCl (aq), and the suspension was stirred for 15 min before use.

4.2.2 Preparation of wood extractive colloidal suspension

Wood extractives (WE) were obtained from hexane extraction of *Pinus radiata* thermomechanical pulp described in the method by Stack et al.[99] Aqueous dispersion of colloidal wood extractives was made by dissolving a fixed amount of extracted wood extractive, taking into account the purity of the wood extractives, in acetone (<1 mL). This acetone-extractive mixture was then added to 20 mL of 6 mM NaCl (aq) and stirred for 15 min before use, giving a colloidal suspension of about 600 mg L^{-1}.

4.2.3 Preparation of model surfaces

Glass, cellulose and chromium surfaces used in force measurement studies were prepared as given below.

Glass surface: Glass coverslips (ProSciTech, Coverglass, No. 1, 18 mm) were wiped with 70 % ethanol solution then with 18 MΩ MilliQ water on lens paper. The cleaned glass coverslips were then dried under a gentle stream of nitrogen gas before use. This was used as a control surface in the experiments.

Cellulose surface: A microcrystalline cellulose modified surface was used to represent a cellulose surface. Freshly prepared 5% microcrystalline cellulose (Serva-Avicel PH 105, ca. 0.019 mm) suspension in 18 MΩ MilliQ water was sonicated for 12 min. The mixture was then filtered through a 0.22 μm syringe filter and the filtrate collected. Glass coverslips were cleaned as above and placed into a 5 mg L^{-1} poly(ethylene)imine (PEI) (MW 25000, Aldrich) solution on an orbital stirrer for 15 min. The PEI-coated cover slips were then gently and thoroughly rinsed with deionised water before being placed into the filtered microcrystalline cellulose suspension on an orbital stirrer for 2 h. The cover slips

were then gently rinsed with deionised water and left to air-dry before use. The cellulose-modified cover slips were not reused during the force measurements (Figure 34).

Chromium surface: Chromium-coated sensors (Q-sense AB) were cleaned with Piranha solution (70 % sulphuric acid and 30 % hydrogen peroxide) for 10 min, then rinsed with 18 MΩ MilliQ water and dried gently under a stream of nitrogen gas. The sensors were then UV-cleaned for 10 min in a Bioforce Nanosciences UV/Ozones Procleaner™, rinsed with 70 % ethanol and dried gently under a stream of nitrogen gas before use.

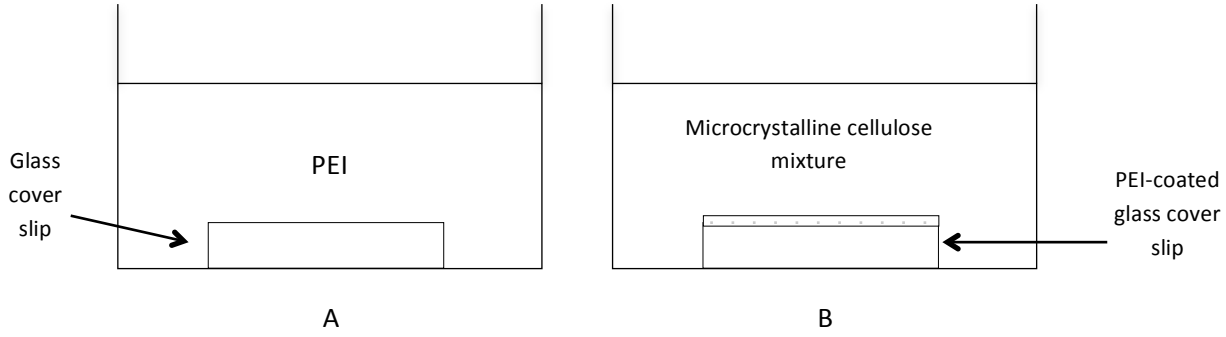

Figure 34 Schematic diagram showing the functionalization of glass cover slip with microcrystalline cellulose. (A) Firstly the cleaned glass cover slip was immersed in a solution of 5 mg/mL poly(ethylene)imine (PEI) solution for 15 min. (B) Then the PEI-coated glass cover slips were rinsed before placing into a microcrystalline cellulose particle-filled suspension for 2 hours. Then cover slip was rinsed with MilliQ water and dried with nitrogen gas gently before use.

4.2.4 Characterisation of model surfaces

Contact angle measurements were carried out on a Dataphysics Contact Angle System OCA instrument. MilliQ water (1 µL of 18 MΩ) was applied to the surface of interest and the deposited drop shape was captured on camera and the contact angle calculated by the SCA 20 software. The average contact angle values of each surface were obtained from four measurements on three replicates of each surface (n = 12).

AFM imaging of model surfaces in air was performed with a MFP-3D AFM (Asylum Research, Santa Barbara, CA). Imaging was performed in AC mode with scan rate of 1 Hz, using commercial silicon nitride cantilevers (Bruker, DNP probes) with an approximate spring constant of 0.25 N/m. Scans (20 µm x 20 µm and 1 µm x 1 µm) were performed on each model surface. The surface roughness (R_{RMS} roughness) was calculated using the AFM software (Igor Pro, Wavemetrics).

4.2.5 Functionalization of AFM cantilever tip surface

Tipless AFM cantilevers (lever A, spring constant ~0.35 N/m, NP-010/tipless/Veeco, Bruker) were used. Different functionalization methods were attempted to find the most suitable cantilever tip surface for secure attachment of the soft colloids. The methods attempted included:

(i) *No functionalization:* The tipless cantilevers were plasma-cleaned for 20 min. Then gently rinsed with ethanol, acetone followed by MilliQ water, before drying under a gentle stream of nitrogen gas.

(ii) *Positively charged functionalization:* Plasma-cleaned tipless cantilevers were functionalized with poly-L-lysine solution before rinsing off excess solution with MilliQ water. The cantilever was then dried under gentle stream of nitrogen before use.

(iii) *Hydrophobic functionalization:* The surfaces of AFM tipless cantilevers were hydrophobically functionalized to aid in attachment of colloids to the cantilever. These tipless cantilevers were plasma cleaned before treatment was applied.

a. The 1, 3-(trimethoxysilyl)propylmethacrylate (Sigma-Aldrich) was mixed with ethanol in 1:1 ratio. The cantilevers were left in the mixture for at least 5 min. The functionalised cantilevers were then rinsed with ethanol to remove excess solution and dried under a gentle stream of nitrogen gas before use.

b. The 1H, 1H, 2H, 2H-perfluorooctyltriethoxysilane (Sigma-Aldrich) was mixed with ethanol at 1:1 ratio. The cantilevers were left in the mixture for at least 5 min. The functionalised cantilevers were then rinsed with ethanol to remove excess solution and dried under a gentle stream of nitrogen gas before use.

4.2.6 Sensitivity and spring constant determination of AFM cantilever

The sensitivity of the mounted tipless cantilever was determined (before the spring constant determination) by measuring the slope of the retracting curve of the cantilever from a clean surface (in this case, a clean microscope glass cover slip). Once the sensitivity was determined, the spring constant of the particular cantilever was measured using the thermal method[121] in the MFP-3D-AFM Asylum software. Both the sensitivity and spring constant determination were done in an ambient air environment.

4.2.7 Attachment of colloid onto functionalized AFM tip

Figure 35(A)-(C) shows a scheme of how colloid attachment to the functionalized cantilever was carried out in colloidal suspension. Firstly, a drop of aqueous colloidal suspension was pipetted onto a clean glass cover slip and positioned on the AFM sample stage. Immobilised and dispersed colloidal droplets of various sizes were observed on the glass cover slip using the light microscope attached to the AFM instrument. A functionalized tip was then secured on the AFM tip holder and lowered into the colloidal suspension. The tip was left to stabilise in the suspension for several minutes before proceeding with the attachment process. The movable X-Y stage was adjusted to position the AFM cantilever above a suitable colloid. Suitable colloids for attachment were those with a diameter no smaller than half the length of the cantilever tip, nor larger than the tip itself to ensure no attached colloids spread onto the legs of the cantilever. With the AFM feedback on (in 'engage' mode) the cantilever was slowly lowered, until the tip made contact with the colloid. Attachment of the colloid usually occurred readily after 10-20 seconds, however the contact force on the colloid was slightly increased to ensure attachment. Too much applied force was observed to deform the colloid onto the glass surface, leading to its rupture and subsequent formation of a film on the substrate. The cantilever was then lifted away from the surface and checked to ensure that the colloid was bound to the tip. An image of the attached colloid was then taken using the mounted camera to measure the radius of the colloid for later use during analysis of the force curve. This method enabled colloids to be attached *in situ*. Observation of the different colloids on the cantilever is discussed under section 4.3.2.

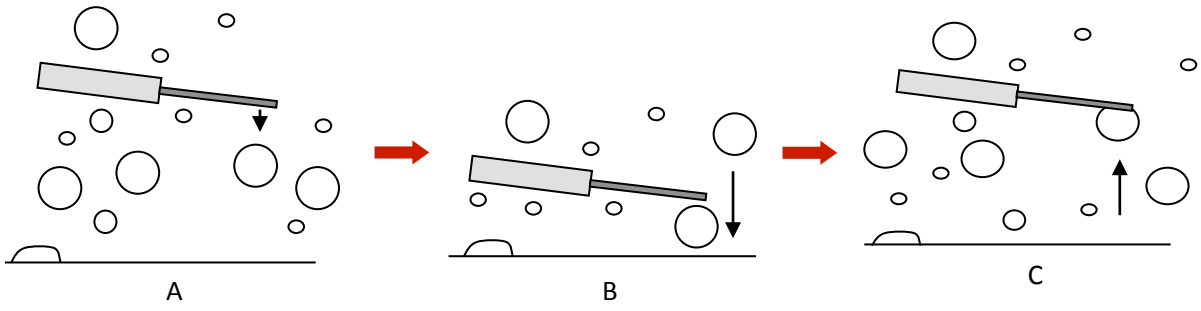

Figure 35 (A) - (C) shows the schematic of how the colloid was attached onto the functionalized tip. (A) A suitable size colloid was selected and positioned under the cantilever. (B) Cantilever tip lowered slowly onto the colloid, pushing the colloid to the surface until the colloid attaches onto the cantilever tip. (C) Lift the cantilever tip up from the surface after the colloid attaches onto the cantilever tip.

4.2.8 Force measurement on different surfaces using the colloidal tip

AFM force spectroscopy experiments were performed on a MFP-3D AFM (Asylum Research, Santa Barbara, CA) in contact mode. Force measurements were conducted in an aqueous environment. "Force" is used as the trigger channel; the trigger mode was set to "relative" and the trigger threshold determined. Relative trigger mode means that all force curves have the same preset maximum cantilever deflection relative to the cantilever's deflection at the beginning of the curve (zero deflection).[2] Different force measurement settings (such as scan rate, scan distance and force applied) were trialled and the final settings used were scan distance = 1.00 µm and scan velocity = 1.00 µm/s and force applied (trigger point) = 400 pN.

Each model surface was cleaned with (in order) ethanol, acetone, then MilliQ water followed by gently drying under a gentle stream of nitrogen gas before use. The surfaces were placed side by side on a glass microscope slide, held in place by capillary action of water between the surface and microscope slide (Figure 36). A drop of 6 mM NaCl (aq) was then placed on a glass surface (the clean model surface). The cantilever with the attached colloid was removed from the colloidal suspension and transferred into the NaCl (aq) droplet on the cleaned surface of interest. The mounted cantilever was gradually lowered until the colloid registered its first force measurement on contact with the surface. For each colloidal probe at least four force measurements were taken on each x-y location with at least three different positions on the same surface. The colloidal probe was then moved to another model surface to carry out the force measurements, unless the colloid had been lost from the mounted cantilever.

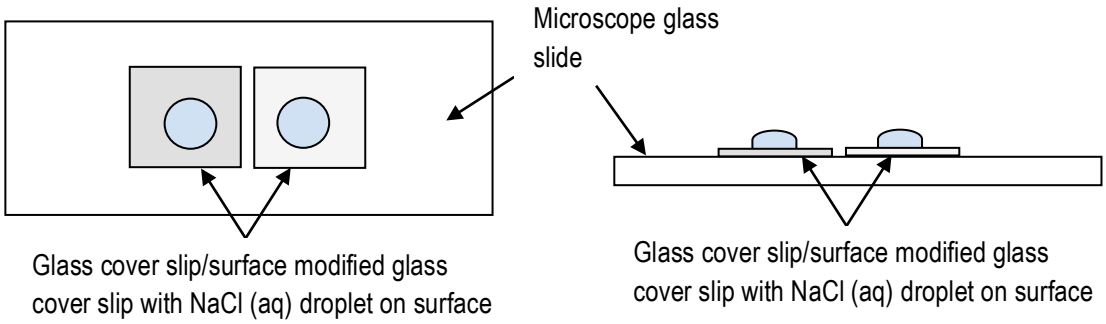

Figure 36 Schematic diagram of how the modified glass cover slips or glass cover slips, which were used as model surfaces, were placed on a microscope glass slide, which were mounted on the AFM movable stage.

4.2.9 Analysis of force curves

All the force curves collected were analysed with the MFP-3D-AFM Asylum software with the sensitivity and spring constant information included during the force-distance conversion. The zero point of each curve was adjusted and the y-axis changed to force value before the maximum adhesion force value was recorded. These force values were normalised with the radius of the colloid (measured from the 2D photo captured when the cantilever was still mounted), to obtain the adjusted force of adhesion values. The colloids were regarded as spheres, even though some of the colloids (OA, TrO and WE) were slightly spread, these were best approximated as a sphere.

4.3 Results & discussion

4.3.1 Characterisation of model surfaces

Figure 37 shows both 20 µm and 1 µm AFM height images of microcrystalline cellulose surfaces (Figure 37A and B), chromium-coated sensors (Figure 37C and D) and glass cover slips (Figure 37E and F), imaged under ambient conditions. The AFM height images show that microcrystalline cellulose-coated glass cover slips consisted of small, granule-like structures (R_{RMS} roughness = 0.80 ± 0.10 nm), whereas commercial chromium-coated sensors had larger, more closely packed, nodular structures (R_{RMS} roughness = 0.92 ± 0.08 nm). The surface of glass cover slip was the smoothest (R_{RMS} roughness = 0.21 ± 0.03 nm) with no observable surface structure. All model surfaces have significantly low surface roughness even though they have different surface morphologies. Such low surface roughness is unlikely to have any governing effect on the interaction between the softer colloids and surfaces during the colloidal probe-AFM force measurements.

The contact angles of the three model surfaces were determined and, as Figure 38 indicates, the values for each of these materials are quite different. The glass surface was the most hydrophilic (31° ± 4°), followed by the chromium surface (49° ± 3°) and the microcrystalline cellulose surface (62° ± 9°). Measurements for each model surface were recorded in triplicate and on each replicate four measurements were obtained, resulting in n=12.

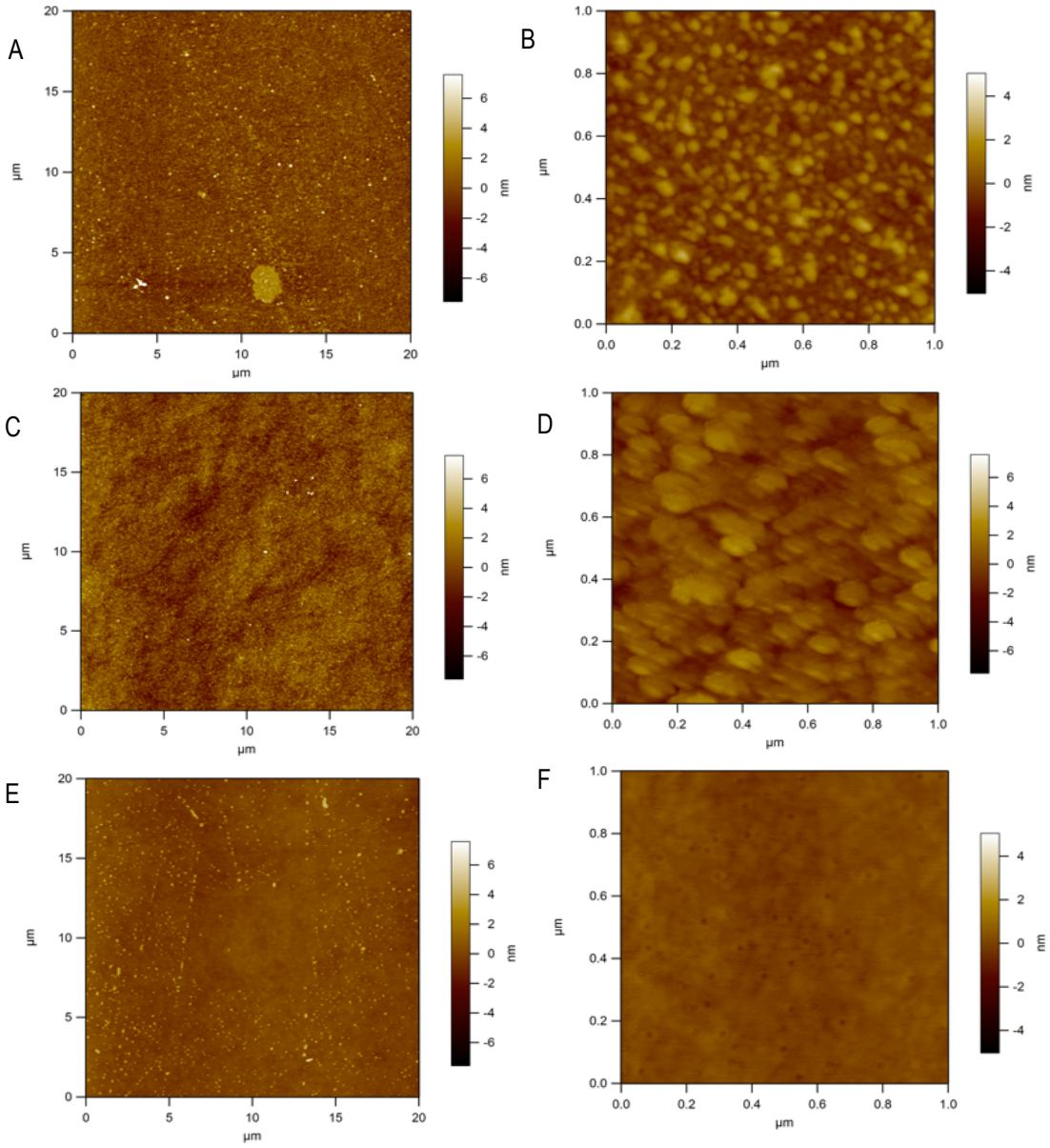

Figure 37 AFM height images obtained in AC mode. (A), (C) and (E) have dimensions of 20.0 µm x 20.0 µm; (B), (D) and (F) have dimensions 1.0 µm x 1.0 µm. Microcrystalline cellulose modified surface (A) – (B), chromium surface (C) – (D), and glass cover slip surface (E) – (F).

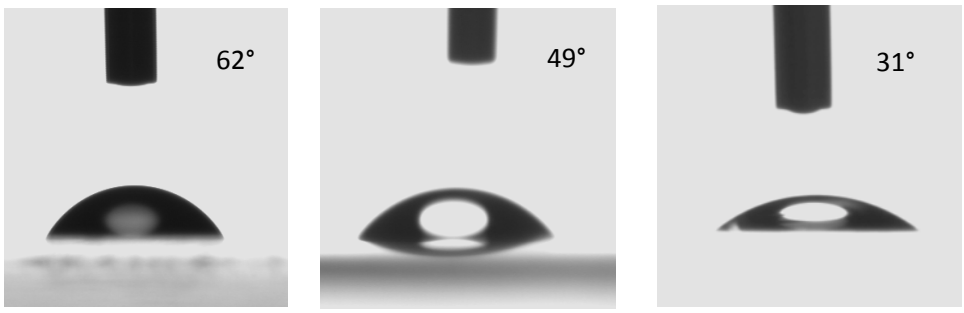

Figure 38 Contact angle measurements of surfaces – (A) microcrystalline cellulose (62° ± 9°), (B) chromium sensor (49° ± 3°) and (C) glass (31° ± 4°). (n=12)

4.3.2 Attachment of wood extractive/model compound colloids onto AFM cantilever (Colloidal probe-AFM)

AFM colloidal probes were made by attaching colloids onto tipless cantilevers as described in section 4.2.7. Many attempts were made to develop a new method of attaching these soft colloids onto the cantilever surface. The following variables were investigated while developing the new attachment method:

1) Concentration of colloidal suspension;
2) Background salt solution;
3) Surface on which the droplet of colloidal suspension was placed;
4) The use of colloids or colloid-coated silica beads;
5) Functionalization of cantilever surface.

Firstly, it was necessary to determine the appropriate concentration of the colloidal suspensions. This was to ensure both stability of colloids and a sufficient number of colloids for observation under the light microscope. This in turn meant there were sufficient colloids in solution to choose from for attachment while not covering the entire surface of the glass slips during the attachment process. In these experiments, the appropriate mass of model compound weighed out was determined to be a colloidal concentration of about 600 mg L^{-1}.

Secondly, both KNO_3 and NaCl solutions were trialled as an electrolyte used to make up the colloidal suspensions. It was observed that colloids prepared in KNO_3 solution had only poor adhesion to an un-functionalized cantilever. In particular any AA colloids that were attached could not withstand the meniscus pull of the water droplet during the transfer between solutions and fell from the tip as it was withdrawn. On the other hand, colloids (especially AA colloids) made up in NaCl solution, adhered more easily and attached more strongly to both functionalised and unfunctionalised cantilevers. When attached to a functionalised cantilever in a sodium chloride solution the colloids were readily able to withstand the transferring process between solutions.

Thirdly, the surface on which the colloidal droplets were placed and, hence, the surface from which the attachment of colloids onto the cantilever was to be made, was assessed. Initially, a glass surface (in form of a glass cover slip) was used. Though abietic acid colloids prepared in KNO_3 solution, remained as colloids in solution when placed on the glass and exhibited good adherence to the unfunctionalised

cantilever surface, colloids of triolein, oleic acid and wood extractives formed films on the glass surface quite quickly. To overcome the problem of oily films of OA, TrO and WE forming on the glass surface, methoxy polyethyleneglycol (PEG) was used to coat gold-coated glass cover slips to create a hydrophobic surface. In this case colloids of oleic acid, triolein and wood extractives remained in the colloidal form on the PEG surface. However even though triolein colloids could be readily picked up with the cantilever, oleic acid and wood extractive colloids could not be successfully attached. Qualitative observation showed that the colloids might be wedged in grooves on the PEG-modified surface. The cantilever was observed not to make contact with the surface or the colloid on the surface, evident by the breaking of the cantilever as z-piezo was adjusted. A literature search showed that PEG tails extend outward from the surface, forming side-by-side "mountains", which may explain the groove-like behaviour of the colloids.[122] With the colloids being stuck in grooves, the cantilevers could not contact them even though it was positioned directly on top of the colloid. Moreover, soft colloids, such as that of oleic acid, triolein and wood extractives, were easily squashed when attempting to adhere them to the cantilever, clearly an undesirable outcome for measuring the adhesion forces.

In a separate approach to make a colloidal probe, silica beads coated with wood extractives and model compounds, to be glued to the cantilever, were trialled. The two methods attempted were based on method developed by Wallqvist[2]:

1) Droplets of wood extractive suspension were carefully placed over silica beads and allowed to dry, resulting in a wood extractive film covering the silica beads. Attempts made to glue these beads onto the cantilevers failed, as the silica beads could not be removed from the oil films.

2) Cantilevers with silica beads glued to the end were carefully dipped into oleic acid and wood extractive oil films, so that the beads were covered in the material and then used for force measurements. This method was once again unreliable as there was no control of the thickness of the film layer that covered the beads.

These attempts to use colloidal material-coated silica beads were deemed unsuitable for force measurements, as there could be difference in position, composition and uniformity at the interacting colloid surfaces and this will not reflect the general interaction that it aims to model.

Since the functionalization of the surface from which the colloids were to be picked up and coating silica beads were considered impractical for making colloidal probes for force measurement studies, functionalization of the cantilever surface was trialled. Different functionalization methods of the cantilever surfaces were investigated to aid in the attachment the colloid to the cantilever.

1) Unfunctionalized cantilever – Initially adhesion of colloids onto the cantilever was trialled without functionalization. These unfunctionalised cantilevers were able to pick up abietic acid colloids quite successfully. However it was observed that when transferring from colloidal suspensions into a clean solution the attached AA colloid either moved along the cantilever or was detached from the cantilever surface by the 'meniscus force' of the colloidal suspension droplet. In the cases of oleic acid, triolein and wood extractive colloids, the colloids failed to adhere to the unfunctionalised cantilever surface at all.

2) Poly-L-lysine modified cantilever – As the surface of colloids is slightly negatively charged, as it is partially deprotonated at the particular working pH of about 5, the cantilever was functionalised with positively charged poly-L-lysine to test if colloids would attach onto this by electrostatic interaction. As none of the colloids adhered to the positively charged cantilever this functionalization was considered unsuitable.

3) Hydrophobically functionalized cantilever – As Lee et al. observed that colloids adhere to hydrophobic surfaces[35] the surface of cantilever was next hydrophobically functionalised (as described in section 4.2) to trial colloid adhesion to this type of surface. Two different hydrophobic chemicals differing in degree of hydrophobicity were used: 1, 3-(trimethoxysilyl)propylmethacrylate and the more hydrophobic 1H, 1H, 2H, 2H-perflurooctyltriethoxysilane.

a. When using 1, 3-(trimethoxysilyl)propylmethacrylate coated cantilever, OA, AA, TrO and wood extractive colloids were observed to adhere to the surface readily. However, the force of adhesion between colloid and functionalised surface was not sufficiently strong to overcome the surface tension of the water droplet when transferring from the colloidal suspension to clean solution for force measurements. The colloids either detached from the cantilever or moved from the attached position at the tip of the cantilever, along the arm of the cantilever.

b. For cantilevers functionalised with 1H, 1H, 2H, 2H-perflurooctyltriethoxysilane, the colloids were also observed to adhere to the functionalized surface readily. AA colloids maintained a more rigid structure, whereas OA, TrO and wood extractive colloids tended to spread slightly on the functionalized surface. The interaction between the colloid and functionalized surface was sufficiently strong in this case to prevent the colloids from moving from the attached position or being lost from the cantilever due to the "meniscus force" when transferring from the colloidal suspension to clean solution for force measurement.

From this the chosen method for attaching colloids onto the cantilever for force measurements was determined to be functionalization with 1H, 1H, 2H, 2H-perflurooctyltriethocysilane and attaching the colloid from a glass surface. (Detailed description in section *4.2.7 Attachment of colloid onto functionalized AFM tip*)

Figure 39 (A)-(C) shows optical images of colloids attached to the AFM cantilever tips in an aqueous environment. Abietic acid (AA) colloids were observed to be mainly spherical, rigid and qualitatively stiffer, as they did not deform or spread when in contact with the functionalized cantilever surface (Figure 39A). Oleic acid (OA), triolein (TrO) and wood extractive (WE) colloids were qualitatively observed to be much softer and tended to spread more, forming a hemisphere when in contact with the functionalized cantilever (two such colloid examples shown in Figure 39B-C). Wood extractive colloids are known to spread more on hydrophobic silanized glass compared to hydrophobic surfaces. They are shown to not retain their spherical shape on a hydrophobic surface, but wet the surface giving rise to lower contact angle values and over time form a film.[35] It is proposed that the hydrophobic components of the wood extractives migrate towards the hydrophobic surface while the hydrophilic components of the wood extractives reorientate toward the water interface.[2, 27] Compared to the other colloids, the retainment of a spherical structure and less spreading of AA colloids suggest that their hydrophobic groups maintain stable intra-colloid interactions and/or have weaker hydrophobic interactions, thus preventing their reorganisation toward the hydrophobic functionalised AFM cantilever.

4.3.3 Soft colloid force measurement

A number of different types of force curves were observed during these studies and these possibly give an insight into the behaviour of the colloids when interacting with different surfaces. The force curves were analysed and a number of different force curve profiles were apparent throughout the experiment. The magnitude of each force curve may be different depending on the type of colloid and the surface on which the forces were measured. Figure 40 shows the main types of force curve profiles that represent specific types of interaction between the colloids and different model surfaces:

(A) “Direct adhesion”;

(B) “Saturated adhesion”;

(C) “Deformation adhesion”.

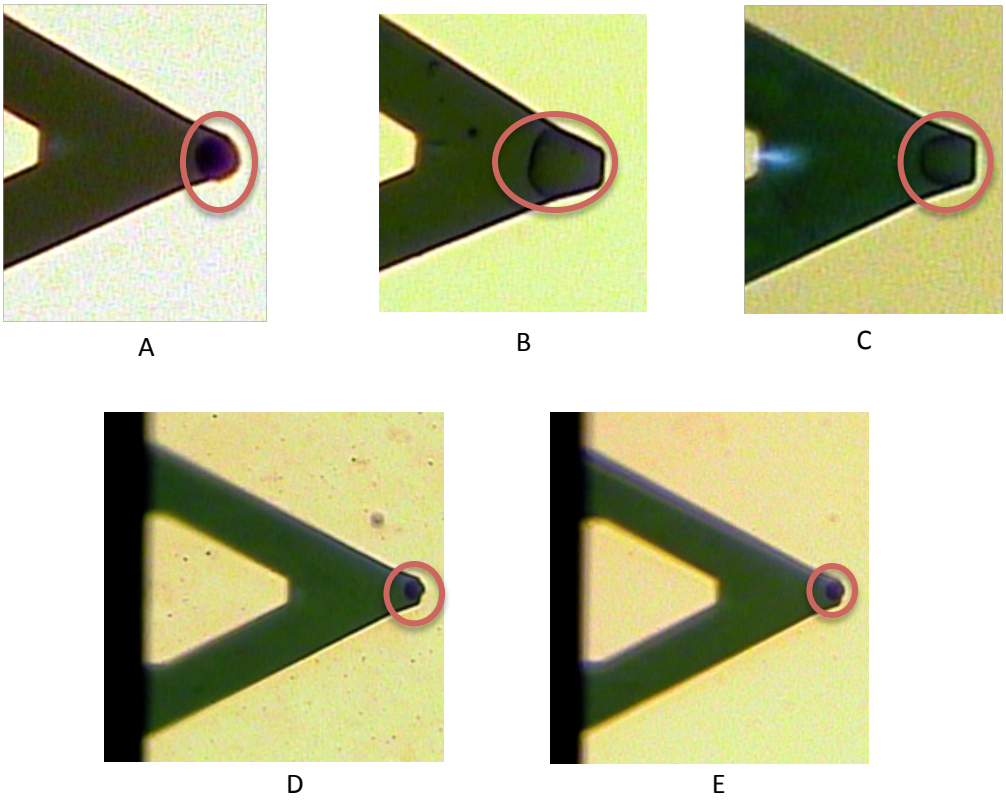

Figure 39 (A) - (E) are images taken after the colloid was attached onto the cantilever. (A) shows shape of abietic acid colloid – round and rigid. (B) and (C) shows possible shapes of colloid belonging to the other colloids used – oleic acid, triolein and wood extractives. (D) shows the colloid attached onto the cantilever tip still in colloidal suspension, whereas (E) shows the colloid still attached to the cantilever tip after being transferred from the colloidal suspension into clean NaCl (aq) for force measurements.

The "direct adhesion" curve (Figure 40A) was the most common force curve pattern observed for all four colloidal types (OA, AA, TrO and WE). This shows a short-range attraction upon approach to the surface, followed by direct adhesion and then "pull-off" as the probe was retracted from the surface. The short-range attraction indicates the presence of van der Waals interactions and subsequent adhesion just prior to the "pull-off" force as the colloid is drawn off the surface.

Figure 40B, referred to as "saturated adhesion" curve, shows a force curve analogous to that of Figure 40A. The difference is that the force values exceed the measurement range of the AFM detection system and "flat lines". The interaction between the colloid and surface in Figure 40B is similar to that in Figure 40A, except that it indicates significantly greater adhesion experienced by colloids than those in "direct adhesion".

For the force curves represented in Figure 40C, also referred to as "deformation adhesion" curves, the force profiles show a distinctly different interaction where the colloid did not "pull-off" instantaneously (in which case the force would return to zero instantaneously) but remained "bridged" between the surface

and cantilever. In this case the colloid underwent deformation in the form of neck-thinning as the probe retracted further from the surface. At some point, when the force pulling the colloid away from the surface exceeded the adhesion of the colloid to the surface, the colloid detached from the surface completely. This deformation profile is shown to occur during the adhesion of viscous liquid droplets, oil droplets or biological systems.[123]

A comparison of the proportion of each type of curve for the different colloids and the surfaces is given in Figure 41. The “direct adhesion” force curve (A) is the most prevalent type of interaction for all four types of colloids (OA, AA, TrO and WE) on cellulose and chromium surfaces (Figure 41A-B). This has a relatively high occurrence, ranging from 65 % - 97 % for these colloids on these surfaces. Interaction of OA and TrO colloids with cellulose also showed high occurrence for “saturated adhesion” curves at 18.9 % and 28.3 %, respectively (Figure 41A), indicating that these colloids exhibit very strong adhesion to cellulose. For AA and WE colloids strong adhesion was observed on chromium, with high occurrences of 21.3 % and 22.9 %, respectively, of “saturated adhesion” force curves. This suggests that OA and TrO have a stronger interaction onto cellulose surface than AA and WE. Conversely, AA and WE adhered more strongly to chromium than to the cellulose surface.

Adhesion onto glass by OA, AA, TrO and WE colloids was observed to be predominately of the “direct adhesion” force curve type, with the proportion of force curves of this type ranging from 63 % - 94 %. However, for model compounds (OA, AA and TrO), the “deformation adhesion” force to glass occurred a number of times, but “saturated adhesion” force was not observed at all for this interaction. WE on glass showed very small percentage (6 %) of the “saturated adhesion” force curves and no “deformation adhesion” curves.

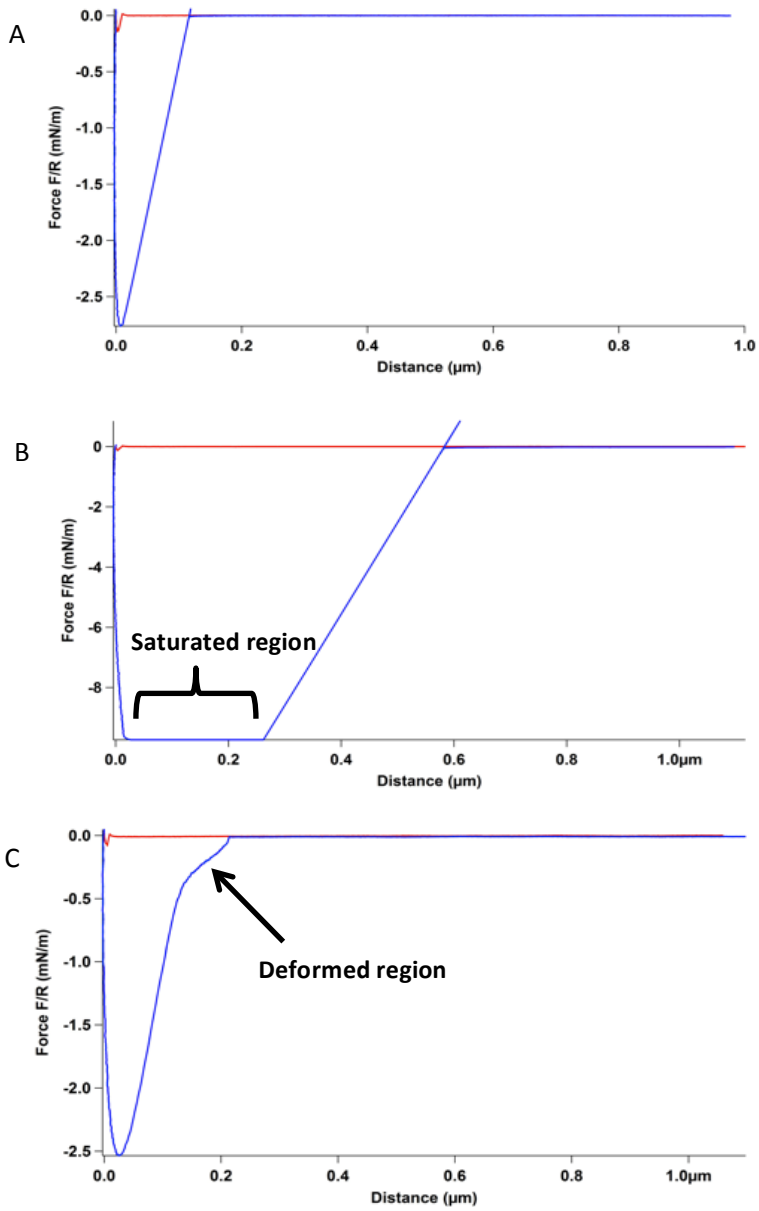

Figure 40 Force curves representative for all four types of colloids used in force measurement studies onto different surfaces. Red trace line – approaching curve of cantilever to substrate; blue trace line – retracting curve of cantilever to substrate. The corresponding percentage of occurrence is compared in Figure 41.

I

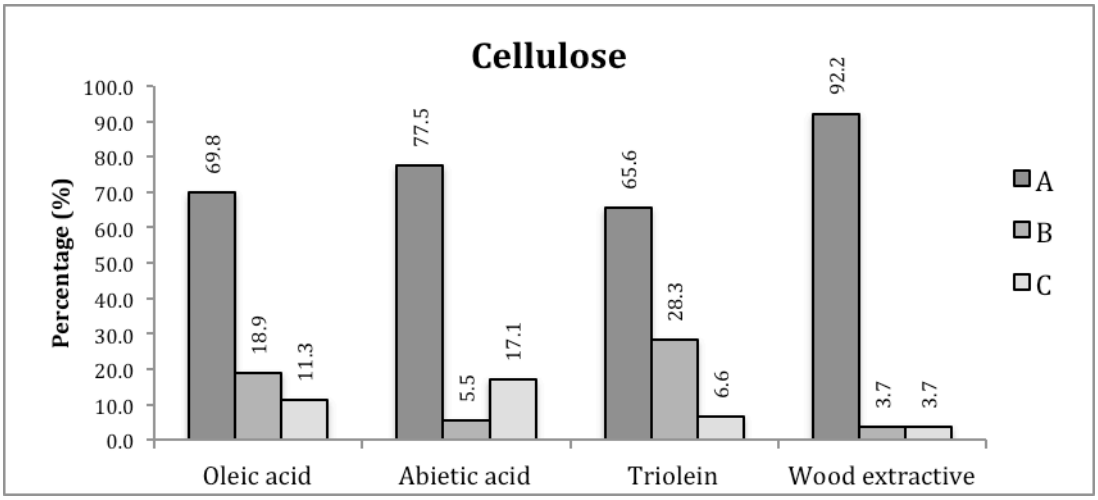

II

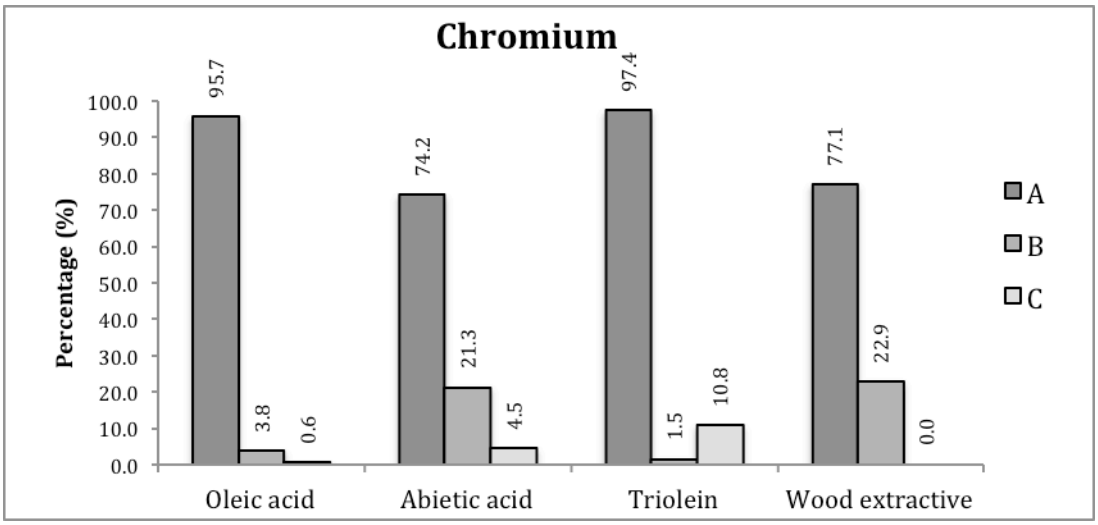

III

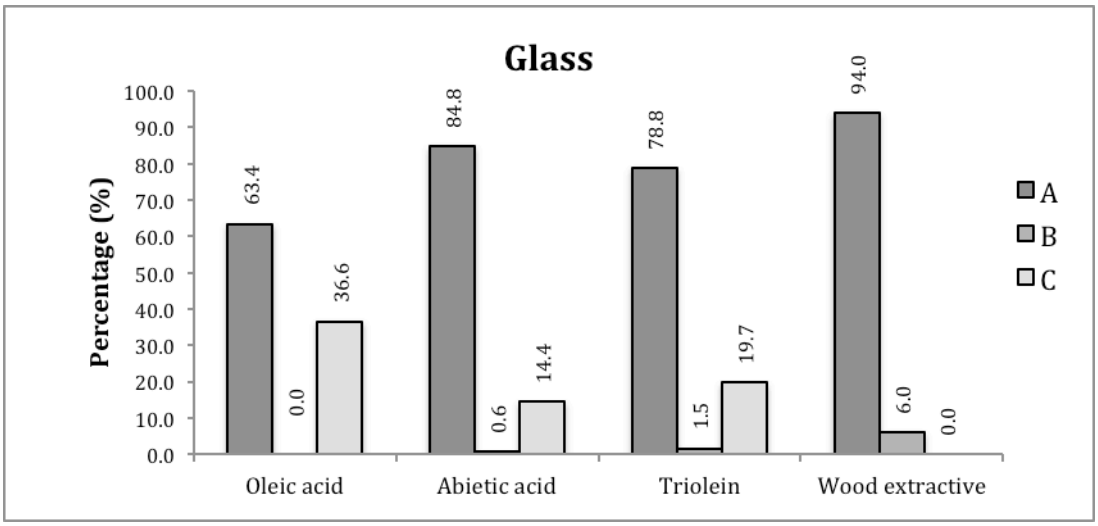

Figure 41 Graphs showing and comparing the percentage of force curve type A-C for each colloid type used (oleic acid, abietic acid, triolein and wood extractives) on cellulose (I), chromium (II) and glass (III) surfaces respectively.

“Deformation adhesion” force curves (C) occurred either infrequently or not at all for all four types of colloids (OA, AA, TrO and WE) on cellulose and chromium surfaces. However, the occurrence of “deformation adhesion” curves was comparably higher than “saturation adhesion” curves for interaction of model compounds colloids with glass surface. The fact that the majority of the force curves were of “direct adhesion” and “saturated adhesion” force curve types provides evidence that the colloids which were attached to the cantilever did not undergo significant change. They maintained their shape with repeated force measurements even though they can be considered as soft colloids (with the exception of abietic acid colloids). The occurrence of “deformation adhesion” force was found not to correlate with higher adhesion forces. Deformation of soft colloids may occur as the colloid maintains adhesion to the tip and surface under the applied tensile stress as the tip was retracted. The occurrence of “deformation adhesion” curves on glass were higher than on the other two surfaces, suggesting that this effect is dependent on the colloid-surface interaction and not solely the inherent physico-chemical properties of the colloid. In general, the occurrence of “deformation adhesion” curves did not correlate with higher adhesion force.

In addition to the commonly observed force curve profiles, an interaction phenomenon specific to OA on the different surfaces (Figure 42) was also seen. For each set of measurements with a new colloid probe, a “direct adhesion” curve or “saturated adhesion” curve was observed for the first force curve indicating strong adhesion. However, the subsequent curves of the same colloid at the same x-y position did not show any adhesion. This suggested that the initial adhesion event and associated deformation of the colloid modified the interfacial chemistry of the colloid by:

1. Causing rearrangement of the colloid interacting surface groups, or
2. Modifying the glass, chromium and cellulose surfaces due to adhesion-induced extraction and deposition of colloidal material, possibly as thin film deposit, onto the respective surfaces.

Either of the above two points could apply to the reduction or total absence of adhesion at the same x-y position when force measurements were repeated. However, when the x-y position was changed after the initial force measurements were performed the strong adhesion in the first curve was again apparent with subsequent curves again showing very little or no adhesion. This would not be expected if it was the rearrangement of the colloid surface that led to the reduction or absence of adhesion. Hence, the most likely cause of this series of interactions would be due to the deposition of colloidal material on the surface. This pattern occurred for 65 % of all OA force curves on cellulose, 14 % on chromium and 59 % on glass surfaces, indicating strong adhesion of OA to cellulose and glass but no or extremely small adhesion to its own surface deposits. It is worth noting that “saturated adhesion”

curves were observed mainly on the cellulose surface, while the “direct adhesion” curves on glass all had small adhesion values. Note that in these cases, the adhesion values of oleic acid in Figure 43 represent those obtained from the initial force curves and/or in new x-y positions where adhesion was observed.

Figure 43 compares the resultant average adhesion force of the different colloidal types on different surfaces. These values are taken from the peak maximum force (mN), then normalised by the radius (m) of the colloid to give adhesion values of units mN m^{-1}. Whilst the colloids, shown in Figure 39 (B) and (C), are not perfectly round and are more spread (less in height than width), a more complicated calculation and approximation will not make any significant difference to existing results. Hence, it is still best to approximate the adhesion values using radius-normalised adhesion values. Colloidal adhesion of model compounds (OA, AA and TrO) was significantly stronger onto cellulose, than onto chromium or glass surfaces. Wood extractive colloids are the exception, where the greatest adhesion was onto the glass surface (7.0 ± 1.7 mN m^{-1}) followed by cellulose (4.3 ± 1.0 mN m^{-1}) and then chromium (3.9 ± 0.7 mN m^{-1}). These force measurements were carried out in aqueous solution at about pH 4-5, where the surface of OA, AA, TrO and WE colloids are believed to be largely protonated. The difference in degree of protonation of each surface may give rise to differences in strength of hydrogen bonding. The presence of hydroxyl and carboxyl surface groups on both model surfaces and colloids contributes to hydrogen bonding, leading to adhesion between colloids and the model surfaces. For example, hydrogen bonding of surface carboxyl groups on oleic acids, abietic acids and wood extractive colloids with surface-rich hydroxyl groups on a cellulose surface, may explain greater adhesion onto these surfaces. As for triolein, colloids or aggregates are not stable in solution due to the extension of hydrophobic hydrocarbon chains into the solution. This may be responsible for the increased adhesion of triolein onto surfaces because of poor solute-solvent interaction.

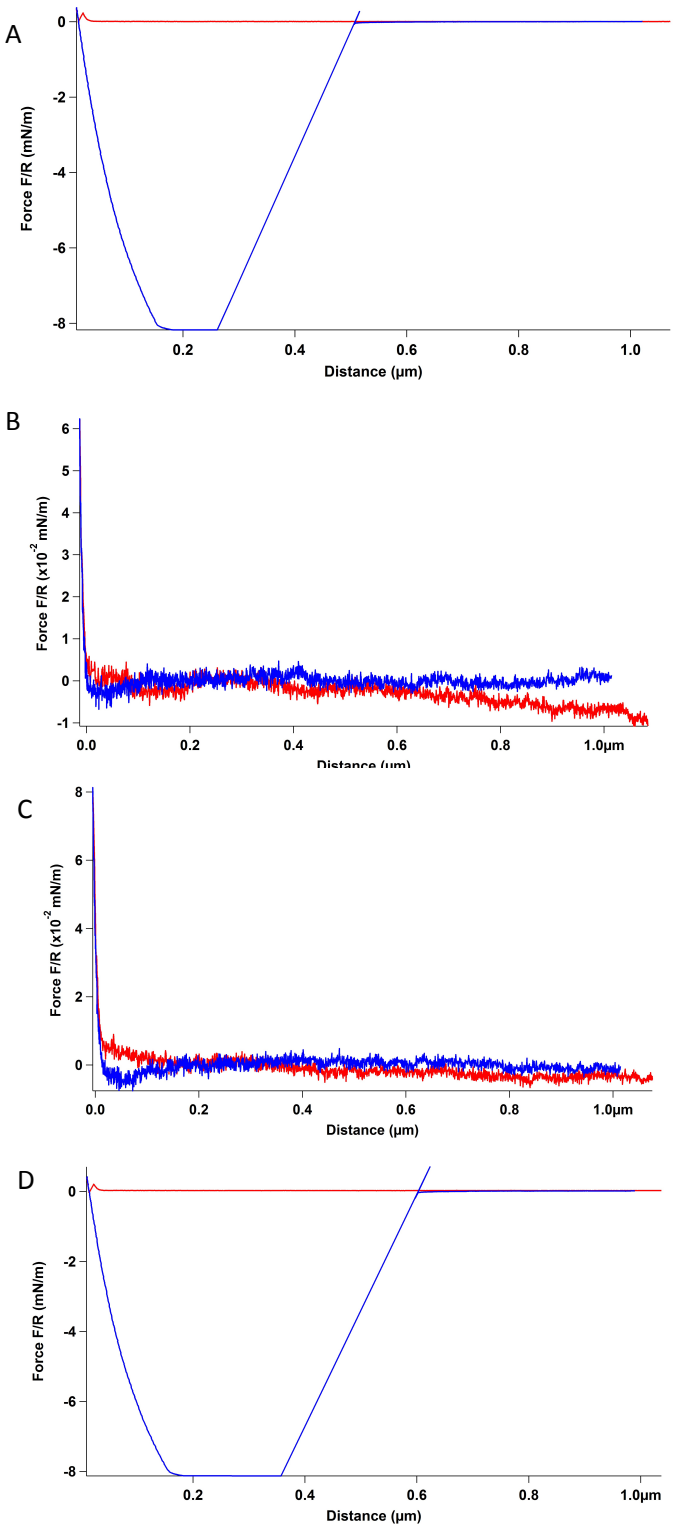

Figure 42 An observation for interaction of oleic acid colloid with surface – (A) shows adhesion force on the first contact with surface, but subsequent contact with the surface shows no adhesion (B) – (C). However, when move to different position on the surface, adhesion once again was observed for the first contact (D) but subsequent force curves do not have adhesion.

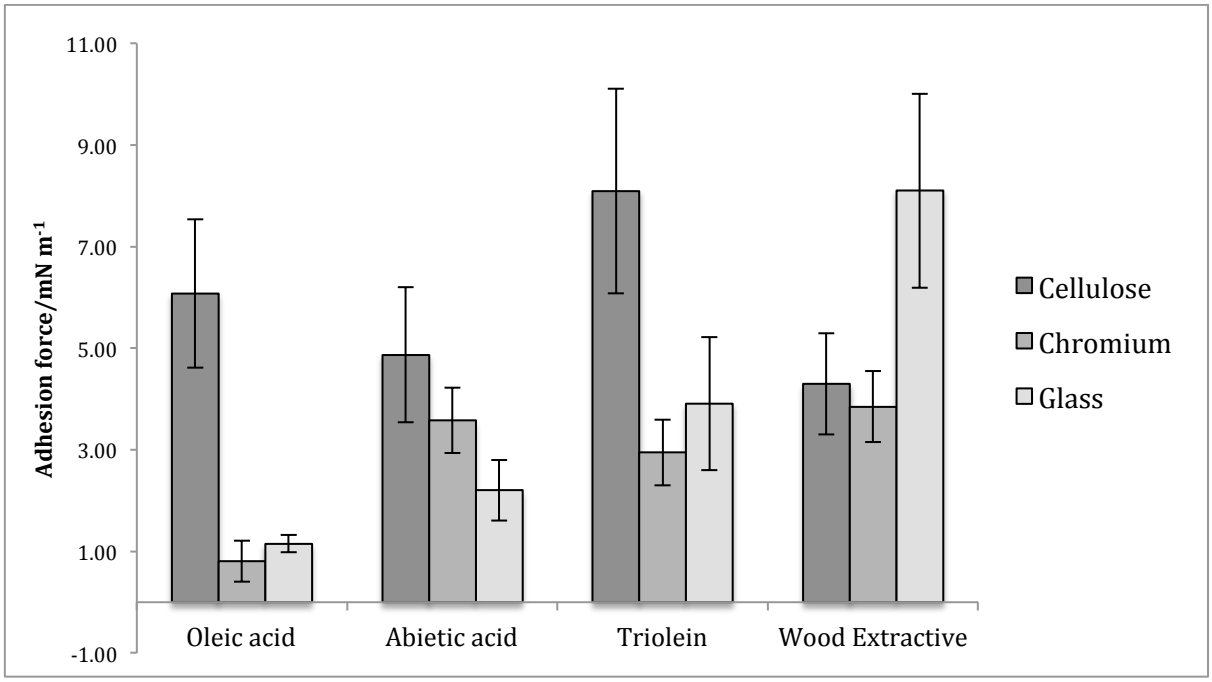

Figure 43 Graph comparing average adhesion data for all colloidal types (oleic acid, abietic acid, triolein and wood extractive) on the three different surfaces (cellulose, chromium and glass).

A comparison between the different colloids shows that the TrO (8.1 ± 2.0 mN m^{-1}) had the greatest adhesion to cellulose followed by OA (6.1 ± 1.5 mN m^{-1}); while the adhesion of AA (4.9 ± 1.3 mN m^{-1}) and WE (4.3 ± 1.0 mN m^{-1}) to cellulose were comparable. Significantly stronger adhesion values for TrO and OA on cellulose were also consistent with higher occurrence of "saturated adhesion" force, as shown in Figure 41. The adhesion forces of OA and TrO onto cellulose were 6 and 2.5 times, respectively, stronger than that onto chromium. This would clearly indicate that OA and TrO would bind preferentially to cellulose rather than to chromium and even though the force of adhesion of TrO to chromium (3.0 ± 0.6 mN m^{-1}) was not significantly different to that of AA (3.6 ± 0.6 mN m^{-1}) and WE (3.9 ± 0.7 mN m^{-1}), TrO would strongly favour adhesion to chromium rather than cellulose. The comparable adhesion forces of AA and WE to cellulose (4.9 ± 1.3 and 4.3 ± 1.0 mN m^{-1}, respectively) and chromium (3.6 ± 0.6 mN m^{-1} and 3.9 ± 0.7 mN m^{-1}, respectively) may point to AA occupying the outer layer of a WE colloid, which is in line with the model of WE colloid suggested by Lee et al.[27] The combination of similar adhesion forces between AA and cellulose and AA and chromium, the observation that AA occupies the outer layer of a WE colloid, and that adhesion of both OA and TrO to cellulose is strongly favoured over those to chromium explains the greater tendency of resin acids to adhere to chromium coated surfaces rather than remain adhered to a cellulose surface or as part of a WE colloid.

Whilst the WE showed significantly high adhesion (7.0 ± 1.7 mN m^{-1}) to the glass, the extent of adhesion by other colloids to this surface was variable (i.e. TrO (3.9 ± 1.3 mN m^{-1}), AA (2.2 ± 0.6 mN m^{-1}) and OA (1.2 ± 0.2 mN m^{-1})). The other notable observation was that adhesion of OA to chromium (0.8 ± 0.4 mN m^{-1}) and glass (1.2 ± 0.2 mN m^{-1}) was very low compared to the other colloid types.

4.4 Conclusion

The AFM colloidal probe technique has been used to investigate the interaction forces of model compounds and wood extractives with cellulose, chromium and glass surfaces. The colloidal probes used in these experiments, were prepared by the newly developed method of adhering the model compound colloids and wood extractive colloids *in situ* onto hydrophobically functionalised AFM tipless cantilevers. The strength of adhesion of oleic acid and triolein onto cellulose is significantly higher than onto chromium surface, whereas the strength of adhesion of abietic acid and wood extractives (believed to have an external layer of abietic acid) onto cellulose and chromium surfaces were comparable. This would explain the observed phenomena in the pulp and paper industry where it is shown that abietic acid preferentially desorbs from cellulose surface and adheres onto chromium surface, while oleic acid and triolein preferentially remain bound to cellulose surface.

Oleic acids and abietic acids are shown through adsorption isotherm modelling (chapter 2) to have greatest adsorption onto cellulose than WE at 50°C. However by increasing to a higher temperature, the surface properties of colloidal materials as well as cellulose surface will be affected, hence it is difficult to draw direct comparison with the results of this chapter. QCM-D deposition experiments showed that deposition of wood extractives and oleic acids onto chromium was greater than onto cellulose, whereas deposition of abietic acid and triolein onto chromium and cellulose were comparable (chapter 3). These QCM-D result trends were notably different from results of force measurements because the type of interaction measured by these two experimental methods is different. AFM force measurements only measure the surface interaction between colloids and model surfaces, whereas results from QCM-D adsorption experiments include the interaction forces between the colloids and model surfaces as well as interaction between colloids. This may explain why the adhesion results from QCM-D adsorption differ from that of AFM force measurements.

Chapter 5 Computational Modelling of Interactions

5.1 Introduction

Computational chemistry, also known as molecular modelling, is used to investigate chemical problems by computational means, most commonly to compliment and provide comparison for experimental data. This technique provides another angle for looking at the interaction energies between molecules by performing experiments on computers instead of traditional chemical experiments. Computational chemistry is used to investigate molecular geometry, energies and transition states of molecules, chemical reactivity, physical properties of substances, enzyme-substrate interaction, and IR/UV/NMR spectra.[124]

There are three broad approaches to computational modelling. The simplest of the three approaches is the use of empirical methods. This is then followed with increasing complexity by the semi-empirical (SeE) methods and *ab initio* quantum methods, the most complicated of the three approaches.

Semi-empirical (SeE) methods are based on the Hartree-Fock methods. Semi-empirical calculations are less demanding and can be performed faster than the *ab initio* calculations. This method is parameterized by curve-fitting in a few parameters or numbers, in order to give the best possible agreement with experimental data, thus reducing the number of integrals to be calculated.[124] This method is useful in organic chemistry where molecules are of moderate size with few elements. It can be also be programmed specifically for inorganic chemistry.[125] Examples of SeE methods are the simple Hückel method, extended Hückel method, and a range of self-consistent field (SCF) SeE methods with the most popular being AM1 and PM3.

Ab initio quantum methods refer to computations that are derived directly from theoretical principals and are mostly quantum mechanical calculations. These quantum mechanical calculations solve the Schrödinger wave equation (of a molecule):

$$\hat{H}\Psi=E\Psi \qquad \text{(Equation 7)}$$

where Ψ= wavefunction; $\hat{H}$= Hamiltonion operator; E=total energy of the system.

The Schrödinger equation provides the energy and wavefunction for the molecule. In turn the wavefunction is a mathematical function that can be used to calculate the electron distribution.

Schrödinger's equation cannot be solved exactly for molecules or multi-electron atoms so approximations are used.[126] The most common *ab initio* quantum method is the Hartree-Fock (HF)

approximation/calculation. The HF approximation is based on the Born-Oppenheimer and orbital approximations.[126] The Born-Oppenheimer approximation says that in a molecule the nuclei are stationary compared to the electrons. This allows a focus on electronic energy with the addition of nuclear repulsion energy at a later state during computational calculations. The primary approximation of HF is the central field approximation where only the net effect of Coulombic electron-electron repulsion is considered in the calculations. The secondary approximation of HF is the wave functions used to approximate the molecular orbitals. The most commonly used functions are Slater type orbitals (STO) and Gaussian type orbitals (GTO). These wave functions are linear combinations of atomic orbitals or basis functions. Correlated methods are built on HF calculations by correcting for explicit electron-electron repulsion.[124]

Generally for small to intermediate sized molecules, HF calculations give reliable geometries but fail to predict other molecular properties due to electron correlation errors introduced by orbital approximations. Post-Hartree-Fock (PHF) methods introduce electron correlation into the calculations rather than the STO/GTO type wave functions. However this means calculations are computationally expensive even though the results can be quantitatively similar.[126]

An alternative *ab initio* quantum method that is commonly used is density functional theory (DFT), which is also based on the Schrödinger equation.[124] More accurately, it is based on two Hohenberg-Kohn theorems, which state that the ground state properties of an atom or molecule are determined by its electron density function, and that a trial electron density must give energy greater than or equal to the true energy.[124] The total energy is expressed in terms of total electron density rather than wave function. DFT calculations generally scale as the third power of the size of the basis set, rather than the fourth power of the HF methods.[125] Some examples of commonly used functionals in DFT are B3LYP, MP2, pBP and BP86.

In general, *ab initio* quantum methods are expensive as they require very large amounts of computer CPU time, memory and disk space.[125] The main uses of *ab initio* quantum methods are calculating molecular geometries, energies, vibrational frequencies, spectrometric features (IR, UV, NMR), ionisation potentials and electron affinities, and properties (e.g. dipole moments) that are directly connected to electron distribution.[124]

Both the *ab initio* and semi-empirical approaches need to define a level of theory and a basis set for calculations. A basis set is a set of mathematical functions (basis functions) used to describe the electron distribution of an atom and combining atomic basis functions yield the electron distribution in the molecule.[124] Molecular orbitals and wave functions are created by taking linear combinations of

basis functions (usually called the LCAO) and angular functions.[124, 127] Basis functions such as hydrogen-like functions (based on Schrödinger equation), polynomial functions (with adjustable parameters), Slater functions and Gaussian functions have all been used. Slater and Gaussian functions are mathematically the simplest.[124] Slater functions are used in semi-empirical calculations. Gaussian functions are employed in molecular *ab initio* programs. The STO-3G basis set is the smallest basis function used in standard *ab initio* quantum calculations by commercial programs.[124] It is referred to as a minimal basis set. It also has a good speed versus accuracy compromise.[124]

Though the STO-3G basis set is not considered acceptable for research, the speed and the ease with which the molecular orbitals can be dissected into atomic orbital contributions makes it advantageous, especially for comparison purposes.[124, 127] The basis set 3-21G is known as the split valence basis set. It splits each valence orbital into two parts, where two Gaussians are used to represent the inner shell and one Gaussian to represent the outer shell (hence the 21). The "3" refers to three Gaussians for each basis function representing the core orbitals. 3-21G is considered a small basis set. For example, for the molecule acetone, the total number of basis functions is 26 and 48 if using the STO-3G and 3-21G basis sets, respectively. Variations added to the basis sets include polarization (*) and diffuse functions (+), however in this part of the research these variations are not utilised.[128]

A common method when using an empirical approach is molecular mechanics (MoM). This method uses a single classical expression, such as the harmonic oscillator, to minimise the molecular potential energy.[126] This method is usually employed if the molecule is too big to be effectively modelled with semi-empirical methods or quantum mechanics. Molecular mechanics views molecules as balls held together by springs[124] and is set up as a simple algebraic expression of the total energy of the compound. The energy expression consists of simple classical equations that describe the energy associated with bond stretching, bending, rotation and intermolecular forces (VDW interactions and hydrogen bonding). Experimental data or *ab initio* quantum calculations are needed for the constants in these equations. With this method, a set of parameters and functions called a force field, which need to have direct relevance to the molecule or compound, are used. However with this method, there are many chemical properties not defined and so may not adequately describe a system.[125]

Two MoM methods used widely are Molecular Dynamics and Monte Carlo methods. Molecular Dynamics (MD) is useful especially in biochemistry: in the study of protein-folding, alternative minimal energy states of macromolecules and areas such as enzyme-substrate docking. It consists of examining the time dependant behaviour of a molecule, such as vibrational motion, computed by the numerical integration of Newton's laws of motion.[125, 126] Monte Carlo methods are based on the

generation of random changes in the variables of a system, followed by reliance on criteria for deciding whether the changes lead to a valid or significant new state of the system.[126]

In general, molecular mechanics (MoM) is suitable to study very large molecules since using SeE, *ab initio* and DFT methods would be too time consuming. *Ab inito* and DFT methods are probably more suitable to study new molecules compared to MoM and SeE methods. Depending on the type of results required when calculating energies of molecules, the type of method used will be different, for example SeE, *ab initio* and DFT methods are usually used in studying reactivity of molecules.[124, 129, 130]

When studying the non-covalent interaction between two molecules using computational methods, it is important to consider both enthalpic (ΔH) and entropic contributions ($-T\Delta S$). If these interactions are spontaneous, it is associated with negative Gibbs' free energy change (ΔG) that may be either enthalpy- or entropy driven.[131] The Gibbs' free energy change (ΔG) is the sum of an enthalpic and an entropic term, given by the following Equation 8:

$$\Delta G = \Delta H - T\Delta S \qquad \text{(Equation 8)}$$

where ΔG is Gibbs' free energy change, ΔH is enthalpy change, ΔS is entropy change and T is the temperature in Kelvin.

Values $\mathrm{of}\ \Delta G$ can be similar, but the driving force of the interaction may be very different from one case to another (enthalpic driven or entropic driven). The phenomenon of enthalpy-entropy compensation is highly system dependent and enthalpic and entropic contributions are related. Restriction of mobility of the interacting molecules will increase the enthalpy while decreasing the entropic contributions (enthalpy-entropy compensation).[132] However enthalpy-entropy compensation, though widely observed, does not always occur. Cooperativity can also contribute to thermodynamic terms, which will not be discussed here.

Enthalpic contributions can be simply associated with specific, non-covalent interactions. The enthalpic component reflects the specificity and strength of the interactions between the two molecules. Examples of specific interactions shown to contribute to the enthalpy term are hydrogen bonding, electrostatic, multipolar, hydrophobic and Van der Waals interactions. A gain in enthalpy can occur due to contributions from desolvation resulting from hydrogen bonding. Similarly a gain in enthalpy can also occur due to hydrophobic interactions. A hydrophobic solute disrupting the bulk water structure is enthalpy favoured as water molecules are restructured around the molecules (hydrophobic effect).[131] Simply put, formation and breaking of many individual bonds, such as solvent reorganisation, loss of

hydrogen bonding with water molecules, formation of Van der Waals interaction and many more, will result in changes to enthalpy.

The entropic contribution to the free energy is a measure of the dynamics of the overall system. For ΔS, the term may be calculated directly from ΔG and ΔH, according to Equation 8. The main contributing effect of ΔS is the solvent effects. Solvation effects can contribute (both favourably and unfavourably) to the entropic term of free energy.[131] Water molecules exist either tightly bound to molecules or as interfacial molecules to the bulk solution. There will be an effect on ΔS due to the displacement of these water molecules after 'binding'. For example, a positive entropic change can point to water molecules being released from the complex-surface[133] or interfacial water remaining after 'binding'[134]. Ignoring the contributing effects of water molecules can lead to substantial errors in the free energy prediction.[135] On the other hand, reduction in the free motion of molecules, due to changes to the translational and rotational restrictions, is shown to be entropically unfavourable.[131]

Very few studies have been undertaken applying computational methods to wood extractives and their interactions. Vercoe et al. modelled interactions between the components of wood extractives, as well as interactions between model compounds with components in wood such as hemicellulose. These modelling calculations were carried out with MM3 (molecular mechanics) and PM3 (semi-empirical method).[105] Modelling using higher levels of theory has not been reported largely due to the limitations on the computing power available to perform the calculations due to the size of the molecules particularly the size of the triglycerides (167 atoms).

5.1.1 Aim

The aim of using computational modelling is to gain a more detailed understanding of the interaction between wood extractive components and different surfaces. The wood extractives will be modelled using model compounds that represent the three major classes of compounds present in the wood extractives, namely oleic acid (OA) for fatty acids, abietic acid (AA) for resin acids, and triolein (TrO) for the triglycerides. The model surfaces will be glucose molecule(s) and a chromium unit.

The interaction will be studied through:

1. Calculation of the stabilising energies (SE) and free energies of interaction (ΔG) of two-component combinations of an extractive component and a model surface at different level of theory and basis sets (under vacuum and at 298 K);

2. Study of the solvation and thermodynamic effects on the interaction between the extractive components and the surface;

3. Comparison of the calculations to the experimental findings especially from the AFM force measurements (Chapter 4).

The program Gaussian09 has been used for calculations. This program has capabilities for electronic structure modelling and is widely used to predict the energies, molecular structures, vibrational frequencies and molecular properties of molecules and reactions.[128]

5.2 Methods

5.2.1 Program

GaussView 5.0 (Gaussian Inc.) was used to build up the molecule structures as well as obtaining the results for the energy values of each calculation. Molecular structures of the model compounds (oleic acid (OA), abietic acid (AA), triolein (TrO)), glucose unit(s) and chromium unit were created on GaussView 5.0 (ball-stick representations of each molecule used are shown in Figure 44 - Figure 48). Computational calculations were performed using the modelling on Gaussian09 program on the supercomputers (Raijin) at the National Computational Infrastructure Facility (NCI).

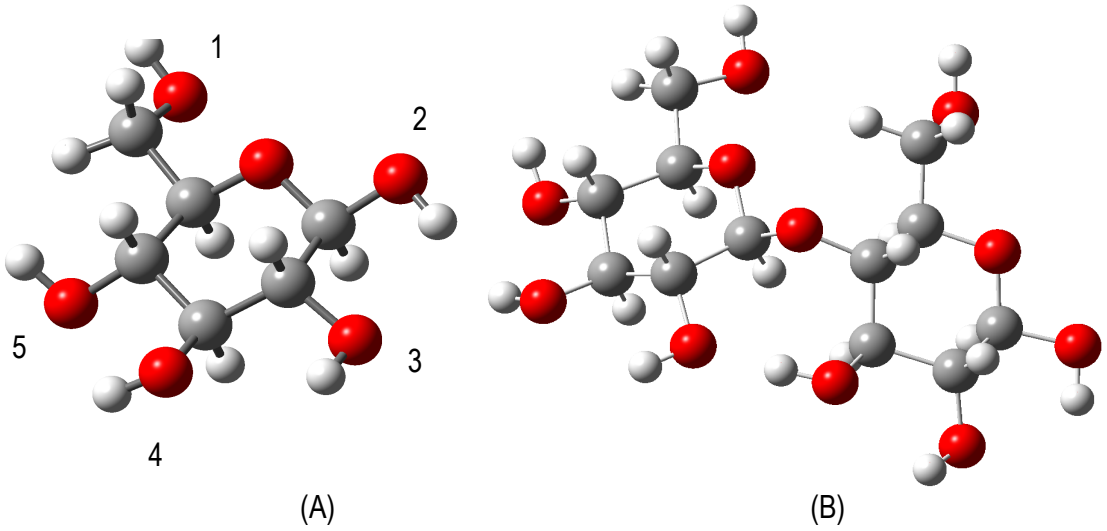

Figure 44 Optimised structures of glucose molecule (Glc) (A) and two units of linked glucose units (Glc-Glc), 'maltose' (B). The –OH groups on (A) were numbered.

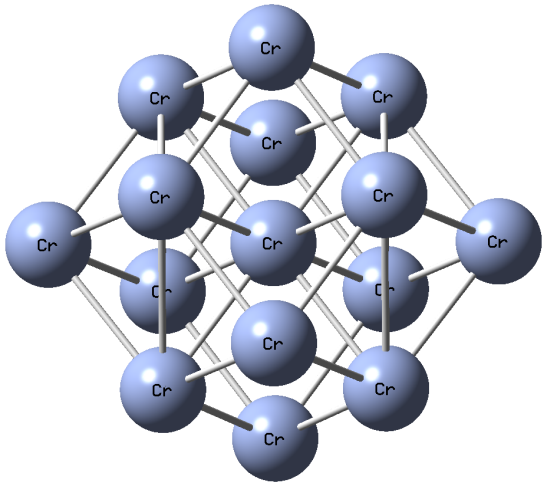

Figure 46 Optimised chromium unit (at BP86/STO-3G)

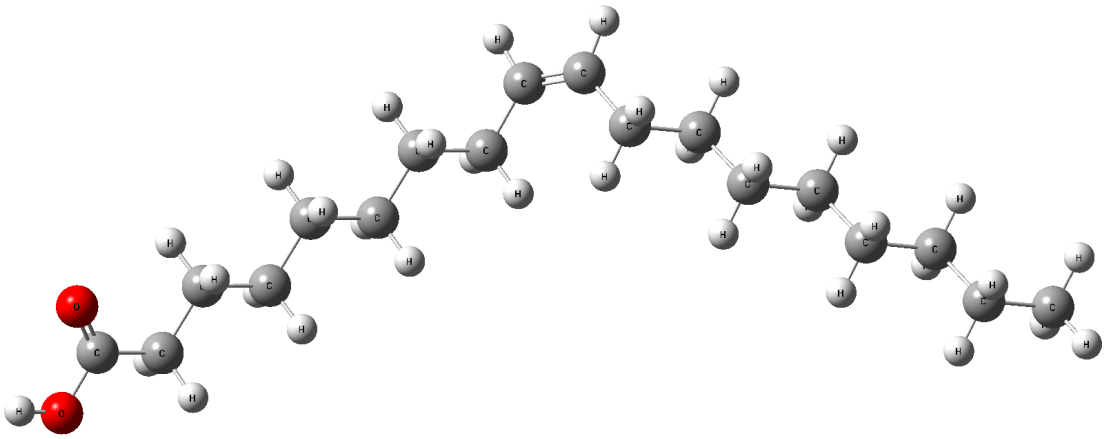

Figure 47 Optimised oleic acid molecule (OA)

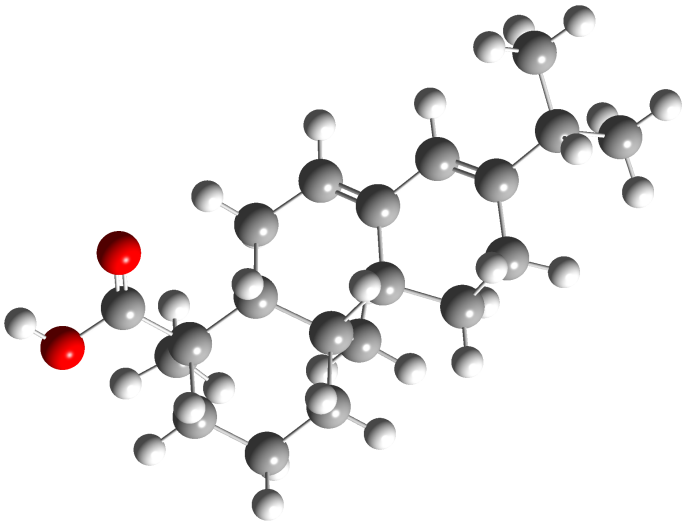

Figure 45 Optimised abietic acid molecule (AA)

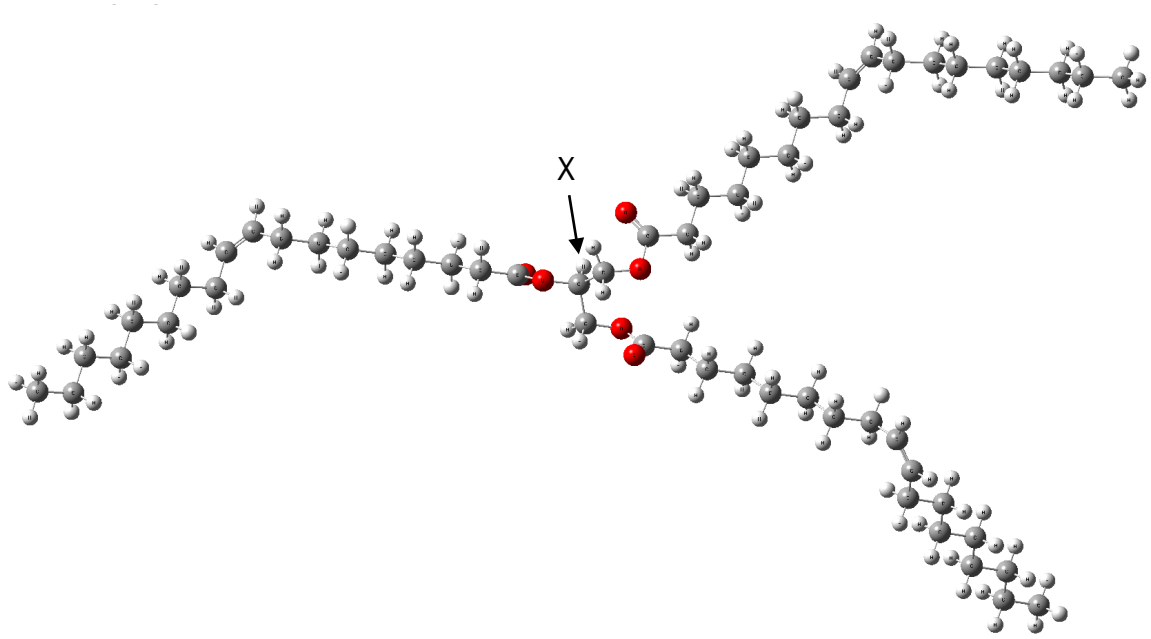

Figure 48 Optimised triolein molecule (TrO). Hydrogen marked 'X', referred to in section 5.3.1.

well as thermal correction values for enthalpy change (ΔH) and Gibbs free energy change (ΔG) for each calculation at the chosen level of theory and basis sets.

Solvation effects, in this case due to water, were also considered during the modelling calculations. The polarizable conductor calculation model (CPCM) was used. In this model the calculation was performed by treating the solvent as a continuum characterised by a bulk dielectric constant with the solute being placed in a cavity in the solvent. The surface of the cavity was divided into 240 small tesserae of area 0.30 au^2. The United Atom Topological Model (UAHF) was applied. An example of the command lines used is presented in the Appendix D.

Combinations of two molecules of OA, AA, TrO, glucose (one unit (Glc) or two-unit (Glc-Glc)) and chromium (Cr) (as shown in Table 16) were placed together and then submitted for optimisation of geometries where the lowest energy of formation was determined. Frequency calculations were carried out on the optimised geometry. Stabilisation energies (SE) and Gibbs free energies (ΔG) of the interaction were then calculated. The levels of theory and basis sets used were HF/STO-3g, B3LYP/3-21g, and M06/3-21g or BP86/STO-3G (for complexes involving chromium (Cr)).

Table 16 Molecules included in the two-component modelling studies are OA, AA, TrO, glucose (one unit (Glc) or two-unit (Glc-Glc)) and chromium (Cr).

Molecule	OA	AA	TrO
Combinations	Glc-OA Glc-Glc-OA Cr-OA	Glc-AA Glc-Glc-AA Cr-AA	Glc-TrO (Glc-Glc-TrO Cr-TrO TrO-OA TrO-AA TrO-TrO

Stabilisation energy (SE) was calculated from the ΔH_f of the complex and single components. SE gives a measure of the difference in total electronic energy values (ξ) between the complex and the two single components.[105] Stabilisation energies at 0 K and 298 K as well as free energies of interaction (ΔG) at 298 K and the solvation effect (ΔG solv (298K)) were calculated based on the following equations:

$$SE\ (0\ K) = \xi_{(complex)} - \xi_{(reactants)}$$

$$SE\ (298\ K) = SE\ (0\ K) + (H_{corr(complex)} - \Sigma\ H_{corr(reactants)})$$

$$\Delta G\ (298\ K) = SE\ (0\ K) + (G_{corr(complex)} - \Sigma\ G_{corr(reactants)})$$

$$\Delta G\ solv\ (298\ K) = \Delta G\ (298K) + (\xi_{(solv)complex} - \Sigma\ \xi_{(solv)reactants})$$

Values of ξ, H_{corr} (thermal correction to enthalpy) and G_{corr} (thermal correction to Gibbs free energy) were obtained from the Gaussian output (Figure 49).

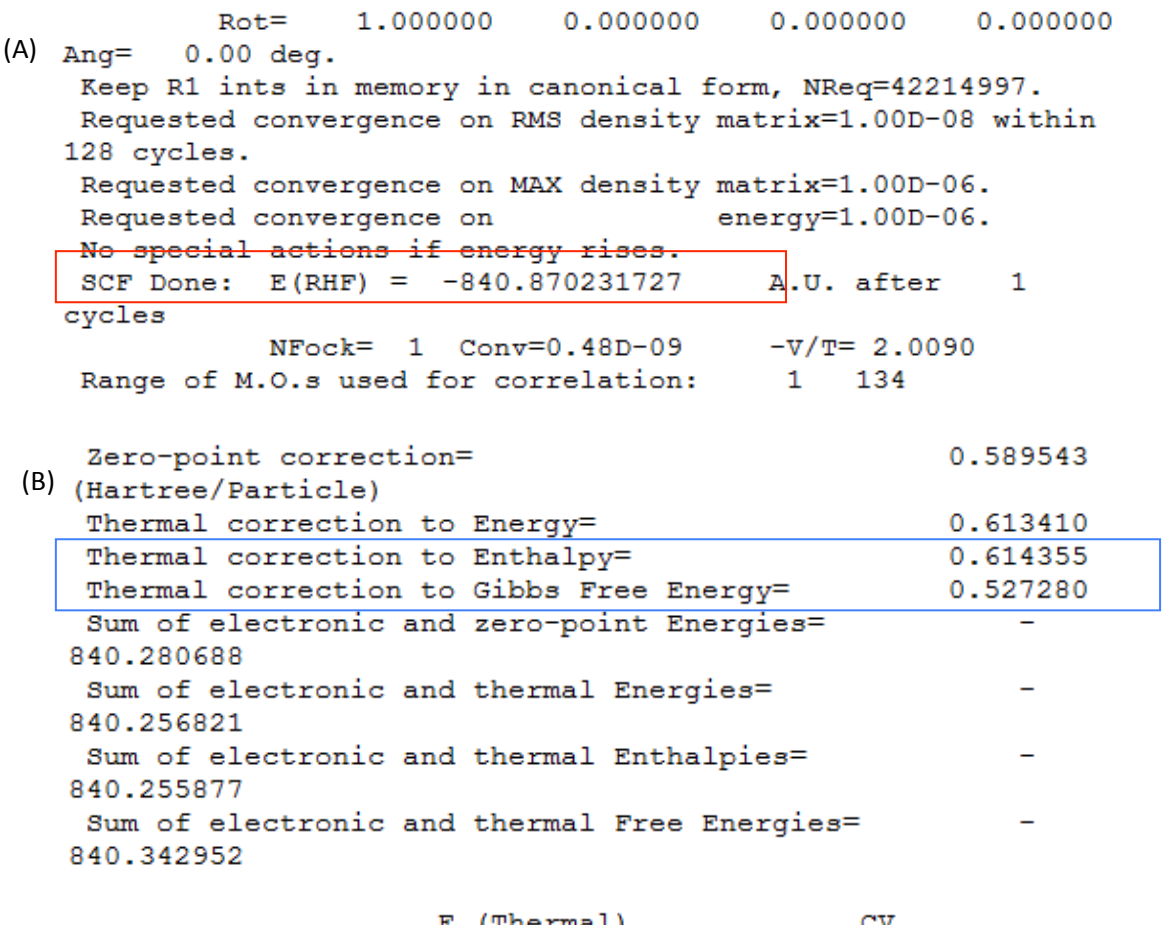

Figure 49 Sections from the output file showing where the relevant values (in unit a.u.) were obtained. (A) Total electronic energy value, ξ (in red lineated box) (B) Thermal correction values to enthalpy (H_{corr}) and Gibbs free energy (G_{corr}) (in blue lineated box).

The energy values were converted from a.u. to kJ mol^{-1} using the conversion of 1 a.u. = 2625.5 kJ mol^{-1}.

5.3 Results and discussion

The output of the Gaussian09 calculations for the ξ values for the individual molecules representing wood extractives (OA, AA and TrO), model surfaces (Glc, Glc-Glc, and Cr) and the complexes are presented in the Appendix F and used to calculate the stabilisation energy (SE) and Gibbs free energy (ΔG).

5.3.1 Modelling the interaction between wood extractives and cellulose

For the modelling of the interaction between wood extractives and cellulose (simulating the paper surface), a simple glucose molecule (Glc) and a dimer of two glucose rings (maltose) (Glc-Glc) were

used for calculations. The interaction between different wood extractive components (OA, AA and TrO) and the glucose molecules was modelled at different positions (namely the different hydroxide (–OH) groups) around the glucose molecule. These positions are indicated in Figure 44A as 1 - 5.

5.3.1.1 Interaction of triolein (TrO) with cellulose at different –OH positions (on glucose molecule)

The interaction between triolein and glucose was modelled using the lowest and simplest level of theory and basis set (HF/STO-3G) and the more complex B3LYP/3-21G. The results show the effect of varying the position of triolein around the glucose molecule when applying HF/STO-3G (Table 17) and B3LYP/3-21G (Table 18). The hydrogen attached to the triolein (marked 'X' in Figure 48) was chosen to be the initial point of interaction. Negative values of stabilisation energies (SE) indicate that the interaction is favoured while a negative Gibbs' free energy (ΔG) points to spontaneous interaction. This means that the larger the negative values, the more stable the interaction.

The most stable conformation was found to be when triolein-H was placed at –OH group #4 on the glucose when modelling with HF/STO-3G. When B3LYP/3-21G was used (Table 18), even though stable conformation were achieved at either –OH groups #2, #4, or combination of #1 & #5, the #4 position resulted in the most stable conformation (lowest SE and ΔG). The bond length was also the shortest indicating stronger hydrogen bonding between the molecules. Figure 50 and Figure 51 show the optimised complex resultant from modelling with B3LYP/3-21G.

Table 17 SE and ΔG values of interaction between triolein (TrO) and glucose (Glc) modelled with HF/STO-3G.

HF/STO-3G				
–OH #	SE	SE (298K)	ΔG (298K)	Bond length (Å)
1	38.1	30.2	-15.2	1.81
2	-1710	-1670	-1710	1.77
3	12.5	5.40	-36.0	1.83
4	-1710	-1670	-1710	1.77
1 & 5	30.7	21.2	-32.3	1.82/1.95

Table 18 SE and ΔG values of interaction between triolein (TrO) and glucose (Glc) modelled with B3LYP/3-21G.

B3LYP/3-21G				
–OH #	SE	SE (298K)	ΔG (298K)	Bond length (Å)
1	79.2	70.9	154	1.89
2	-1660	-1640	-1570	1.73
3	127	115	183	1.67
4	-1720	-1690	-1610	1.69
1 & 5	-1680	-1640	-1570	1.75/1.74

A possible reason for the unfavourable interaction with –OH at position #1 and #3 compared to those in position #2, #4 and #1-#5, may be due to steric hindrance/repulsion experienced from the orientation and position of the glucose (at those positions) with regards to the triolein molecule.

After careful consideration, however, the interaction of glucose with the hydrogen marked 'X' (in Figure 47) on triolein should not be possible as this particular hydrogen or the particular space chosen for modelling, would encounter significant steric hindrance as the hydrogen is shielded due to the stable conformation adopted by the triolein molecule.

5.3.1.2 Interaction with a glucose (Glc) and maltose (two glucose-linked units, Glc-Glc)

The modelling of the interactions between model compounds (OA, AA and TrO) and a single glucose unit (Glc) and a maltose unit (two glucose-linked units, Glc-Glc) was carried out at different levels of theory and basis sets, namely HF/STO-3G, B3LYP/3-21G AND M06/3-21G. Interactions of OA and AA with Glc and Glc-Glc were also modelled at HF/STO-3G at –OH positions of #1, #2 and #5. The resultant ξ values showed that the complexes were of similar stability. Results in Table 19 - Table 22, with regards to Glc-OA, Glc-AA, Glc-Glc-OA and Glc-Glc-AA, are based on modelling at the interaction at the –OH #1 position of glucose as the resultant complexes were found to be the most stable. Any attempts to increase the complexity of basis set from 3-21G to 6-31G were unsuccessful due to the molecules (especially the triolein molecule) being too big, with calculations exceeding the computing capacity and available computing time granted.

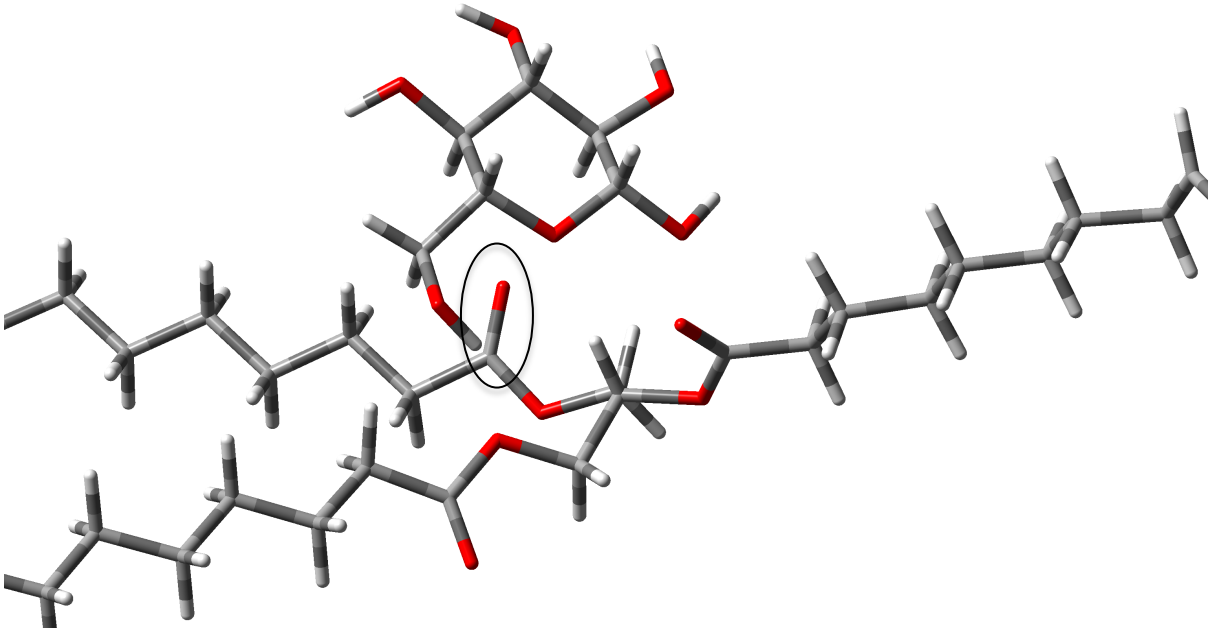

Figure 50 (Close up) Interaction between triolein and glucose molecules. Probable hydrogen bonding (marked in circle) occurring between the -OH #1 (of glucose) with the oxygen (-C=O) of triolein molecule. The bond length measured here is 1.89 Å.

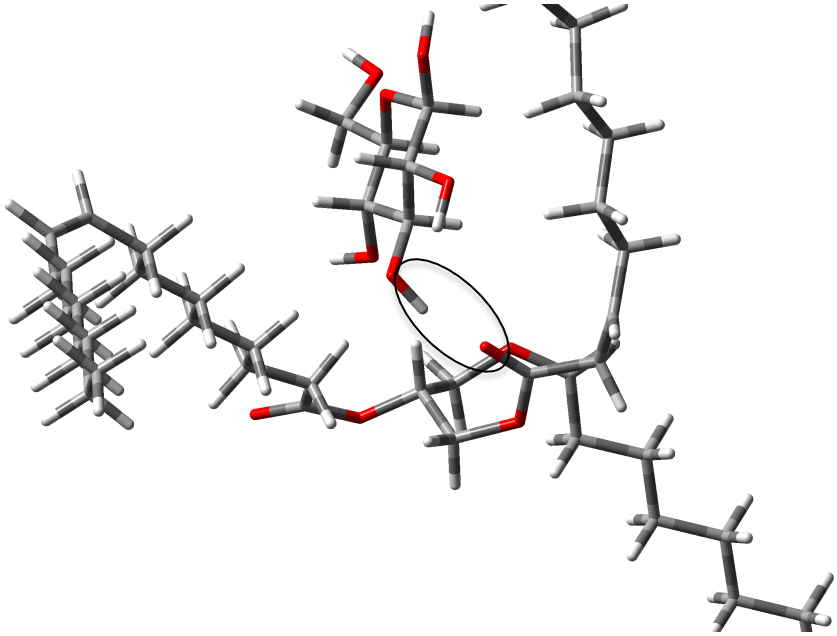

Figure 51 Interaction between triolein and glucose molecule that is more favourable. Probable hydrogen bonding occurring between -OH #4 (of glucose) with the oxygen (-C=O) of triolein molecule. The bond length measured to be 1.69 Å.

Table 19 and Table 20 give the results of the calculations for the interaction between the model compounds and Glc, whereas Table 21 and Table 22 show results for modelling each model compound with Glc-Glc. The modelling of the interaction between TrO and Glc was carried out by placing the glucose molecule at the tail end of the triolein molecule. After careful consideration, this would probably be the most likely position for the interaction as in the real system it is believed that the tail portion of triolein would be protruding into the aqueous solution open to interaction with surrounding molecules.

The different levels of theory were found to give quite different results. In some cases these appear to be unreliable, for example the very large positive values of SE and ΔG obtained using M06/3-21G. Of the three calculations B3LYP/3-21G would appear to give the most reliable and consistent results and also predicts stable interactions for all model compounds with Glc and Glc-Glc. Hence, for further discussions only results from B3LYP/3-21G will be considered when modelling cellulose interactions.

Based on the SE values given in Table 19, OA and AA formed more stable complexes with Glc than did TrO. Similarly, when the number of glucose units was increased OA and AA formed more stable complexes with Glc-Glc than did TrO with Glc-Glc (Table 21). By increasing one glucose unit to two units, the SE (298K) results show that interactions of model compounds with Glc-Glc are more stable. This may be due to increased hydrogen bonds with the model compounds (OA and AA) or increased hydrophobic interactions between TrO and the glucose units, shown by increased SE values. Based on ΔG values from Table 20, the results predict that interactions of OA, AA and TrO with Glc should be spontaneous. However Table 22 predicts that only interactions of OA and AA with Glc-Glc should be spontaneous, and the interaction of TrO with Glc-Glc is non-spontaneous. The Glc-Glc-OA interaction was found to be less favourable than the Glc-OA interaction. On the other hand, the Glc-Glc-AA interaction became more favourable than Glc-AA. Solvation effects cannot be ignored and the introduction of water molecules would greatly affect the entropic contribution and free energy of interaction. When solvation effects were considered (Table 20), only the Glc-AA interaction became non-favourable whereas the Glc-OA and Glc-TrO interactions were still favourable. On the other hand, the Glc-Glc-TrO interaction became favourable and, instead, Glc-Glc-OA and Glc-Glc-AA interactions became unfavourable (Table 22). The Glc-TrO and Glc-Glc-TrO interactions seem to increase in stability. This may be due to repulsive interaction with the water molecules (poor solute-solvent interaction). For interactions with OA and AA, the solvation effect leads to a significant positive gain in ΔG, which may be caused by displacement of water molecules or reorganisation of water molecules causing a loss in entropy. Interaction of OA with a single glucose unit is still favourable, however by increasing to 'maltose' (Glc-Glc), the interaction between OA becomes unfavourable. The interaction of AA is unfavourable with either Glc or Glc-Glc when solvation effects were introduced.

Table 19 SE and ΔS values for two-component calculations - model compounds with one glucose unit (Glc).

	(kJ mol^{-1})		HF/STO-3G	B3LYP/3-21G	M06/3-21G
SE	Glc	OA	-42.7	-136	10900
		AA	-1790	-95.5	9850
		TrO	-3.10	-22.5	-74.4
SE (298K)	Glc	OA	-32.1	-127	10900
		AA	-1560	-89.6	9860
		TrO	2.30	-16.1	-60.8
ΔS	Glc	OA	-0.19	0.28	-0.25
		AA	-0.94	-0.14	-0.20
		TrO	-0.10	0.30	-0.26

Table 20 ΔG and ΔG (solv) for two-component calculations - model compounds with one glucose unit (Glc).

	(kJ mol^{-1})		HF/STO-3G	B3LYP/3-21G	M06/3-21G
ΔG	Glc	OA	14.3	-219	11000
		AA	-1510	-54.4	9910
		TrO	27.7	-111	3.40
ΔG (solv)	Glc	OA	250	-35.7	182
		AA	283	28.9	9990
		TrO	-1920	-2040	-1840

Table 21 SE and ΔS values for two-component calculations - model compounds with two glucose-linked unit (Glc-Glc).

	(kJ mol^{-1})		HF/STO-3G	B3LYP/3-21G	M06/3-21G
SE	Glc-Glc	OA	-56.1	-169	10900
		AA	-38.1	-226	-103
		TrO	-13.2	-45.8	-106
SE (298K)	Glc-Glc	OA	-45.3	-162	10900
		AA	-30.6	-215	-92.3
		TrO	-8.20	-38.4	-87.3
ΔS	Glc-Glc	OA	-0.19	-0.21	-0.28
		AA	-0.16	-0.28	-0.24
		TrO	-0.13	-0.22	-0.31

Table 22 ΔG and ΔG (solv) for two-component calculations - model compounds with two glucose-linked unit (Glc-Glc).

	(kJ mol^{-1})		HF/STO-3G	B3LYP/3-21G	M06/3-21G
ΔG	Glc-Glc	OA	2.0	-107	11000
		AA	10.3	-142	-32.9
		TrO	25.8	21.0	-13.1
ΔG (solv)	Glc-Glc	OA	-80.5	36.6	79.4
		AA	-193	29.6	12.3
		TrO	-1830	-1820	-1770

5.3.1.3 Interaction of model compounds with glucose (Glc) and with chromium (Cr)

The calculations performed for interactions with glucose using HF, B3LYP and M06 were found to be unsuitable for modelling interactions with metal molecules. Modelling of the interaction between model compounds and chromium was thus carried out with BP86/STO-3G. Any attempts to model these interactions with more complex theories/basis sets were unsuccessful. At the same time, BP86/STO-3G was also used to model the interaction between model compounds and glucose, to allow a comparison between the interaction with chromium and glucose.

Table 23 compares the results of modelling the interactions of OA, AA and TrO with Cr and OA, AA and TrO with Glc when the molecular structures and complexes were optimised with BP86/STO-3G. Negative SE values indicate that complexes formed by the interactions of OA and AA with Cr, and OA, AA and TrO with Glc are stable, with more negative values indicating a more stable the complex. However, ΔG values show that interaction of Cr and OA would not be favourable. The complex formed from the interaction between TrO and Cr is predicted to be unstable and unfavourable, shown by having a largely positive SE and ΔG values. Only the interaction of AA with Cr is favourable, based on modelling with BP86/STO-3G.

The similar SE values observed for the interaction of OA and AA with Glc may be explained by similar strength in hydrogen bonding between these two interacting molecules. Similar ΔS values suggest that the entropic components due to loss of conformational degree of freedom for each complex (Glc-OA and Glc-AA) are also similar. The negative ΔG for the interaction of TrO with Glc predicts that the interaction is still favourable, however, the enthalpic contribution to this interaction (Glc-TrO) is much less than that with OA and AA possibly due to hydrophobic interactions and not hydrogen bonding which occurs with OA and AA.

Table 23 SE, ΔS and ΔG values values of two-component calculations with BP86/STO-3G.

(kJ mol^{-1})		SE	SE (298K)	ΔS	ΔG (298K)
Glc	OA	-187	-173	-0.21	-125
	AA	-188	-177	-0.22	-122
	TrO	-37.3	-33.8	-0.11	-5.9
Cr	OA	-73.6	-113	-0.44	57.1

	AA	-93.0	-114	-0.22	-26.2
	TrO	2050	1990	-1.20	2410

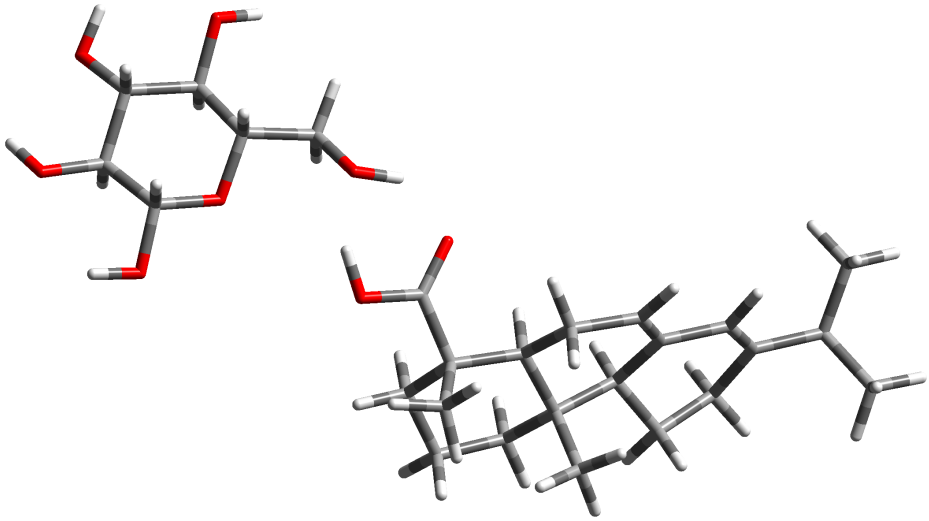

Figure 52 Interaction of an abietic acid molecule with a glucose molecule modelled at BP86/STO-3G.

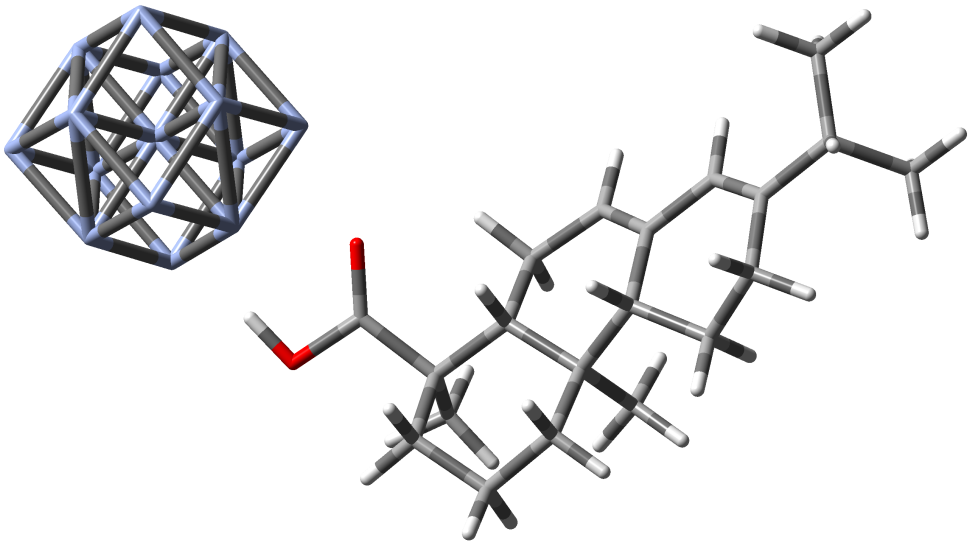

Figure 53 Interaction of an abietic acid molecule with a chromium unit modelled at BP86/STO-3G.

5.3.1.4 Interaction between model compound molecules

The results of modelling the interaction between individual model compound molecules using HF/STO-3G are presented in Table 24 and Table 25. The SE (298 K) values show that TrO-OA forms the most

stable complex followed by TrO-TrO, however TrO-AA complex is not stable. The ΔG values (with or without solvation effects) show that all interactions (TrO-OA, TrO-AA and TrO-TrO) are unfavourable. However, ΔG (solv) results indicate that TrO prefers interacting with OA than with AA, whereas the most unfavourable interaction is TrO with itself. This observation is in agreement with the three-layered model of wood extractive colloid model proposed by Lee et al., where triglycerides (TrO) interact with fatty acids (OA) instead of resin acids (AA).[27] Therefore, as AA (or resin acids) occupies the outermost layer of the wood extractive colloids, it may be more readily lost than OA (or fatty acids) or TrO (triglycerides) when wood extractive colloids come into contact with other surfaces such as chromium (due to the interaction of Cr-AA being favoured over any other).

Table 24 SE and ΔS values for modelling between triolein and each model compounds with HF/STO-3G

(kJ mol^{-1})		SE	SE (298 K)	ΔS
TrO	OA	0.001	-5.0	-0.15
	AA	5.40	7.40	-0.14
	TrO	-1.10	-1.10	-0.03

Table 25 ΔG and ΔG (solv) values between triolein and each model compounds with HF/STO-3G

(kJ mol^{-1})		ΔG (298 K)	ΔG (solv) (298 K)
TrO	OA	44.8	145
	AA	47.0	728
	TrO	7.30	1270

5.3.2 Comparison with experimental results

The very large negative ΔG (solv) of interaction of TrO with glucose unit(s) (Table 20 and Table 22), shows that this interaction is greatly favoured. This result agrees with the observation made by the QCM-D adsorption experiments (Chapter 3), where there was a very strong interaction between TrO and the cellulose surface, which may indicate a very strong interaction of triglycerides with cellulose. Additionally, the fact that resin acids (exemplified by AA in this work) are shown to occupy the

outermost layer of the wood extractive colloids (section 5.3.1.4) reinforces the explanation of the results of Chapter 2. That is, surface properties of wood extractives colloids are altered to become more "fatty acid-like" due to deprotonation and solubilisation of resin acids when the pH of suspension was perturbed. Then these resin acids do not return to the wood extractive colloids when the pH is readjusted after perturbation. The results from adsorption isotherms (Chapter 2) and QCM-D adsorption experiments also showed that the strength of interaction of AA with cellulose is greater than that of OA with cellulose, which agrees with the trend observed from modelling experiments where interactions of Glu-Glu with AA was more favourable than that with OA.

The modelling experiments that compared the interaction with Cr and with Glc (section 5.3.1.3) showed that only AA has a favourable interaction with Cr (negative ΔG), as opposed to all three colloidal types (OA, AA and TrO) having favourable interactions with Glc. This observation supports the trend of the adhesion force results from Chapter 4, where it was shown that the strength of adhesions of OA and TrO with cellulose were much greater than the respective adhesion strengths with chromium. The interaction of Glc-AA and Cr-AA, however, are both favourable interactions, which agrees with the AFM results that adhesion of AA onto chromium is comparable in strength to cellulose. Additionally, the strength of adhesion of OA and AA onto cellulose are comparable in the AFM force measurements, which agrees qualitatively with observation made of ΔG (solv) values on interaction of OA-Glc-Glc and AA-Glc-Glc (section 5.3.1.2). The results from section 5.3.1.2 also showed that the ΔG values indicate that the interaction of Glc-OA and Glc-TrO are more spontaneous (significantly more negative) than for Glc-AA and a spontaneous interaction also occurs for Glc-Glc-TrO. When the solvation effect was introduced, the interaction of AA with Glc or Glc-Glc becomes unfavourable.

When taken together, these observations support the notion that triglycerides (represented by TrO) and fatty acids (represented by OA) have stronger interaction with paper (modelled by Glc or Glc-Glc) than do resin acids (represented by AA). This may explain the observation that resin acids preferentially desorb from paper onto chromium surface. The apparent difference between the modelling calculations and the AFM experiments is bought about because the molecule used to represent cellulose in computational modelling experiments is only a single glucose molecule or maltose molecule (with α-1, 4-glycosidic bond). Hence the results from computational modelling experiments can only be used as a qualitative comparison.

5.4 Conclusion

Different levels of theory and basis sets were used to model interactions of model compounds (OA, AA and TrO) with representations of model surfaces (Glc, Glc-Glc and Cr). The results of these modelling calculations are useful as a qualitative comparison to the experimental results (Chapters 2, 3 and 4). The very strong interaction of TrO with glucose unit(s) agrees with QCM-D adsorption experiments, where the TrO was tightly bound to cellulose surface. The results (5.3.1.4) also showed that interaction between the three components agreed with the proposed three-layered wood extractive model. Thus placing resin acids on the outermost layer of the colloid may explain why resin acids are more readily lost and transferred from the paper surface to another surface that it comes in contact with. Lastly, the interaction of model compounds with Glc as compared to that with Cr, where only AA has favourable interaction with chromium (Cr), agreed with the AFM adhesion results that fatty acids and triglycerides interact more strongly with cellulose than chromium, whereas resin acids can interact with both cellulose and chromium.

The main issue faced was insufficient computing time and capacity to carry out the desired calculations. As mentioned previously, triolein is too big to model with anything except the lower level of theory and basis set if using *ab initio* quantum calculations. In addition, only BP86 could be used for modelling with Cr. Solvation effects were important in considering the favourability of interaction, and in many cases result in interaction being unfavourable, indicating that a different approach is needed to model these interactions fully.

5.4.1 Future work

There are endless possibilities in the study of interactions for these complexes when using computational methods. This current work attempted to simplify the system to a level to allow the modelling in a reasonable timeframe, including modelling with one to two glucose rings as a model for cellulose. It would be profitable for future calculations to build up the number of glucose units to reflect more accurately the structure of cellulose. To better understand the real system, it would also be useful to increase the number of fatty acid, resin acid and triglyceride molecules interacting with the glucose units (or metal surface); to have complexes of two or more different model compounds (fatty acid, resin acid or triglyceride molecules) interacting with glucose unit(s) (or metal surface) and thus study the effect of these possible combinations and compare it with experimental data. These future calculations are however dependent on the cost and time required performing them, as well as the capability of the computational program to carry out these calculations.

A different approach may be needed to carry out the calculations with metal or inorganic surfaces. The current established method is only useful for the most basic of *ab initio* quantum calculations. It may be worth exploring other computational programs other than Gaussian09 to carry out these calculations. An alternative is to employ the ONIOM capability in Gaussian09 to attempt calculations with metal surfaces. However, even with all these considerations, the main issue to address is the use of quantum mechanical calculations for modelling and whether it is the correct approach. The size of the system that can be analysed will limit the choice of level of theory and basis sets that can be used.

Chapter 6 General Conclusion

The interactions of wood extractives and model compound colloids with cellulose and chromium surfaces were studied using a number of different techniques, and the possible modes/mechanisms and strength of interactions with these surfaces were investigated. The outcomes of experimental and theoretical evaluations gives some insight into why the resin acid component of the wood extractives incorporated into paper (represented by pulp fibre or microcrystalline cellulose) would be transferred onto paper making or printing machine surfaces (represented by chromium model surface) during manufacture or processing of paper.

Two new experimental techniques were developed as part of this work: first a technique to coat surfaces with microcrystalline cellulose, and second, a technique to attach colloids directly to an AFM tip. The method for modifying a surface with microcrystalline cellulose as a surrogate paper surface was developed and used extensively in QCM-D adsorption experiments and AFM force measurement studies. The *in situ* attachment of a soft colloid to the AFM cantilever tip was successfully developed for the AFM force measurement experiments and proved to be crucial to maintain the native structure of the colloid during the adhesion experiments.

The behaviour of the adsorption of colloids onto model surfaces was studied through fitting a number of models for adsorption isotherms from gas chromatography analysis of deposition experiments. The Freundlich model was found to have a better fit to the results than the Langmuir model, thus concluding that the adsorption of all colloidal types follow multilayer adsorption behaviour. The BET model, with exceptions of adsorption of wood extractives and oleic acid onto microcrystalline cellulose, was not suitable as the negative C_{BET} values obtained are unrealistic. The Langmuir isotherm results showed that oleic acid and abietic acid have greater adsorption intensity (n) and capacities (K_F) to microcrystalline cellulose than pulp fibres. On the other hand, WE showed greater adsorption intensity and capacity to pulp fibres than microcrystalline cellulose. The isotherm results also showed that without pH perturbation, wood extractives behaved like abietic acid but with pH perturbations wood extractives behaved more like oleic acid. Thus showing that surface properties of wood extractives colloids changed when subjected to pH perturbations. This may be explained by the deprotonation and solubilisation of resin acids at increased pH (from 5 to 7). These normally occupy the outermost layer of a wood extractives colloid, but once solubilised they do not return to the wood extractives colloid when pH was returned to 5. This results in fatty acids now being exposed on the outermost layer of a wood extractives colloid.

Similar to results from adsorption isotherms, QCM-D adsorption experiments showed that wood extractives and model compound colloids with model surfaces follow multilayer adsorption behaviour. QCM-D adsorption experiments concluded that wood extractives have greater adsorption onto chromium surfaces than onto cellulose surfaces. This is similar to the deposition trend observed in the same adsorption experiments where abietic acid (a representative of resin acids) deposited to a larger extent onto chromium than onto cellulose in comparison to triolein (a representative of triglycerides) and oleic acid (a representative of fatty acids). QCM-D results of the amount of wood extractive colloids and mixed model compound colloids deposited were not significantly different. This showed that the deposition behaviour onto both model surfaces does not differ even though the concentrations of each component in the colloids were different. From the AFM force measurement studies (Chapter 4) it is also clear that abietic acid and wood extractives have comparable strength of adhesion onto cellulose and chromium, whereas the strengths of adhesion of triolein and oleic acid was significantly greater onto cellulose than onto chromium. Computational modelling of the interaction between oleic acid, abietic acid and triolein also showed that triolein prefers interacting with oleic acid rather than abietic acid. Altogether, these results agree with the wood extractive colloid model suggested by Lee et al.[27], where resin acids occupy the outermost layer of a wood extractive colloid.

Even though computational modelling of interactions was useful, the *ab initio* quantum calculations, especially at higher levels of theory and basis sets, were not suitable for modelling metal compounds or large organic compounds such as triolein or multiple linked glucose molecules, due to restriction on the computing capacity and time available. Therefore, different computing programs and approaches may be needed to carry out modelling these interactions effectively.

By comparing both experimental results and computational modelling results, the trends with regards to the strength of interaction of each model compound with cellulose and with chromium would suggest that unlike abietic acid colloids, triolein and oleic acid colloids have very strong affinity to cellulose. Coupled with the change in the trend observed in the Freundlich isotherm when pH perturbations were investigated this points to the surface properties of wood extractive colloids changing from resin-acid like to fatty acid-like. These observations and results suggest that resin acids have higher tendency to adsorb onto metal surfaces rather than remain on paper surfaces during papermaking and printing processes, especially after colloids in suspension have been subjected to pH perturbations. In order to minimise the transfer of resin acids from paper surfaces onto metal surfaces they come into contact with, it would be beneficial to maintain a constant pH in solution to avoid any change to surface properties of the colloid that might lead to colloid instability.

Reference

1. Grubb, M.; Wray, H.; Richardson, D., The use of flow cytometry for managing extractives associated with pitch deposits. In *Appita Conference and Exhibition (63rd : 2009 : Melbourne, Vic.)*, Appita Inc.: Carlton, Vic., 2009; pp 347-352.
2. Wallqvist, V.; Claesson, P. M.; Swerin, A.; Schoelkopf, J.; Gane, P. A. C., Interaction Forces between Talc and Pitch Probed by Atomic Force Microscopy. *Langmuir* 2007, *23*, 4248-4256.
3. Dreisbach, D. D.; Michalopoulos, D. L., Understanding the behavior of pitch in pulp and paper mills. *Tappi J.* 1989, *72*, 129-34.
4. The Boyer mill in Tasmania has converted totally to softwood plantation fibre and is no longer using native timber. http://www.norskeskog.com/People-and-press/Press-room/Prior-articles/Boyer-conversion.aspx (29 April, 2011),
5. Wilderness Society, Norske Skog congratulated on ruling out native forests. In *Tasmanian Times*, Tuffin, Lindsay: 2009.
6. Opedal, M. T.; Stenius, P.; Johansson, L., Review: Colloidal Stability and Removal of Extractives from Process Water in Thermomechanical Pulping. *Nord. Pulp Pap. Res. J.* 2011, *26*, 248-257.
7. Thornton, J. Dissolved and colloidal substances in the production of wood-containing paper. PhD thesis, Åbo Akademi University, Åbo, 1993.
8. Sundberg, K. Effects of wood polysaccharides on colloidal wood resin in papermaking. PhD thesis, Åbo Akademi University, Åbo, 1995.
9. Richardson, D. E.; Parsons, T.; van den Bosch, J.; Harden, P. E. In *Factors affecting the formation and control of pitch deposits in newsprint manufacture from mechanical pulp and recycled fibre*, 50th Appita Annual General Conference Proceedings, Auckland, New Zealand, 1996; Auckland, New Zealand, 1996; pp 499-506.
10. Stack, K. R.; Stevens, E. A.; Richardson, D. E.; Parsons, T.; Jenkins, S. In *Factors affecting the deposition of pitch in process waters and model dispersions*, 52nd Appita Annual General Conference Proceedings, Brisbane, Australia, 1998; Brisbane, Australia, 1998; pp 59-66.
11. Stack, K.; Stevens, E. *Study of factors affecting pitch deposition*; School of Chemistry, Report; University of Tasmania: Hobart, 2000.
12. McLean, D. S.; Stack, K.; Richardson, D. In *Wood pitch deposition versus composition*, WPP 2003 Chemical Technology of Wood, Pulp and Paper International Conference, Bratislava, Slovak Republic, September 17–19, 2003; Bratislava, Slovak Republic, 2003; pp 115-120.
13. Mosbye, J. Colloidal Wood Resin: Analyses and Interactions. PhD thesis, NTNU Trondheim Norwegian University of Science and Technology, Trondheim, 2003.
14. Mosbye, J.; Laine, J.; Moe, S., The effect of dissolved substances on the adsorption of colloidal extractives to fines in mechanical pulp. *Nordic Pulp and Paper Research Journal* 2003, *18*, 63-68.
15. Qin, M.; Hannuksela, T.; Holmbom, B., Physico-chemical Characterisation of TMP Resin and Related Model Mixtures. *Colloids Surf., A* 2003, *221*, 243-254.
16. Qin, M.; Hannuksela, T.; Holmbom, B., Deposition tendency of TMP resin and related model mixtures. *Journal of Pulp and Paper Science* 2004, *30*, 279-283.
17. Sundberg, A.; Strand, A.; Vahasalo, L.; Holmbom, B., Phase Distribution of Resin and Fatty Acids in Colloidal Wood Pitch Emulsions at Different pH-Levels. *J. Dispersion Sci. Technol.* 2009, *30*, 912-919.
18. Kallio, T.; Lindfors, J.; Laine, J.; Stenius, P., Spreading and Adhesion of Lipophilic Extractives on Surfaces in Paper Machines. *Nord. Pulp Pap. Res. J.* 2008, *23*, 108-119.

19. Featherstone, A.; Viney, D.; Mosbye, J.; Richardson, D. E. In *Deposit Control: Does Adsorption of Colloidal Extractives to Bentonite Affect the Dissolution of Resin Acids?*, 60th Appita Annual Conference, Melbourne, Australia, 2006; Appita: 2006; pp 417-420.
20. Ekman, R.; Holmbom, B., Chapter 2 - The chemistry of wood resin. In *Pitch Control, Wood Resin and Deresination*, 1st ed.; Back, E. L.; Allen, L. H., Eds. TAPPI Press: Atlanta, 2000; pp 37-76.
21. Ekman, R., Chapter 7 - Resin during storage and in biological treatment. In *Pitch Control, Wood Resin and Deresination*, 1st ed.; Back, E. L.; Allen, L. H., Eds. TAPPI Press: Atlanta, 2000; pp 185-204.
22. Sjöström, E., Chapter 5 - Extractives. In *Wood Chemistry. Fundamentals and Applications*, 2nd ed.; Academic Press: San Diego, 1993; pp 90-108.
23. Norske Skog Boyer. http://www.norskeskog.com/Business-units/Australasia/Norske-Skog-Boyer.aspx (30th April, 2011),
24. Back, E. L., Chapter 1 - The locations and morphology of resin components in the wood. In *Pitch Control, Wood Resin and Deresination*, 1st ed.; Back, E. L.; Allen, L. H., Eds. TAPPI Press: Atlanta, 2000; pp 1-35.
25. Vercoe, D.; Stack, K. R.; Blackman, A.; Richardson, D. E., A Multicomponent Insight into the Interactions Leading to Wood Pitch Deposition. *Appita J.* 2005, *58*, 208-213.
26. Vercoe, D.; Stack, K.; Blackman, A.; Richardson, D. In *Interaction of pitch components at a molecular level*, WPP 2003 Chemical Technology of Wood, Pulp and Paper International Conference, Bratislava, Slovak Republic, September 17.–19. 2003, 2003; Bratislava, Slovak Republic, 2003; pp 127-133.
27. Lee, R.; Stack, K. R.; Lewis, T. W.; Garnier, G.; Richardson, D. E.; Ottaviani, M. F.; Jockusch, S.; Turro, N. J., Structure of Wood Extract Colloids and Effect of $CaCl_2$ on the Molecular Mobility. *Nord. Pulp Pap. Res. J.* 2012, *27*, 639-646.
28. MacNeil, D.; Sundberg, A.; Vahasalo, L.; Holmbom, B., Effect of calcium on the phase distribution of resin and fatty acids in pitch emulsions. *Journal of Dispersion Science and Technology* 2011, *32*, 269-276.
29. Mosbye, J.; Moe, S.; Tammelin, T.; Saarinen, T.; Laine, J., The ability of PEO to remove model colloidal extractives from solutions with different types of fines. *Nordic Pulp and Paper Research Journal* 2004, *19*, 59-66.
30. Kallio, T.; Kekkonen, J., Fouling in the paper machine wet end. *Tappi Journal* 2005, *4*, 20-24.
31. Porubská, J.; Alince, B.; van de Ven, T. G. M., Homo- and heteroflocculation of papermaking fines and fillers. *Colloids and Surfaces A: Physicochemical and Engineering Aspects* 2002, *210*, 223-230.
32. Wu, M. R. P., Jean; van de Ven, Theo G. M, Polyethylene oxide induced fines flocculation and retention: from bench top experiments to paper machine performance. *Nordic Pulp & Paper Research Journal* 2006, *21*, 646-652.
33. Lee, R.; Stack, K. R.; Richardson, D. E.; Lewis, T. W.; Garnier, G., Study of Pitch Colloidal Stability using a Photometric Dispersion Analyser. *Appita J.* 2010, *63*, 387-406.
34. Lee, R.; Stack, K.; Lewis, T. W.; Garnier, G.; Richardson, D.; De Van, T. V. In *Measurement of pitch deposition by impinging jet microscopy: Effect of divalent salts.*, In: 64th Appita Annual Conference & Exhibition, Melbourne, Australia., 18-21 April, 2010; Melbourne, Australia., 2010; pp 1-7.
35. Lee, R.; Garnier, G.; Lewis, T. W.; Richardson, D. E.; Van De Ven, T. G. M.; Stack, K. R., Pitch Deposition at the Solid–Liquid Interface: Effect of Surface Hydrophobicity/Hydrophilicity and Cation Specificity. *Colloids Surf., A* 2011, *388*, 84-90.
36. Murray, G.; Stack, K.; McLean, D. S.; Shen, W.; Garnier, G., Dynamics of colloidal pitch adsorption at the solid-liquid interface by surface plasmon resonance. *Colloids and Surfaces A: Physicochemical and Engineering Aspects* 2009, *341*, 127-133.

37. Vahasalo, L.; Degerth, R.; Holmbom, B., The use of flow cytometry in wet end research. *Paper Technology* 2003, *44*, 45-49.
38. Rissanen, R.; Leinonen, A.; Haapala, A.; Kyyronen, P., Comparison of sample pre-treatment methods on flow cytometry measurement of mechanical pulp. In *PEERS Conference*, TAPPI: 2011.
39. Saarimaa, V.; Vahasalo, L.; Sundberg, A.; Pranovich, A.; Holmbom, B.; Svedman, M.; Orsa, F., Influence of pectic acids on aggregation and deposition of colloidal pitch. *Nordic Pulp & Paper Research Journal* 2006, *21*, 613-619.
40. McLean, D. S.; Stack, K. R.; Richardson, D. E.; Haddad, P. R. In *Wood pitch fixative selection by laser particle size analysis*, 60th Appita Annual General Conference Proceedings, Melbourne, Australia, 3-5 April, 2006; Appita: Melbourne, Australia, 2006; pp 413-416.
41. Woods, D. A. Dynamics of surfactant adsorption at solid-liquid interfaces. University of Durham, Durham theses, 2011.
42. Shaw, D. J., Chapter 8 Colloid stability. In *Introduction to Colloid and Surface Chemistry*, 4th ed.; Butterworth-Heinemann: Oxford, 1992; pp 211-243.
43. Boufi, S.; Gandini, A., Formation of polymeric films on cellulosic surfaces by admicellar polymerization. *Cellulose* 2001, *8*, 303-312.
44. Liu, S., Cooperative adsorption on solid surfaces. *Journal of Colloid and Interface Science* 2015, *450*, 224-238.
45. Tien, C., *Adsorption calculations and modeling*. Butterworth-Heinemann: New York, 1994; p 244.
46. Rahimi, M.; Vadi, M., Langmuir, Freundlich and Temkin adsorption isotherms of propranolol on multi-wall carbon nanotube. *Journal of Modern Drug Discovery and Drug Delivery Research* 2014, *3*, 1-3.
47. Foo, K. Y.; Hameed, B. H., Insights into the modeling of adsorption isotherm systems. *Chemical Engineering Journal* 2010, *156*, 2-10.
48. Scatchard, G., Adsorption isotherms and liquid solutions. *Science* 1949, *110*, 440.
49. Piccin, J. S.; Dotto, G. L.; Pinto, L. A. A., Adsorption isotherms and thermochemical data of FD&C Red n° 40 binding by Chitosan. *Brazilian Journal of Chemical Engineering* 2011, *28*, 295-304.
50. Toth isotherm. http://micro-report.com/isotherm-models/toth/ (26 June 2015),
51. Theimer, O., On multilayer adsorption isotherms. *Transactions of the Faraday Society* 1952, *48*, 326-331.
52. Ebadi, A.; Mohammadzadeh, J. S. S.; Khudiev, A., What is the correct form of BET isotherm for modeling liquid phase adsorption? . *Adsorption* 2009, *15*, 65-73.
53. Moradi, O., *Thermodynamics of Interfaces, Thermodynamics - Interaction Studies - Solids, Liquids and Gases*. INTECH Open Access Publisher: 2011.
54. Lowell, S.; Shields, J. E., *Powder surface area and porosity*. 1 ed.; Springer Netherlands: 1984; p 234.
55. Bungay, H. R. B.E.T. Equation. http://www.rpi.edu/dept/chem-eng/Biotech-Environ/Adsorb/bet.htm (28 September 2015),
56. McMillan, W. G.; Teller, E., The Assumptions of the BET Theory. *Journal of Physical and Colloid Chemistry* 1951, *55*, 17-20.
57. Heier, D. Adsorption of wood extractives and model compounds onto bentonite. University of Tasmania, Hobart, 2013.
58. Park, Y.; Ayoko, G. A.; Horvárth, E.; Kurdi, R.; Kristof, J.; Frost, R. L., Structural characterisation and environmental application of organoclays for the removal of phenolic compounds. *Journal of Colloid and Interface Science* 2013, *393*, 319-334.
59. Gurumayum Sharma, S. D.; Moreton, D.; Vincent, B., Adsorption isotherm and atomic force microscopy studies of the interactions between polymers and surfactants on

steel surfaces in hydrocarbon media. *Journal of Colloid and Interface Science* 2003, *263*, 343-349.
60. Agarwal, A. K.; Kadu, M. S.; Pandhurnekar, C. P.; Muthreja, I. L., Langmuir, Freundlich and BET adsorption isotherm studies for zinc ions onto coal fly ash. *International Journal of Application or Innovation in Engineering and Management* 2014, *3*, 64-70.
61. Palme, A. Study of wood pitch emulsions-interactions with Nile red and influence of pH. Chalmers University of Technology, Goteborg, 2011.
62. McLean, D. S.; Vercoe, D.; Stack, K. R.; Richardson, D., The colloidal pK_a of lipophilic extractives commonly found in *Pinus radiata*. *Appita Journal* 2005, *58*, 362-366.
63. Asselman, T.; Garnier, G., Adsorption of model wood polymers and colloids on bentonites. *Colloids and Surfaces a-Physicochemical and Engineering Aspects* 2000, *168*, 175-182.
64. Höök, F.; Rodahl, M.; Brzezinski, P.; Kasemo, B., Energy dissipation kinetics for protein and antibody-antigen adsorption under shear oscillation on a quartz crystal microbalance. *Langmuir* 1998, *14*, 729-734.
65. Henry, C., Product review: measuring the masses: quartz crystal microbalances. *Analytical Chemistry* 1996, *68*, 625A-628A.
66. King, W. H., Piezoelectric sorption detector. *Analytical Chemistry* 1964, *36*, 1735-1739.
67. Marx, K. A., Quartz crystal microbalance: A useful tool for studying thin polymer films and complex biomolecular systems at the solution−surface interface. *Biomacromolecules* 2003, *4*, 1099-1120.
68. O'Sullivan, C. K.; Guilbault, G. G., Commercial quartz crystal microbalances: Theory and applications. In Gizeli, E.; Lowe, C. R., Eds. 2002; pp 291-303.
69. Fundamentals of Quartz Oscillators. In *Electronic Counters Series*, Hewlett-Packard Company: USA, 1997; pp 1-28.
70. Kurtz, O.; Barthelmes, J.; Ruether, R.; Wuensche, M.; Donner, C., Quartz crystal microbalance used to characterize electrochemical metal deposition. *J. Electrochem. Plat. Technol.* 2010, *1*, 33-49.
71. Schumacher, R., The quartz microbalance - A novel approach to the in-situ investigation of intergacial phenomena at the solid/liquid junction. *Angewandte Chemie - International Edition in English* 1990, *29*, 329-343.
72. Gast, T.; Brokate, T.; Robens, E.; Ali, Z.; Pavey, K., Survey on mass determination systems: Part I. Fundamentals and history. *Journal of Thermal Analysis and Calorimetry* 2003, *71*, 19-23.
73. Rodahl, M.; Höök, F.; Krozer, A.; Brzezinski, P.; Kasemo, B., Quartz crystal microbalance setup for frequency and Q-factor measurements in gaseous and liquid environments. *Review of Scientific Instruments* 1995, *66*, 3924-3930.
74. Rodahl, M.; Höök, F.; Kasemo, B., QCM operation in liquids: An explanation of measured variations in frequency and Q factor with liquid conductivity. *Analytical Chemistry* 1996, *68*, 2219-2227.
75. Rodahl, M.; Kasemo, B., A simple setup to simultaneously measure the resonant frequency and the absolute dissipation factor of a quartz crystal microbalance. *Review of Scientific Instruments* 1996, *67*, 3238-3241.
76. Handley, J., Product review: quartz crystal microbalances. *Analytical Chemistry* 2001, *73*, 225 A-229 A.
77. Bouzidi, L.; Narine, S. S.; Stefanov, K. G.; Slavin, A. J., High-stability quartz-crystal microbalance for investigations in surface science. *Review of Scientific Instruments* 2003, *74*, 3039-3044.
78. Hamilton, C.; Gedeon, A., A gas analyser based on the quartz crystal adsorption technique. *Journal of Physics E: Scientific Instruments* 1986, *19*, 271.

79. Weerawardena, A.; Drummond, C. J.; Caruso, F.; McCormick, M., Real time monitoring of the detergency process by using a quartz crystal microbalance. *Langmuir* 1998, *14*, 575-577.
80. Lin, Z.; Hill, R. M.; Davis, H. T.; Ward, M. D., Determination of wetting velocities of surfactant superspreaders with the quartz crystal microbalance. *Langmuir* 1994, *10*, 4060-4068.
81. Lin, Z.; Stoebe, T.; Hill, R. M.; Davis, H. T.; Ward, M. D., Improved accuracy in dynamic quartz crystal microbalance measurements of surfactant enhanced spreading. *Langmuir* 1996, *12*, 345-347.
82. Okahata, Y.; Ariga, K., In situ weighing of water-deposited Langmuir-Blodgett films on a piezoelectric quartz plate. *Journal of the Chemical Society, Chemical Communications* 1987, 1535-1537.
83. Okahata, Y.; Ebara, Y., Observation of phospholipase A2 activity towards the hydrolysis of phospholipid Langmuir-Blodgett films deposited on a quartz-crystal microbalance. *Journal of the Chemical Society, Chemical Communications* 1992, 116-117.
84. Thompson, M.; Arthur, C. L.; Dhaliwal, G. K., Liquid-phase piezoelectric and acoustic transmission studies of interfacial immunochemistry. *Analytical Chemistry* 1986, *58*, 1206-1209.
85. Nivens, D. E.; Chambers, J. Q.; Anderson, T. R.; White, D. C., Long-term, on-line monitoring of microbial biofilms using a quartz crystal microbalance. *Analytical Chemistry* 1993, *65*, 65-69.
86. Gryte, D. M.; Ward, M. D.; Hu, W. S., Real-time measurement of anchorage-dependent cell adhesion using a quartz crystal microbalance. *Biotechnology Progress* 1993, *9*, 105-108.
87. Dultsev, F. N.; Ostanin, V. P.; Klenerman, D., "Hearing" bond breakage. measurement of bond rupture forces using a quartz crystal microbalance. *Langmuir* 2000, *16*, 5036-5040.
88. Pham, N. T.; McHale, G.; Newton, M. I.; Carroll, B. J.; Rowan, S. M., Application of the quartz crystal microbalance to the evaporation of colloidal suspension droplets. *Langmuir* 2004, *20*, 841-847.
89. Johnsen, I.; Stenius, P.; Tammelin, T.; Osterberg, M.; Johansson, L.-S.; Laine, J., The influence of dissolved substances on resin adsorption to TMP fine material. *Nordic Pulp and Paper Research Journal* 2006, *21*, 629-637.
90. Tammelin, T.; Johnsen, I. A.; Osterberg, M.; Stenius, P.; Laine, J., Adsorption of colloidal extractives and dissolved hemicelluloses on thermomechanical pulp fiber components studied by QCM-D. *Nordic Pulp & Paper Research Journal* 2007, *22*, 93-101.
91. Kou, J.; Tao, D.; Xu, G., Fatty acid collectors for phosphate flotation and their adsorption behavior using QCM-D. *International Journal of Mineral Processing* 2010, *95*, 1-9.
92. Kou, J.; Tao, D.; Sun, T.; Xu, G., Application of the quartz crystal microbalance with dissipation method to a study of oleate adsorption onto a hydroxyapatite surface. *Minerals & Metallurgical Processing* 2012, *29*, 47-55.
93. Kontturi, K. S.; Tammelin, T.; Johansson, L.-S.; Stenius, P., Adsorption of cationic starch on cellulose studied by QCM-D. *Langmuir* 2008, *24*, 4743-4749.
94. Gustafsson, E.; Johansson, E.; Wagberg, L.; Pettersson, T., Direct adhesive measurements between wood biopolyrner model surfaces. *Biomacromolecules* 2012, *13*, 3046-3053.
95. Kontturi, E.; Suchy, M.; Penttila, P.; Jean, B.; Pirkkalainen, K.; Torkkeli, M.; Serimaa, R., Amorphous characteristics of an ultrathin cellulose film. *Biomacromolecules* 2011, *12*, 770-777.

96. Olszewska, A.; Eronen, P.; Johansson, L. S.; Malho, J. M.; Ankerfors, M.; Lindstrom, T.; Ruokolainen, J.; Laine, J.; Osterberg, M., The behaviour of cationic nanofibrillar cellulose in aqueous media. *Cellulose* 2011, *18*, 1213-1226.
97. Kittle, J. D.; Du, X. S.; Jiang, F.; Qian, C.; Heinze, T.; Roman, M.; Esker, A. R., Equilibrium water contents of cellulose films determined via solvent exchange and quartz crystal microbalance with dissipation monitoring. *Biomacromolecules* 2011, *12*, 2881-2887.
98. Edgar, C. D.; Gray, D. G., Smooth model cellulose I surfaces from nanocrystal suspensions. *Cellulose* 2003, *10*, 299-306.
99. Stack, K. R.; Lee, R.; Rao, R.; Richardson, D. E.; Garnier, G.; Lewis, T. W., Effect of Pitch Preparation on its Colloidal Properties and Deposition Behaviour. *Appita J.* 2009, 353-358.
100. Mohamad Haafiz, M. K.; Eichhorn, S. J.; Hassan, A.; Jawaid, M., Isolation and characterization of microcrystalline cellulose from oil palm biomass residue. *Carbohydrate Polymers* 2013, *93*, 628-634.
101. Abdelsalam, M. E.; Bartlett, P. N.; Kelf, T.; Baumberg, J., Wetting of regularly structured gold surfaces. *Langmuir* 2005, *21*, 1753-1757.
102. Steele, D. F.; Moreton, R. C.; Staniforth, J.; Young, P.; Tobyn, M.; Edge, S., Surface energy of microcrystalline cellulose determined by capillary intrusion and inverse gas chromatography. *The American Association of Pharmaceutical Scientists (AAPS) Journal* 2008, *10*, 494-503.
103. Kuze, E.; Teramoto, T.; Yukimura, K.; Maruyama, T., Contact angle of water on chromium nitride thin film prepared on three-dimensional materials by chromium plasma-based ion implantation. *Surface and Coatings Technology* 2002, *158*, 577-581.
104. Jodar-Reyes, A. B.; Mendez-Vilas, A.; Gonzalez-Martin, M. L., Experimental contribution to the understanding of wetting of solid surfaces at the meso-- and nano-scale using dynamic AFM. *Modern Research and Educational Topics in Microscopy* 2007, *2*, 500-512.
105. Vercoe, D. Study of the interactions leading to wood resin deposition. PhD, University of Tasmania, Hobart, 2004.
106. Rogan, K. R., Adsorption of oleic acid and triolein onto various minerals and surface treated minerals. *Colloid & Polymer Science* 1994, *272*, 82-98.
107. Maher, L.; Stack.K; McLean, D.; Richardson, D., Adsorption behaviour of cationic fixatives and their effect on pitch deposition. *Appita Journal* 2007, *60*, 112-119, 128.
108. McLean, D. S.; Stack, K. R.; Richardson, D. E., The effect of wood extractives composition, pH and temperature on pitch deposition. *Appita Journal* 2005, *58*, 52-55, 76.
109. Gantenbein, D.; Schoelkopf, J.; Matthews, G. P.; Gane, P. A. C., Influence of the temperature on the adsorption of dissolved and colloidal substances from a thermo mechanical pulp filtrate onto talc. *Nordic Pulp & Paper Research Journal* 2011, *26*, 329-335.
110. Froix, M. F.; Goedde, A. O., The effect of temperature on the cellulose/water interaction from NMR relaxation times. *Macromolecules* 1976, *9*, 428-430.
111. Ödberg, L.; Forsberg, S.; McBride, G.; Persson, M.; Stenius, P.; Ström, G., Surfactant behavior of wood resin components. Part 2. Solubilization in micelles of rosin and fatty acids. *Svensk Papperstidning* 1985, *88*, R118-R125.
112. Palonen, H.; Stenius, P.; Ström, G., Surfactant behavior of wood resin components. The solubility of rosin and fatty acid soaps in water and in salt solutions. *Svensk Papperstidning* 1982, *85*, R93-R99.
113. Senden, T. J., Force Microscopy and Surface Interactions. *Current Opinion in Colloid & Interface Science* 2001, *6*, 95-101.
114. Butt, H.-J.; Cappella, B.; Kappl, M., Force Measurements with the Atomic Force Microscope: Technique, Interpretation and Applications. *Sur. Sci. Rep.* 2005, *59*, 1-152.

115. Shahin, V.; Ludwig, Y.; Schafer, C.; Nikova, D.; Oberleithner, H., Glucocorticoids remodel nuclear envelope structure and permeability. *Journal of cell science* 2005, *118*, 2881-9.
116. Butt, H. J.; Berger, R.; Bonaccurso, E.; Chen, Y.; Wang, J., Impact of atomic force microscopy on interface and colloid science. *Adv Colloid Interface Sci* 2007, *133*, 91-104.
117. Dagastine, R. R.; Chau, T. T.; Chan, D. Y. C.; Stevens, G. W.; Grieser, F., Interaction Forces between Oil-Water Particle Interfaces - Non-DLVO Forces. *Faraday Discuss.* 2005, *129*, 111-124.
118. Manor, O.; Vakarelski, I. U.; Stevens, G. W.; Grieser, F.; Dagastine, R. R.; Chan, D. Y. C., Dynamic Forces between Bubbles and Surfaces and Hydrodynamic Boundary Conditions. *Langmuir* 2008, *24*, 11533-11543.
119. Dagastine, R. R.; Manica, R.; Carnie, S. L.; Chan, D. Y. C.; Stevens, G. W.; Grieser, F., Dynamic Forces between Two Deformable Oil Droplets in Water. *Science* 2006, *313*, 210-213.
120. Lockie, H.; Manica, R.; Tabor, R. F.; Stevens, G. W.; Grieser, F.; Chan, D. Y. C.; Dagastine, R. R., Anomalous Pull-Off Forces between Surfactant-Free Emulsion Drops in Different Aqueous Electrolytes. *Langmuir* 2012, *28*, 4259-4266.
121. Hutter, J. L.; Bechhoefer, J., Calibration of Atomic-Force Microscope Tips *Rev. Sci. Instrum.* 1993, *64*, 1868-1873.
122. Perry, J. L.; Reuter, K. G.; Kai, M. P.; Herlihy, K. P.; Jones, S. W.; Luft, J. C.; Napier, M.; Bear, J. E.; DeSimone, J. M., PEGylated PRINT nanoparticles: The impact of PEG density on protein binding, macrophage association, biodistribution, and pharmacokinetics. *Nano Letters* 2012, *12*, 5304-5310.
123. Tabor, R. F.; Lockie, H.; Mair, D.; Manica, R.; Chan, D. Y. C.; Grieser, F.; Dagastine, R. R., Combined AFM−Confocal Microscopy of Oil Droplets: Absolute Separations and Forces in Nanofilms. *J. Phys. Chem. Lett.* 2011, *2*, 961-965.
124. Lewars, E., *Computational chemistry - Introduction to the theory and applications of molecular and quantum mechanics*. Kluwer Academic Publishers: 2004.
125. Young, D. Introduction to computational chemistry. http://www.ccl.net/cca/documents/dyoung/topics-orig/compchem.html
126. Rioux, F. Computational chemistry. http://www.chemistryexplained.com/Co-Di/Computational-Chemistry.html
127. Young, D. C., Using existing basis sets. In *Computational Chemistry*, John Wiley & Sons, Inc.: 2002; pp 78-91.
128. Gaussian 09: Expanding the limits of computational chemistry. http://www.gaussian.com/g_prod/g09b.htm (16 June 2015),
129. Cramer, C. J., *Essentials of computational chemistry: Theories and models*. 2nd ed.; John Wiley & Sons Ltd: England, 2004; p 596.
130. Jensen, F., *Introduction to computational chemistry*. 2nd ed.; John Wiley & Sons, Ltd: West Sussex, England, 2007; p 599.
131. Bronowska, A. K., Thermodynamics of ligand - protein interactions: Implications for molecular design. In *Thermodynamics - Interaction Studies - Solids, Liquids and Gases*, PirajĀin, J. C. M., Ed. InTech: 2011; p 918.
132. Dunitz, J. D., Win some, lose some: enthalpy-entropy compensation in weak intermolecular interactions. *Chemistry & Biology* 1995, *2*, 709-712.
133. Jelesarov, I.; Bosshard, H. R., Isothermal titration calorimetry and differential scanning calorimetry as complementary tools to investigate the energetics of biomolecular recognition. *Journal of Molecular Recognition* 1999, *12*, 3-18.
134. Fisher, S.; Verma, C. S., Binding of buried structural water increases the flexibility of proteins. *Proceedings of the National Academy of Sciences* 1999, *96*, 9613-9615.

135. Michel, J.; Tirado-Rivers, J.; Jorgensen, W. L., Energetics of displacing water molecules from protein binding sites: consequences for ligand optimization. *Journal of American Chemical Society* 2009, *131*, 15403-15411.

Appendix A – Plot of loading concentration vs equilibrium concentration, C_e of adsorption experiments onto microcrystalline cellulose without pH changes to colloidal suspension

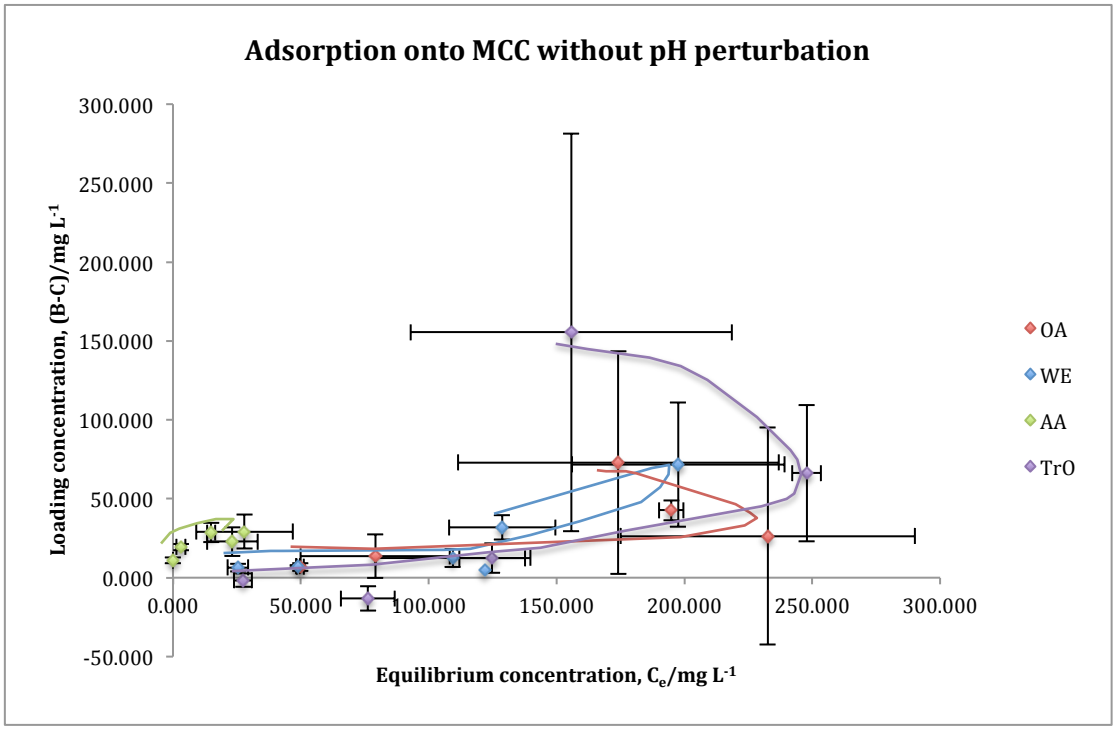

Figure A1 Plot of loading concentration vs equilibrium concentration, C_e of adsorption of oleic acid (OA, abietic acid (AA), triolein (TrO) and wood extractives (WE) onto microcrystalline cellulose (MCC) without pH perturbation to colloidal suspension.

Appendix B – Frequency and dissipation values of all QCM-D deposition experiments

Table B1 Frequency and dissipation values at point of maximum deposition and end of rinsing as well as the percentage desorbed onto cellulose.

Conditions		max deposited			aft rinsing			% desorbed
		F_1	D	F/D	F_2	D	F/D	$(F_1 - F_2)/F_1$
OA	**25deg**	-12.00	0.88	-13.64	-5.49	0.43	-12.77	54.25%
OA	**25deg**	-11.81	1.07	-11.04	-5.54	0.67	-8.27	53.09%
OA	**25deg**	-13.46	1.20	-11.22	-5.24	0.37	-14.16	61.08%
OA	**50deg**	-50.28	10.24	-4.91	-14.21	-2.91	4.88	71.73%
OA	**50deg**	-54.41	8.87	-6.13	-32.22	4.01	-8.04	40.78%
OA	**50deg**	-88.52	21.86	-4.05	-43.69	7.63	-5.73	50.65%
OA	**50deg**	-51.33	6.95	-7.39	-17.54	0.96	-18.28	65.82%
AA	**25deg**	-545.30	129.65	-4.21	-77.55	18.32	-4.23	85.78%
AA	**25deg**	-210.25	71.21	-2.95	-37.25	13.89	-2.68	82.28%
AA	**25deg**	-310.84	109.57	-2.84	-72.46	23.73	-3.05	76.69%
AA	**25deg**	-883.53	133.53	-6.62	-399.16	76.85	-5.19	54.82%
AA	**25deg**	-531.67	66.65	-7.98	-253.61	45.90	-5.53	52.30%
AA	**25deg**	-155.71	55.70	-2.80	-100.64	36.22	-2.78	35.36%
AA	**25deg**	-95.14	25.53	-3.73	-70.82	18.96	-3.74	25.57%
AA	**25deg**	-159.82	48.45	-3.30	-110.20	33.86	-3.25	31.05%
AA	**50deg**	-802.45	113.33	-7.08	-375.89	50.17	-7.49	53.16%
AA	**50deg**	-847.87	114.79	-7.39	-183.07	24.56	-7.45	78.41%

AA	**50deg**	-720.18	70.73	-10.18	-167.62	17.69	-9.47	76.73%
TrO	**25deg**	-363.86	52.16	-6.98	-366.73	52.76	-6.95	-0.79%
TrO	**25deg**	-515.71	62.00	-8.32	-559.14	56.25	-9.94	-8.42%
TrO	**25deg**	-397.77	49.35	-8.06	-417.61	45.83	-9.11	-4.99%
TrO	**25deg**	-194.86	55.47	-3.51	-212.94	58.21	-3.66	-9.28%
TrO	**50deg**	-384.07	46.63	-8.24	-383.41	46.51	-8.24	0.17%
TrO	**50deg**	-283.14	137.74	-2.06	-270.67	123.52	-2.19	4.40%
TrO	**50deg**	-547.99	97.33	-5.63	-491.56	86.35	-5.69	10.30%
MM	**25deg**	-16.95	0.43	-39.42	-9.93	0.78	-12.73	41.42%
MM	**25deg**	-60.30	8.94	-6.75	-17.63	1.88	-9.38	70.77%
MM	**25deg**	-63.56	8.95	-7.10	-22.40	2.46	-9.11	64.76%
MM	**25deg**	-32.77	8.19	-4.00	-18.98	5.25	-3.62	42.07%
MM	**50deg**	-157.73	54.74	-2.88	-110.67	40.78	-2.71	29.83%
MM	**50deg**	-44.66	15.31	-2.92	-32.59	12.34	-2.64	27.03%
MM	**50deg**	-25.31	9.47	-2.67	-16.36	6.90	-2.37	35.37%
MM	**50deg**	-141.14	51.21	-2.76	-97.57	34.38	-2.84	30.87%
WE	**25deg**	-36.17	7.79	-4.64	-18.06	4.73	-3.82	50.08%
WE	**25deg**	-24.71	4.32	-5.72	-19.70	1.15	-17.13	20.27%
WE	**25deg**	-17.35	4.16	-4.17	-10.30	1.89	-5.45	40.66%
WE	**25deg**	-17.61	3.70	-4.76	-9.20	2.28	-4.03	47.77%
WE	**50deg**	-73.29	14.12	-5.19	-31.69	7.15	-4.43	56.76%

WE	**50deg**	-118.59	20.40	-5.81	-55.49	10.46	-5.30	53.21%
WE	**50deg**	-86.17	14.62	-5.89	-47.73	7.41	-6.44	44.61%
WE	**50deg**	-122.12	21.77	-5.61	-56.44	12.47	-4.53	53.79%

F_1 = Frequency recorded at point of maximum deposition (Hz); F_2 = Frequency recorded after 4 h rinsing (Hz); D = dissipation factor.

Table B2 Frequency and dissipation values at point of maximum deposition and end of rinsing as well as the percentage desorbed for deposition onto chromium.

Conditions		**max deposited**			**aft rinsing**			**% desorbed**
		F_1	**D**	**F/D**	**F_2**	**D**	**F/D**	**$(F_1 - F_2)/F_1$**
OA	**25deg**	-151.29	34.50	-4.39	-150.38	29.46	-5.10	0.60%
OA	**25deg**	-200.77	37.55	-5.35	-188.29	32.61	-5.77	6.21%
OA	**25deg**	-103.67	30.07	-3.45	-102.25	23.91	-4.28	1.37%
OA	**50deg**	-189.49	18.78	-10.09	-112.49	4.08	-27.57	40.64%
OA	**50deg**	-152.30	21.26	-7.16	-85.30	6.43	-13.27	44.00%
OA	**50deg**	-108.09	17.55	-6.16	-37.59	2.28	-16.49	65.23%
AA	**25deg**	-800.26	48.87	-16.38	-598.50	49.27	-12.15	25.21%
AA	**25deg**	-690.77	41.39	-16.69	-504.83	43.02	-11.73	26.92%
AA	**25deg**	-783.03	41.45	-18.89	-645.60	44.89	-14.38	17.55%
AA	**50deg**	-640.11	41.77	-15.32	-389.53	26.69	-14.59	39.15%
AA	**50deg**	-676.49	37.30	-18.14	-269.10	15.53	-17.33	60.22%
AA	**50deg**	-632.68	29.98	-21.10	-130.59	4.18	-31.27	79.36%
TrO	**25deg**	-392.00	84.29	-4.65	-411.83	78.51	-5.25	-5.06%

TrO	**25deg**	-482.47	68.07	-7.09	-485.20	59.09	-8.21	-0.57%
TrO	**25deg**	-470.97	64.81	-7.27	-476.45	55.35	-8.61	-1.16%
TrO	**50deg**	-400.29	73.65	-5.44	-408.31	68.47	-5.96	-2.00%
TrO	**50deg**	-410.67	66.41	-6.18	-411.94	62.51	-6.59	-0.31%
TrO	**50deg**	-430.45	68.35	-6.30	-432.90	62.14	-6.97	-0.57%
MM	**25deg**	-438.81	44.47	-9.87	-334.73	40.89	-8.19	23.72%
MM	**25deg**	-371.97	43.94	-8.47	-262.39	44.35	-5.92	29.46%
MM	**25deg**	-313.13	50.48	-6.20	-204.19	44.35	-4.60	34.79%
MM	**50deg**	-277.15	34.20	-8.10	-189.99	18.55	-10.24	31.45%
MM	**50deg**	-305.00	40.55	-7.52	-200.05	24.61	-8.13	34.41%
MM	**50deg**	-278.22	26.72	-10.41	-176.86	17.80	-9.94	36.43%
WE	**25deg**	-183.33	21.53	-8.52	-100.29	12.04	-8.33	45.30%
WE	**25deg**	-175.67	25.83	-6.80	-114.80	16.59	-6.92	34.65%
WE	**25deg**	-209.54	21.16	-9.90	-115.34	11.76	-9.81	44.96%
WE	**25deg**	-189.22	21.56	-8.78	-111.58	13.07	-8.54	41.03%
WE	**50deg**	-275.83	42.65	-6.47	-156.63	21.26	-7.37	43.22%
WE	**50deg**	-267.84	36.95	-7.25	-144.92	14.07	-10.30	45.89%
WE	**50deg**	-257.47	29.97	-8.59	-132.49	12.67	-10.46	48.54%
WE	**50deg**	-175.05	27.34	-6.40	-80.88	5.27	-15.35	53.80%

F_1 = Frequency recorded at point of maximum deposition (Hz); F_2 = Frequency recorded after 4 h rinsing (Hz); D = dissipation factor.

Appendix C – An example of input file for oleic acid (OA) optimization and frequency calculations at HF/STO-3G

```
%nproc=4
%mem=4gb
%chk=/short/dw5/yyt581/oa-hfsto3g.chk
#hf/sto-3g opt freq

Opt Freq OA

0 1
 C                 -7.41027434   -1.78628229    0.06288514
 H                 -7.56935154   -2.44615969   -0.76424789
 H                 -6.84057716   -2.28933439    0.81606942
 C                 -8.76947729   -1.35886652    0.64727784
 H                 -8.61045857   -0.69907464    1.47450464
 H                 -9.33920292   -0.85574047   -0.10582095
 C                 -9.53753102   -2.60528386    1.12498525
 H                 -8.96777473   -3.10840796    1.87808364
 H                 -9.69651108   -3.26503244    0.29773736
 C                -10.89675800   -2.17807292    1.70942078
 H                -11.46651765   -1.67492337    0.95635258
 H                -10.73779393   -1.51835870    2.53670186
 C                -11.66474898   -3.42454699    2.18703189
 H                -11.09498217   -3.92771044    2.94007954
 H                -11.82372116   -4.08425450    1.35972937
 C                -13.02398327   -2.99738173    2.77150470
 H                -13.59377260   -2.49420700    2.01846575
```

Command line – updated accordingly

H	-12.86502149	-2.33769497	3.59881003
C	-13.79193070	-4.24388411	3.24908276
H	-13.22212690	-4.74707219	4.00209204
H	-14.73632184	-3.94710650	3.65521539
H	-13.95091580	-4.90355723	2.42176385
C	-6.64203192	-0.54008188	-0.41509625
H	-6.48293015	0.11988879	0.41196886
H	-7.21166036	-0.03703612	-1.16833470
C	-5.28288348	-0.96788323	-0.99933968
H	-4.79179849	-1.84240062	-0.62656511
C	-4.70873423	-0.23693388	-1.98558278
H	-3.76450118	-0.53453459	-2.39150257
C	-5.41510165	1.02191211	-2.52221060
H	-6.05308490	0.75253431	-3.33788893
H	-6.00021934	1.46247168	-1.74219364
C	-4.36104451	2.03432520	-3.00765998
H	-3.77596441	1.59361744	-3.78764401
H	-3.72304331	2.30376936	-2.19203426
C	-5.06726205	3.29314706	-3.54455195
H	-5.70540344	3.02363816	-4.36005073
H	-5.65219483	3.73403527	-2.76456747
C	-4.01314653	4.30527010	-4.03045105
H	-3.42820105	3.86425988	-4.81036196
H	-3.37501549	4.57490594	-3.21498597
C	-4.71934321	5.56397082	-4.56765453
H	-5.30416383	6.00511249	-3.78773482
H	-5.35758195	5.29424873	-5.38300517
C	-3.66523899	6.57590446	-5.05393472
H	-3.08041822	6.13468110	-5.83381239

H	-3.02700543	6.84569429	-4.23860418
C	-4.37137912	7.83455952	-5.59131820
H	-4.95618845	8.27585861	-4.81147108
H	-5.00965281	7.56479489	-6.40664824
C	-3.31716876	8.84634190	-6.07768093
O	-2.18236618	8.88251802	-5.53499177
O	-3.62778965	9.74473092	-7.14599190
H	-3.13225390	10.55921200	-7.03348936

1 2 1.0 3 1.0 4 1.0 23 1.0

2

3

4 5 1.0 6 1.0 7 1.0

5

6

7 8 1.0 9 1.0 10 1.0

8

9

10 11 1.0 12 1.0 13 1.0

11

12

13 14 1.0 15 1.0 16 1.0

14

15

16 17 1.0 18 1.0 19 1.0

17

18

19 20 1.0 21 1.0 22 1.0

20

21

22

23 24 1.0 25 1.0 26 1.0

24

25

26 27 1.0 28 2.0

27

28 29 1.0 30 1.0

29

30 31 1.0 32 1.0 33 1.0

31

32

33 34 1.0 35 1.0 36 1.0

34

35

36 37 1.0 38 1.0 39 1.0

37

38

39 40 1.0 41 1.0 42 1.0

40

41

42 43 1.0 44 1.0 45 1.0

43

44

45 46 1.0 47 1.0 48 1.0

46

47

48 49 1.0 50 1.0 51 1.0

49

```
50

51 52 2.0 53 1.0

52

53 54 1.0

54
```

The appropriate level of theories and basis sets were changed in the command line before submitting for job calculation(s). For example, “# b3lyp/3-21g opt freq” for calculations involving level of theory and basis set B3LYP/3-21G.

Appendix D – An example of input file for oleic acid (OA) solvation calculations at HF/STO-3G

```
%nproc=8
%mem=8GB
%chk=/short/dj8/yyt581/OAs.chk
#hf/sto-3g scrf=(cpcm,solvent=water,read)

OA solvation

0 1
 C                  3.72885900    1.58411500    0.14366400
 H                  3.60640000    1.56055600   -0.94659500
 H                  4.31650100    2.48006900    0.38631300
 C                  4.49652600    0.32758400    0.60797900
 H                  4.61207400    0.35634400    1.70062100
 H                  3.90501200   -0.56709000    0.36780700
 C                  5.89005900    0.20522200   -0.04707600
 H                  6.48342000    1.09782700    0.19550800
 H                  5.77429600    0.17956600   -1.13956900
 C                  6.65602700   -1.05476500    0.41298700
 H                  6.06177000   -1.94698700    0.17069200
 H                  6.77179400   -1.02912500    1.50561700
 C                  8.04918600   -1.17905900   -0.24213500
 H                  8.64464700   -0.28786200    0.00106900
 H                  7.93409800   -1.20334400   -1.33490000
 C                  8.81481000   -2.44017700    0.21534600
 H                  8.21856300   -3.32981200   -0.02760100
```

H	8.92824500	-2.41511400	1.30738500
C	10.20508500	-2.55234800	-0.44664400
H	10.82155600	-1.68107700	-0.19566200
H	10.73169300	-3.45280100	-0.11135100
H	10.10814800	-2.59774900	-1.53780000
C	2.32707000	1.69894100	0.80273700
H	2.45773600	1.69716900	1.89501600
H	1.73707400	0.81348800	0.54402000
C	1.61597500	2.96639000	0.38706900
H	2.11194300	3.88374200	0.70409300
C	0.49461200	3.07187700	-0.33281300
H	0.11890300	4.07018600	-0.55681400
C	-0.36867500	1.94800200	-0.85919000
H	-0.53006300	2.08782000	-1.93816200
H	0.12289800	0.97856600	-0.72633600
C	-1.75389700	1.91340200	-0.15725000
H	-2.24257100	2.89028700	-0.27419900
H	-1.60105900	1.75258500	0.91739300
C	-2.67358400	0.80960000	-0.72234700
H	-2.82214800	0.97682100	-1.79846300
H	-2.17900300	-0.16558500	-0.61066800
C	-4.04812700	0.76441100	-0.01946800
H	-4.54635900	1.73687000	-0.13479400
H	-3.89873600	0.60183900	1.05683000
C	-4.96479400	-0.34582600	-0.57796200
H	-4.46371700	-1.31757200	-0.46486700
H	-5.11555400	-0.18240600	-1.65439200
C	-6.33303800	-0.38877400	0.13194500
H	-6.83993200	0.57720600	0.02211000

H	-6.18944000	-0.54735800	1.20727300
C	-7.24347800	-1.49664500	-0.41898500
H	-6.77805000	-2.48448100	-0.31054500
H	-7.43627100	-1.35778500	-1.49026300
C	-8.57357000	-1.52374800	0.29774400
O	-8.93583000	-0.78571800	1.20606300
O	-9.37618700	-2.52786100	-0.21409200
H	-10.24199400	-2.51538200	0.28182800

tsare=0.3

tsnum=240

radii=uahf

m

Appendix E – Step-by-step modeling command line to enable successful optimization and frequency calculations of chromium unit

For modeling interaction with chromium unit, first single point calculations were carried out with the following command line:

BP86/sto-3g

When single point calculation converge successfully, additional instructions were then included in the command line as follow:

BP86/sto-3G scf=qc

Lastly the optimisation and frequency calculations were carried out.

BP86/sto-3g scf=qc opt freq

Appendix F – Results of all ξ, $\xi_{(solv)}$, H_{corr} and G_{corr} values of each individual molecules and complex at different level of theory and basis sets

Table F1 Results from optimisation and frequency calculations of glucose at different level of theories and basis sets (unit in a.u.).

Glucose	HF/STO-3G	B3LYLP/3-21G	M06/3-21G	BP86/STO-3G
ξ	-674.4699	-683.3592	-683.1438	-678.0287
$\xi_{(solv)}$	-674.4991	-683.4094	-683.1996	-677.9830
$\Delta\ \xi_{(solv)}$	-0.0292	-0.0502	-0.0558	0.0457
H_{corr}	0.2415	0.2071	0.2104	0.2117
G_{corr}	0.1905	0.2090	0.1599	0.1607

Table F2 Results from optimisation and frequency calculations of Glu-Glu at different level of theories and basis sets (unit in a.u.).

Glu-Glu	HF/STO-3G	B3LYLP/3-21G	M06/3-21G
ξ	-1273.9847	-1290.7526	-1290.3477
$\xi_{(solv)}$	-1274.0335	-1290.8688	-1290.4709
$\Delta\ \xi_{(solv)}$	-0.0488	-0.1162	-0.1232
H_{corr}	0.4551	0.3896	0.3950
G_{corr}	0.3794	0.3129	0.3197

Table F3 Results from optimisation and frequency calculation of Cr at BP86/STO-3G (unit in a.u.).

Cr	BP86/STO-3G
ξ	-15503.7137
H_{corr}	0.0493
G_{corr}	-0.013413

Table F4 Results from optimisation and frequency calculations of OA and AA with different positions of -OH on Glu at HF/STO-3G (unit in a.u.).

OA - Glu	position 1	position 2	position 5
ξ	-1515.356	-1515.356	-1515.355
AA - Glu	position 1	position 2	position 5
ξ	-1588.524	-1587.856	-1587.853

Table F5 Results from optimisation and frequency calculations of OA at different level of theories and basis sets (unit in a.u.).

OA	HF/STO-3G	B3LYLP/3-21G	M06/3-21G	BP86/STO-3G
ξ	-840.8702	-852.2048	-856.0114	-846.3327
$\xi_{(solv)}$	-840.8821	-852.2325	-851.8273	-846.3316
$\Delta\ \xi_{(solv)}$	-0.0119	-0.0277	4.1841	0.0011
H_{corr}	0.6144	0.5253	0.5229	0.5515
G_{corr}	0.5273	0.4378	0.4376	0.4654

Table F6 Results from optimisation and frequency calculations of AA at different level of theories and basis sets (unit in a.u.).

AA	HF/STO-3G	B3LYLP/3-21G	M06/3-21G	BP86/STO-3G
ξ	-913.3735	-925.5962	-925.2043	-919.2317
$\xi_{(solv)}$	-913.3603	-925.6158	-925.2166	-919.2569
$\Delta\ \xi_{(solv)}$	0.0132	-0.0196	-0.0123	-0.0253
H_{corr}	0.5753	0.4919	0.4924	0.5150
G_{corr}	0.5070	0.4211	0.4216	0.4412

Table F7 Results from optimisation and frequency calculations of TrO at different level of theories and basis sets (unit in a.u.).

TrO	HF/STO-3G	B3LYLP/3-21G	M06/3-21G	BP86/STO-3G
ξ	-2636.0688	-2671.5381	-2670.2837	-2653.1784

$\xi_{(solv)}$	-2635.3937	-2670.8488	-2669.5866	-2652.4263
$\Delta\ \xi_{(solv)}$	0.6751	0.6894	0.6971	0.7521
H_{corr}	1.8999	1.6264	1.6294	1.7078
G_{corr}	1.6701	1.3996	1.4303	1.4766

Table F8 Results from optimisation and frequency calculations of Glu-OA complex at HF/STO-3G at -OH positions 1,2 and 5 (unit in a.u.).

Glu-OA	1	2	5
Ξ	-1515.3564	-1515.3561	-1515.3545
$\xi_{(solv)}$	-1515.3078	-1515.2644	-1515.2696
$\Delta\ \xi_{(solv)}$	0.0486	0.0917	0.0849
H_{corr}	0.8599	0.8602	0.8593
G_{corr}	0.7395	0.7400	0.7374

Table F9 Results from optimisation and frequency calculations of Glu-OA complex at different level of theories and basis sets (unit in a.u.).

Glu-OA	HF/STO-3G	B3LYLP/3-21G	M06/3-21G
ξ	-1515.3564	-1535.6156	-1534.9959
$\xi_{(solv)}$	-1515.3078	-1535.6238	-1534.9853
$\Delta\ \xi_{(solv)}$	0.0486	-0.0082	0.0105
H_{corr}	0.8599	0.7357	0.7398
G_{corr}	0.7395	0.6151	0.6254

Table F10 Results from optimisation and frequency calculations of Glu-AA complex at HF/STO-3G at -OH positions 1,2 and 5 (unit in a.u.).

Glu-AA	1	2	5
ξ	-1588.5244	-1587.8562	-1587.8529
$\xi_{(solv)}$	-1587.8588		

$\Delta\ \xi_{(solv)}$	0.6656	1587.8562	1587.8529
H_{corr}	0.8207	0.8204	0.8199
G_{corr}	0.7187	0.7175	0.7166

Table F11 Results from optimisation and frequency calculations of Glu-AA complex at different level of theories and basis sets (unit in a.u.).

Glu-AA	HF/STO-3G	B3LYLP/3-21G	M06/3-21G
ξ	-1588.5244	-1608.9917	-1608.3837
$\xi_{(solv)}$	-1587.8588	-1609.0298	-1608.4197
$\Delta\ \xi_{(solv)}$	0.6656	-0.0381	-0.0360
H_{corr}	0.8207	0.7012	0.7056
G_{corr}	0.7187	0.5972	0.6041

Table F12 Results from optimisation and frequency calculations of Glu-TrO complex at different level of theories and basis sets (unit in a.u.).

Glu-TrO	HF/STO-3G	B3LYLP/3-21G	M06/3-21G
ξ	-3310.5399	-3354.9059	-3353.4559
$\xi_{(solv)}$	-3310.6372	-3355.0017	-3353.5170
$\Delta\ \xi_{(solv)}$	-0.0973	-0.0958	-0.0611
H_{corr}	2.1435	1.8360	1.8450
G_{corr}	1.8723	1.5751	1.6198

Table F13 ξ values from optimisation and frequency calculations of Glu-Glu-OA and Glu-Glu-AA complexes at HF/STO-3G at different –OH positions (unit in a.u.).

Glu-Glu-OA	1	2	3 (6)	4 (6)	5	6
ξ	-2114.8827	-2114.8739	-2114.8730	-2114.8739	-2114.8683	-2114.8754
Glu-Glu-AA	1	2	4	5	6	6(2)
ξ	-2187.3774	-2187.3751	-2187.3661	-2187.3757	-2187.3671	-2187.3727

r

Table F14 Results from optimisation and frequency calculations of Glu-Glu-OA complex at different level of theories and basis sets (unit in a.u.).

Glu-Glu-OA	HF/STO-3G	B3LYLP/3-21G	M06/3-21G
ξ	-2114.8763	-2143.0216	-2142.2043
$\xi_{(solv)}$	-2114.9684	-2143.1110	-2142.2993
$\Delta\ \xi_{(solv)}$	-0.0921	-0.0893	-0.0950
H_{corr}	1.0735	0.9177	0.9247
G_{corr}	0.9288	0.7743	0.7887

Table F15 Results from optimisation and frequency calculations of Glu-Glu-AA complex at different level of theories and basis sets (unit in a.u.).

Glu-Glu-AA	HF/STO-3G	B3LYLP/3-21G	M06/3-21G
ξ	-2187.3727	-2216.4349	-2215.5912
$\xi_{(solv)}$	-2187.4858	-2216.5053	-2215.7095
$\Delta\ \xi_{(solv)}$	-0.1131	-0.0704	-0.1183
H_{corr}	1.0332	0.8858	0.8915
G_{corr}	0.9048	0.7660	0.7681

Table F16 Results from optimisation and frequency calculations of Glu-Glu-TrO complex at different level of theories and basis sets (unit in a.u.).

_Glu-Glu-TrO	HF/STO-3G	B3LYLP/3-21G	M06/3-21G
ξ	-3910.0585	-3962.3081	-3960.6718
$\xi_{(solv)}$	-3910.1383	-3962.4378	-3960.7671
$\Delta\ \xi_{(solv)}$	-0.0798	-0.1296	-0.0953
H_{corr}	2.3569	2.0189	2.0316
G_{corr}	2.0644	1.7379	1.7854

Table F17 Results from optimisation and frequency calculations at HF/STO-3G of TrO-OA, TrO-AA and TrO-TrO (unit in a.u.).

HF/STO-3G	TrO-OA	TrO-AA	TrO-TrO
ξ	-3476.9390	-3549.4403	-5272.1380
$\xi_{(solv)}$	-3476.2376	-3548.4926	-5270.3070
$\Delta\ \xi_{(solv)}$	0.7014	0.9477	1.8310
H_{corr}	2.5124	2.4760	3.7998
G_{corr}	2.2144	2.1929	3.3434